Clim. Past, 22, 2067–2109, 2026
https://doi.org/10.5194/cp-22-2067-2026
© Author(s) 2026. This work is distributed under
the Creative Commons Attribution 4.0 License.

Climate of the Past
Open Access
EGU

The Northwest Pacific corals unravel the NPGO- and Victoria Mode-related temperature variability back to the 19th century

Saori Ito[1,2], **Takaaki K. Watanabe**[1,2,3], **Atsuko Yamazaki**[3,4], **Chuan-Chou Shen**[5,6], **Taro Komagoe**[3], and **Tsuyoshi Watanabe**[1,3,4,7]

[1]Department of Natural History Sciences, Faculty of Science, Hokkaido University, Sapporo, 060-0810, Japan
[2]Institute of Geosciences, Kiel University, Kiel, 24118, Germany
[3]KIKAI Institute for Coral Reef Sciences, Kikai Town, Kagoshima, 891-6151, Japan
[4]Graduate School of Environmental Studies, Nagoya University, Nagoya, 464-8601, Japan
[5]High-Precision Mass Spectrometry and Environment Change Laboratory (HISPEC), Department of Geosciences, National Taiwan University, Taipei, 10617, Taiwan, ROC
[6]Research Center for Future Earth, National Taiwan University, Taipei, 10617, Taiwan, ROC
[7]Research Institute for Humanity and Nature, Kyoto, 603-8047, Japan

Correspondence: Saori Ito (saori.ito@ifg.uni-kiel.de)

Received: 19 August 2025 – Discussion started: 4 September 2025
Revised: 25 August 2026 – Accepted: 7 October 2026 – Published: 18 November 2026

Abstract. Atmospheric and oceanic phenomena in the Pacific Ocean, such as the North Pacific Gyre Oscillation (NPGO) and the Victoria Mode (VM), have significant implications for global climate variability through their linkage with temperature variability in the Central Pacific (CP). The NPGO and VM are defined based on sea surface height and basin-wide sea surface temperature anomaly patterns in the North Pacific, respectively, but their variability is often closely coupled. Although recent studies have drawn attention to their connection with temperature variability in the CP, the historical variability of this connection remains poorly understood due to limited instrumental observations. Because coral Sr/Ca records are primarily sensitive to temperature variability, they can capture signals of the temperature expression of the NPGO, the VM, or their covariability (i.e., NPGO–VM-related temperature variability). Here, we present a long-term reconstruction of NPGO–VM-related temperature variability based on a coral Sr/Ca temperature proxy from the Northwest Pacific (NWP), covering the period from 1799 to 2014 Common Era (CE). The coral-inferred temperature record closely aligns with temperature variability in the CP, indicating an extra-tropical linkage between temperature variability in the CP and NPGO–VM-related temperature variability in the NWP via an ocean–atmosphere bridge. The reconstructed NPGO–VM-related variability shows a pronounced negative phase (cool conditions in the NWP) during the 1860s–1900s, and a positive phase (warm-temperature in the NWP) during the 2000s–2010s. We also find a significant correlation between temperature variability in the CP and reconstructed NPGO–VM-related variability from the early 20th century to 2014, except during the 1970s–1980s. This relationship re-emerged in the 1990s, strengthened thereafter, and remained significant from the 2000s onward. Given the strong linkage between NPGO–VM-related variability and temperature anomalies in the CP, as well as the projected increase in CP-centred climate variability under future warming scenarios, the climatic influence of the NPGO and VM in the North Pacific and beyond is expected to intensify.

1 Introduction

Atmospheric and oceanic phenomena in the Pacific Ocean play a significant role in shaping global climate systems, including variations in sea surface temperature (SST) and ocean circulation. Global SST variations are known to be closely associated with Pacific climate phenomena (Messié and Chavez, 2011), such as the El Niño-Southern Oscillation (ENSO) (McPhaden et al., 2006; Philander, 1983), the

Pacific Decadal Oscillation (PDO) (Mantua et al., 1997), and the North Pacific Gyre Oscillation (NPGO) (Di Lorenzo et al., 2008). Recent studies have further classified ocean–atmosphere interactions in the equatorial Pacific into two flavours based on the longitudinal position of the temperature anomalies in the Eastern Pacific (EP; 5° S–5° N, 150–90° W) and the Central Pacific (CP; 5° S–5° N, 160° E–150° W) (Ashok et al., 2007; Kao and Yu, 2009; Larkin and Harrison, 2005; Lee and McPhaden, 2010; Yeh et al., 2009). These phenomena and their associated SST variability have teleconnections on global climate, influencing weather patterns, ecosystems, and socio-economic systems worldwide.

The NPGO is a mode of decadal-scale climate variability in the North Pacific, first introduced by Di Lorenzo et al. (2008). The index for NPGO (Di Lorenzo et al., 2008) quantifies variations in the strength of the central and eastern branches of the clockwise North Pacific gyre circulation, available back to 1950 CE. Dynamically, the NPGO is defined as the second principal component (i.e., the second empirical orthogonal function; EOF2) of sea surface height anomalies (SSHa) in the central-to-eastern North Pacific. The corresponding EOF2 spatial pattern exhibits a meridional dipole-like structure, with a nodal line around 40° N, reflecting large-scale wind-driven gyre circulation changes (Di Lorenzo et al., 2008; Chhak et al., 2009) (Fig. 1c). The NPGO is primarily forced by boreal wintertime wind-stress curl anomalies associated with the North Pacific Oscillation (NPO; Rogers, 1981; Walker and Bliss, 1932), with oceanic adjustment leading to circulation and SSH anomalies that typically peak from boreal late winter to spring, and its effects can be observed even in early summer (Chenillat et al., 2012). The dipole structure of the NPGO closely resembles that of the Victoria Mode (VM) (Bond et al., 2003) (Figs. 1b and A1b), which is defined as the EOF2 of basin-wide sea surface temperature anomalies (SSTa) over the North Pacific (Di Lorenzo et al., 2008) (Figs. 1a and A1a). The VM represents a dominant mode of extratropical SST variability on interannual-to-decadal scales, particularly during boreal winter and spring (Ding et al., 2015; Yu and Kim, 2011; Wen et al., 2024). In contrast to the dynamical ocean-circulation-based NPGO, the VM primarily reflects a thermodynamic surface response to atmospheric forcing by the NPO (Ding et al., 2015), through surface heat fluxes and Ekman advection.

Beyond the similarity of their dipole-like spatial structures observed in the EOF2 patterns of SSHa and SSTa, the NPGO and VM exhibit covariability on interannual-to-decadal timescales (Fig. A2). This relationship is consistent with the influence of NPO-related atmospheric forcing on both modes. In this sense, the NPGO and VM can be regarded as dynamically related but distinct components of a broader extratropical ocean–atmosphere system. The NPO has also been identified as a precursor to ENSO events via the seasonal footprinting mechanism, linking subtropical sea level pressure (SLP) anomalies to tropical Pacific variability (Vimont et al., 2001, 2003). Both the NPGO and VM have been linked to CP-ENSO dynamics, forming bidirectional links that connect extratropical and tropical Pacific climate variability (Di Lorenzo et al., 2010, 2013; Ding et al., 2015; Qi and Mao, 2022). These modes also play important roles in regional climate variability, including East Asian hydrology (e.g., Ye et al., 2016) and the Indian summer monsoon (e.g., Zhang et al., 2024a, b). Despite growing understanding of these mechanisms and their impacts, the long-term interactions and variability among the NPGO, VM, and CP-ENSO remain poorly understood due to the limited temporal coverage of instrumental and satellite observations. Addressing this limitation requires longer-term pre-instrumental archives, such as paleoclimate proxy records.

Modern and fossil reef-building corals can provide high temporal resolution archives of paleoclimatology on scales that can cover more than several hundred years (e.g., Abram et al., 2020; Cobb et al., 2003; D'Olivo et al., 2024; Hendy et al., 2002; Kawakubo et al., 2017; Quinn et al., 1998; Tangri et al., 2018). Notably, the ratio of strontium to calcium (Sr/Ca) in coral aragonite skeletons ($CaCO_3$) has been used as a proxy for paleo-temperature variability (e.g., Cahyarini et al., 2014; D'Olivo et al., 2024; Felis et al., 2018). Coral Sr/Ca records can therefore capture ocean temperature signals associated with the NPGO and VM, and potentially provide information extending beyond the available observational records and climate indices. In the Pacific, long-term coral records that complement or extend instrumental data are primarily concentrated in the tropics (Cobb et al., 2003, 2013; Cole et al., 1993; D'Olivo et al., 2024; McGregor et al., 2013; Nurhati et al., 2011; Rafter et al., 2017; Sanchez et al., 2016). Although several studies have attempted to reconstruct the NPGO mode in the past (Nurhati et al., 2011; Rafter et al., 2017; Sanchez et al., 2016), none have focused on VM variability or NPGO–VM-related temperature variations propagated extra-tropically from the CP. Focusing on the Northwest Pacific (NWP), paleoclimatic coral archives have mostly been used for East Asia monsoon reconstructions based on skeletal oxygen isotope ratio records ($\delta^{18}O$) (Garas et al., 2023; Kajita et al., 2017; Morimoto et al., 2007; Watanabe et al., 2014) and temperature reconstructions based on skeletal Sr/Ca records (Kawakubo et al., 2017; Felis et al., 2010). Here, we introduce a new long-term coral Sr/Ca-based temperature archive from the NWP. We first compare our coral record with previously published coral Sr/Ca-temperature records and then investigate relationships among our record, variability in CP SST, the NPGO, and the VM. Through these relationships, we evaluate the potential of this record to reconstruct NPGO–VM-related variability. This study presents the first coral-based reconstruction of NPGO–VM-related variability derived from the NWP, extending back to the 19th century.

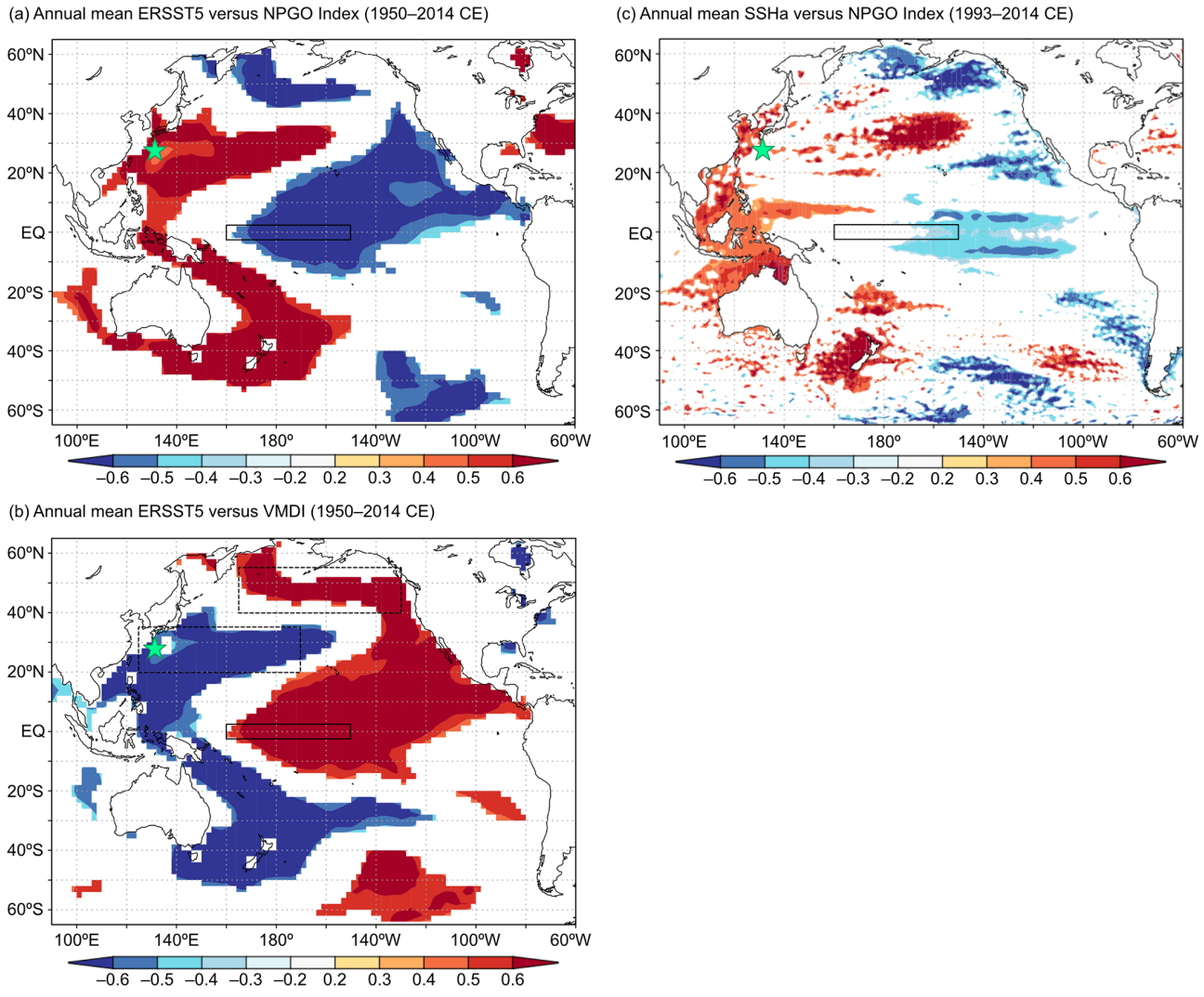


Figure 1. Spatial distribution of the NPGO and VM patterns shown in SST or SSH fields. **(a)** Field correlation map between the annual mean SST time series (ERSST5; Huang et al., 2017) and the NPGO Index (Di Lorenzo et al., 2008) from 1950 to 2014 CE. **(b)** Field correlation map between the annual mean SST time series (ERSST5; Huang et al., 2017) and the Victoria Mode Dipole Index (VMDI; Wen et al., 2024, calculated using ERSST5, grey boxes), from 1950 to 2014 CE. The black dashed boxes indicate the regions used to calculate the VMDI. **(c)** Field correlation map between the annual mean SSHa time series (Copernicus 0.25 × 0.25°, Copernicus Climate Change Service) and the NPGO Index from 1993 to 2014 CE. All correlations are computed using detrended data. Only correlations with p-values < 0.1 are colour-coded. The original figures in each panel were computed using the web application KNMI Climate Explorer (https://climexp.knmi.nl/, last access: 22 October 2026) and plotted using GrADS (v2.2.1). The location of the coral sampling site (Kikai Island, Kagoshima, Japan) is marked by a star. The black solid box indicates the CP region (5° S–5° N, 160° E–150° W). For figure panels **(a)** and **(b)**, an 8–30 year bandpass filter was applied to the datasets before calculation. See also Fig. A1 for the unfiltered analyses.

2 Methods

2.1 Study site and coral core collection

We collected three coral cores from Kikai Island, Kagoshima Prefecture, Japan, which is located in the NWP (Figs. 1 and A3). In June 2015 CE, three *Porites* coral cores were drilled from two colonies using an air drill with a 7.6 cm diameter core barrel at less than 5 m water depth in Shiomichi Bay, northeast of Kikai Island (28.338° N, 130.009° E). One core (Core-1) was collected from a living colony, and the others (Core-2 and Core-3) were collected from a microatoll-shaped sub-fossil colony. The two colonies were located adjacent to each other.

2.2 Sample preparation and coral skeletal Sr/Ca analysis

All cores were cut into 5 mm thick slabs. The slabs were rinsed several times with distilled water in an ultrasonic

bath and then dried at 50 °C for 24 h. X-radiographs (Fig. A4) were taken using a digital X-ray scanner, following the method described by Ito et al. (2020). Clear annual bands were observed in the X-radiographs of Core-1 and Core-3 but not in Core-2 (Fig. A4). Preservation of pristine skeletal aragonites in all specimens was confirmed by powder X-ray diffraction analysis at Hokkaido University (Fig. A5) and by microscopic observations at the KIKAI Institute for Coral Reef Sciences (Fig. A6).

Analytical paths were determined to follow the extending corallites and their growth direction along the major growth axis visible in the X-radiographs (Fig. A4) and on the slab surfaces. Skeletal powder samples for geochemical analysis were obtained using a precise microsampling technique with a 0.8 mm diameter micro-drill mounted on a semi-manually controlled XY stage. Each sample was collected at 1.2 mm intervals with a drilling depth of 1.0 mm. After each sampling, the milled area was cleaned with compressed air to avoid cross-contamination.

Coral skeletal Sr/Ca analysis was performed by inductively coupled plasma optical emission spectrometry (ICP-OES; iCAP 6200 Duo, Thermo Scientific) equipped with an autosampler (ASX-260, Teledyne CETAC Technologies) installed at Hokkaido University, following the method described by Watanabe et al. (2020). The coral Sr/Ca time series from 1989 to 2015 CE (part of Core-1) was previously documented by Kajita et al. (2017). Powdered samples (150 ± 10 µg) were dissolved in 250 µL of 25 % high-purity nitric acid and subsequently diluted with ultrapure water (Milli-Q water, 18.2 Ω cm at 25 °C, Merck Millipore). We calibrated Sr/Ca using the intensity-intensity ratio method (de Villiers et al., 2002) with five matrix-matched standard solutions. The JCp-1 solution (Okai et al., 2002) was measured as a reference material after every five sample measurements to correct for instrumental drift. As reported by Watanabe et al. (2020), the Sr/Ca value of the JCp-1 reference material was 8.838 ± 0.009 mmol mol^{-1} (1σ). Analytical uncertainty was typically 0.1 % relative standard deviation (%RSD, 1σ).

2.3 Chronology and seasonal definition

For the sub-fossil specimens (Core-2 and Core-3), three skeletal fragments were subsampled for uranium–thorium (U–Th) dating (174–413 mg each; Fig. A4). High-precision U–Th dating was conducted at the High-Precision Mass Spectrometry and Environment Change Laboratory (HISPEC), National Taiwan University. U–Th chemistry was performed on a class-100 bench in a class-10 000 clean room (Shen et al., 2003, 2008). Skeletal U and Th isotopic compositions were determined using a multi-collector inductively coupled plasma mass spectrometer (MC-ICP-MS; NEPTUNE, Thermo Fisher) (Shen et al., 2012). The decay constants used were from Cheng et al. (2013) for ^{230}Th and ^{234}U, and from Jaffey et al. (1971) for ^{238}U.

The age model was established based on coral Sr/Ca seasonal cycles, the Optimum Interpolation Sea Surface Temperature (OISST v2.1; Huang et al., 2021, monthly resolved and converted from daily data, see Sect. 2.4), annual density bands, and U–Th dating results (for sub-fossil specimens only). Core-2 showed clear annual cycles in the coral Sr/Ca record without interruption (e.g., no breakdown or abrupt shifts in seasonality), although its annual density bands were indistinct. Therefore, for Core-2, we developed an age model based on the annual cycles in the coral Sr/Ca record and the U–Th dating result. For overlapping periods between cores (1926–1931 CE between Core-1 and Core-2; 1884–1886 CE between Core-2 and Core-3; Fig. A7), the coral Sr/Ca records were recomputed into averaged values for each year. We used tie points to connect the highest (lowest) Sr/Ca values and the coolest (warmest) temperature values derived from the OISST data to establish each year, following the method of Ito et al. (2020). Based on the seasonal cycle in the OISST dataset from September 1981 to June 2015 CE, the annual coolest and warmest temperatures occur in February and August, respectively. For the period prior to August 1981 CE, the age model was established using tie points to connect the highest (lowest) Sr/Ca values and February (August). This method, an age-model approach using an artificial time series composed of repeating mean monthly temperatures, is commonly applied in coral geochemical studies (e.g., Charles et al., 1997; Felis et al., 2000; Pfeiffer et al., 2009; DeLong et al., 2014; Cahyarini et al., 2021); however, this approach can produce approximately 1–2 months of error in any given year for the period prior to the instrumental era. To minimise the influence of this uncertainty on our analysis, we used monthly interpolated summer and winter coral Sr/Ca records, defined by averaging three consecutive months centred on the warmest and coolest months, respectively, based on SST climatology (see Sect. 2.5).

2.4 Instrumental datasets and indices

We used instrumental datasets and climate indices to compare with coral geochemical records. Monthly data from the NOAA Extended Reconstructed Sea Surface Temperature Version 5 (ERSST5; Huang et al., 2017) were obtained from the grid cell covering the coral sampling site (27–29° N, 129–131° E; referred to as "Kikai-SST$_{ERSST5}$") and from the CP (5° S–5° N, 160° E–150° W; referred to as "CP-SST$_{ERSST5}$") for the period 1900–2014 CE. The abbreviations of these instrumental datasets are listed in Table A1. An annual SSHa time series ($0.25 \times 0.25°$ spatial resolution) from the Copernicus Climate Change Service was obtained for the period 1993–2014 CE. Both SST and SSHa data were downloaded via the KNMI Climate Explorer (https://climexp.knmi.nl/, last access: 22 October 2026). Additionally, the monthly NPGO Index (Di Lorenzo et al., 2008) for the period 1950–2014 CE was obtained from the NPGO website (http://www.o3d.org/npgo/index.html, last access: 22 October 2026). Fol-

lowing Wen et al. (2024), the Victoria Mode Dipole Index (VMDI) was calculated as the difference in SSTa between the northeastern North Pacific (40–55° N, 165° E–129° W) and the southwestern North Pacific (20–35° N, 125° E–170° W) for the period 1900–2014 CE. The NPO dataset for the period 1950–2014 CE was calculated from the Hadley Centre Sea Level Pressure dataset (HadSLP2r, Allan and Ansell, 2006; 30–65° N, 160° E–140° W) using the empirical orthogonal function method of Trenberth and Hurrell (1994) at KNMI Climate Explorer.

For establishing the age model for the coral geochemical record, we used the OISST v2.1 dataset (Huang et al., 2021, monthly resolved and converted from daily data) covering Kikai Island as a reference temperature product that reflects local water temperatures at high spatial resolution ($0.25 \times 0.25°$ grid) (see Sect. 2.3 for details of the age model method). A comparison between the instrumental temperature datasets employed in this study (OISST v2.1 and ERSST5) is shown in Fig. A8, indicating a statistically significant correlation at the 99 % confidence level ($r = 0.99$, $n = 406$, monthly resolution, for the period from September 1981 to June 2015 CE).

2.5 Converting coral Sr/Ca record (Kikai-coral Sr/Ca) into Sr/Ca-inferred temperature (°C, centred, Kikai-SST_{coral})

Based on the established age model (Sect. 2.3), we obtained a continuous 217 year coral Sr/Ca record, referred to as "Kikai-coral Sr/Ca". The dataset was then interpolated to a monthly resolution. From this monthly resolved dataset, three derived time series were constructed. First, three-month-averaged Sr/Ca values centred on the lowest and highest Sr/Ca values in each year, corresponding to boreal summer and winter, respectively, and are referred to as "Kikai-coral Sr/Ca_{summer}" and "Kikai-coral Sr/Ca_{winter}." Second, annual mean Sr/Ca values were calculated by averaging the Sr/Ca record from one winter peak to the subsequent winter peak; this time series is referred to as "Kikai-coral $Sr/Ca_{annual\ mean}$." The abbreviations of these time series are listed in Table A1.

We converted Kikai-coral Sr/Ca_{summer} and Kikai-coral Sr/Ca_{winter} (unit in mmol mol^{-1}) into temperature (unit in °C) using a Monte–Carlo technique that accounts for both coral Sr/Ca analytical errors and Sr/Ca-temperature slope uncertainties (Watanabe and Pfeiffer, 2022). For the Monte–Carlo simulation, we adopted four previously published Sr/Ca-temperature slopes derived from corals at Kikai Island (Fig. A9, Kajita et al., 2017; Kawakubo et al., 2014; Morimoto et al., 2007; Watanabe et al., 2020) in order to encompass potential intercolonial differences in the slope at this site. The resulting coral-based temperature record is hereafter referred to as "Kikai-SST_{coral}". When the record was calculated using Kikai-coral Sr/Ca_{summer} (Kikai-coral Sr/Ca_{winter}), the dataset is referred to as "Summer Kikai-SST_{coral} (Winter Kikai-SST_{coral})". This record is presented as a "centred" time series, where the mean value has been subtracted from the data. Centring is a standard statistical procedure (Draper and Smith, 1981) and has been commonly used in previous studies of coral-based temperature reconstructions (e.g., Cahyarini et al., 2008; Felis et al., 2018; Garas et al., 2023; Xu et al., 2015).

2.6 Statistical analysis

We tested the significance of the differences in coral Sr/Ca records for overlapping periods between Core-1 and Core-2, and between Core-2 and Core-3, using t-tests. The significance of variance differences in summer and winter Sr/Ca values among cores was tested using Levene's test. For time series analysis, we applied two temporal filters: an 8–30 year bandpass filter and an 8 year low-pass filter. The selection of these filters was guided by previous NPGO studies and supported by multitaper spectral analyses of the NPGO Index and VMDI (Fig. A10, see Sect. 3.1). The 8–30 year bandpass filter (bandwidth = 0.033–0.125 $year^{-1}$) was used for intercomparison among proxy and instrumental records and for sensitivity analyses. This filter emphasises variability within the targeted decadal band by removing high-frequency variability and attenuating variability at periods longer than 30 years. In contrast, the coral-based reconstruction of NPGO–VM-related variability (see Sect. 2.7) was designed to retain the broader low-frequency variability contained in the proxy record rather than to isolate only the 8–30 year component. For the reconstruction, we therefore applied an 8 year low-pass filter to the Kikai-coral Sr/Ca_{summer} record (bandwidth = 0.000–0.125 $year^{-1}$). This filter removes high-frequency variability while retaining variability at periods longer than 8 years, including periods longer than 30 years. The 8 year low-pass filter has been commonly used in previous NPGO studies (Di Lorenzo et al., 2010; Ding et al., 2015; Nurhati et al., 2011). A 30 year running correlation was calculated to assess the temporal change in the relationship between time series at relatively low frequencies (i.e., using 8 year low-pass filtered data). Multitaper spectral analysis and temporal filtering were performed using Past software (v.5.2, Hammer et al., 2001). A trend change point was estimated using the "SiZer" package on R software (Chaudhuri and Marron, 1999; R Core Team, 2023; Sonderegger et al., 2009). Cross-wavelet coherence analysis was performed using the "biwavelet" package on R software (Gouhier et al., 2021; R Core Team, 2023).

The statistical significance of correlation coefficients, i.e., confidence levels (CL), was tested using the method described by Di Lorenzo et al. (2009, 2010), which accounts for the reduction in effective sample size (N_{eff}) due to filtering. The significance of the correlation coefficient was determined based on the probability distribution functions of the correlation coefficient of two randomly generated red noise time series. These two time series were randomly generated

following the same autoregressive coefficients as those observed in the original two time series. The probability distributions are computed by generating 20 000 realisations of the correlation coefficient of two randomly generated red-noise time series.

In all statistical reports, the correlation coefficient is denoted as r. The number of samples is reported as N_{eff} (for filtered data only) or n (for all other data). The significance of the statistical analyses is reported using p-values (for t-tests, Levene's test, field correlations, and cross-wavelet coherence analyses), confidence intervals (CI; for trend change point analyses), or CLs (for correlations of unfiltered and filtered time series). When the correlation coefficient r was not significant, it is denoted as n. s.

2.7 Reconstruction of NPGO–VM-related variability

In this study, we use the term "NPGO–VM-related variability" to refer inclusively to variability associated with the NPGO, the VM, or their covariability, without implying that the two constitute a single climate mode or a unified index. Based on intercomparison among the NPGO Index, the VMDI, and Kikai-SST$_{\mathrm{coral}}$ time series (Sect. 3.4), we reconstructed NPGO–VM-related variability from the Kikai-coral Sr/Ca$_{\mathrm{summer}}$ time series using the following equation (Eq. 1).

$$Z_{\mathrm{Sr/Ca},t} = -\frac{\mathrm{Sr/Ca}_t - \overline{\mathrm{Sr/Ca}}_{1950\text{–}2014}}{\sigma_{\mathrm{Sr/Ca,\ 1950\text{–}2014}}}, \quad (1)$$

where $\overline{\mathrm{Sr/Ca}}_{1950\text{–}2014}$ and $\sigma_{\mathrm{Sr/Ca,1950\text{–}2014}}$ are the mean and standard deviation, respectively, of the Kikai-coral Sr/Ca$_{\mathrm{summer}}$ time series over 1950–2014 CE. The sign of the standardised Sr/Ca anomaly was reversed because coral Sr/Ca is inversely related to water temperature, with positive (negative) values indicating relatively warmer (cooler) conditions. High-frequency variability was removed by applying an 8 year low-pass filter (bandwidth = 0.000–0.125 year^{-1}). This approach retains variability at periods longer than 8 years, including the decadal and lower-frequency variability represented in the coral record. Both the NPGO Index and VMDI exhibit statistically significant or distinct spectral power at periods longer than 8 years (Fig. A10, 95 % CL for the NPGO Index; 90 % CL for the VMDI, see also Sect. 3.1). Variability at periods longer than 30 years was retained in the reconstruction but was not attributed specifically to either NPGO-related or VM-related variability. It is noted that the standardised Kikai-coral Sr/Ca$_{\mathrm{summer}}$ time series, rather than Kikai-SST$_{\mathrm{coral}}$, was used for the reconstruction. Conversion of coral Sr/Ca to SST (Sect. 2.5) was performed to evaluate the temperature response of the coral Sr/Ca record and to facilitate comparisons with instrumental and coral-based SST records. For the reconstruction, the original coral Sr/Ca record was standardised directly because the target variables, the NPGO Index and the VMDI, are standardised climate indices rather than absolute temperature records. This approach also avoids propagating uncertainties associated with the Sr/Ca–SST calibration into the reconstruction.

3 Results

3.1 Significant frequencies in the NPGO and VM

We conducted spectral analyses of the NPGO Index dataset (Di Lorenzo et al., 2008) and the VMDI dataset (Wen et al., 2024) to identify their significant frequencies. For the unfiltered NPGO Index, significant spectral peaks were detected at 9.8, 6.9, and 3.6 years at the 95 % CL (Fig. A10a). Similar significant spectral peaks were detected after application of a 30 year high-pass filter (9.8, 6.8, and 3.6 years at the 95 % CL; Fig. A10c). For the unfiltered VMDI, spectral peaks exceeding the 90 % CL were identified at 51.2, 10.6, 3.7–3.9, and 2.4–2.5 years (Fig. A10b). However, the 51.2 year peak lies near the limit of the resolvable range and represents only approximately two cycles within the 1900–2014 CE record; it was therefore not regarded as a robustly resolved spectral peak. After applying a 30 year high-pass filter, significant peaks were detected at 12.4 and 10.6 years at the 95 % CL (Fig. A10d). Overall, both indices exhibited distinct decadal-scale spectral peaks within the 8–30 year band.

3.2 Kikai-coral Sr/Ca (this study)

3.2.1 Sr/Ca records from Core-1 to Core-3

Each coral Sr/Ca record obtained from the three coral cores revealed clear annual cycles (defined as from one winter peak to the subsequent winter peak) without interruptions (Fig. 2a; Table 1). No signatures of growth disturbances were observed, such as stress bands or growth cessations (Figs. 2a and A4). The modern coral, Core-1, covered the period from summer 1926 CE to the year of collection (2015 CE). The sub-fossil coral, Core-2, covered the period from autumn 1884 CE to spring 1931 CE, with a U–Th age of 1884 ± 1.5 CE (Table A2). Another sub-fossil coral, Core-3, covered the period from spring 1798 CE to winter 1886 CE, with U–Th ages of 1883 ± 2.5 CE and 1797 ± 2.6 CE (Table A2). There were overlapping periods between Core-1 and Core-2 (1926–1931 CE) and between Core-2 and Core-3 (1884–1886 CE). The accuracy of the age model was verified by comparing datasets for these overlapping periods. The overlapping skeletal Sr/Ca records correlated significantly at the 99 % CL (Core-1 and Core-2: $r = 0.79$, $n = 54$; Core-2 and Core-3: $r = 0.85$, $n = 18$; Fig. A7). In addition, no statistically significant differences were detected in mean Sr/Ca values for the overlapping periods among Core-1, Core-2, and Core-3, except for the mean of winter peaks between Core-1 and Core-2 (Fig. A7; Table A3). Furthermore, variance differences in summer and winter Sr/Ca values among cores were not statistically significant (summer Sr/Ca: p-value = 0.19; winter Sr/Ca: p-value = 0.72, Levene's test). These results confirm that the compiled coral Sr/Ca time

series, i.e., Kikai-coral Sr/Ca, provides a continuous record from 1798 to 2015 CE.

3.2.2 Summer, winter, and mean values of Kikai-coral Sr/Ca

To evaluate the characteristics of the Kikai-coral Sr/Ca record, we compared the summer, winter, and mean Sr/Ca values (Kikai-coral Sr/Ca_{summer}, Kikai-coral Sr/Ca_{winter}, and Kikai-coral $Sr/Ca_{annual\ mean}$; Sect. 2.5) with the annual mean values of the instrumental temperature derived from the grid cell covering the coral sampling site (Kikai-SST_{ERSST5}) for the period 1950–2014 CE. This comparison revealed that the summer, winter, and mean Sr/Ca values did not show significant correlations with Kikai-SST_{ERSST5} without filtering (for Kikai-coral Sr/Ca_{summer}: $r = -0.12$, $n = 65$, n.s.; Kikai-coral Sr/Ca_{winter}: $r = 0.06$, $n = 65$, n.s.; Kikai-coral $Sr/Ca_{annual\ mean}$: $r = 0.03$, $n = 65$, n.s.). In contrast, these coral Sr/Ca time series captured long-term temperature variability around Kikai Island when an 8–30 year bandpass filter was applied (for Kikai-coral Sr/Ca_{summer}: $r = -0.69$, $N_{eff} = 8.02$, significant at the 95 % CL; Kikai-coral Sr/Ca_{winter}: $r = -0.67$, $N_{eff} = 9.29$, significant at the 99 % CL; Kikai-coral $Sr/Ca_{annual\ mean}$: $r = -0.78$, $N_{eff} = 7.58$, significant at the 99 % CL; Fig. A11).

3.2.3 Comparison of coral Sr/Ca records from Kikai Island

On Kikai Island, coral Sr/Ca records have been published by Kawakubo et al. (2017) and Morimoto et al. (2007). We compared our Kikai-coral Sr/Ca record with these previously published records to assess consistency and differences.

In a comparison between our Kikai-coral Sr/Ca record and the previously published record by Kawakubo et al. (2017) for the period 1950–2008 CE, we found a correlation between Kikai-coral Sr/Ca_{summer} and the previously published summer values only at the 90 % CL ($r = 0.50$, $N_{eff} = 8.22$, 8–30 year bandpass filtered; Fig. A11a). In contrast, no significant correlation was observed between Kikai-coral Sr/Ca_{winter} and the previously published winter values ($r = -0.35$, $N_{eff} = 7.14$, n. s., 8–30 year bandpass filtered; Fig. A11b). Additionally, unlike the results from our coral record (Sect. 3.2.2), neither the summer nor the winter values from the previously published record (Kawakubo et al., 2017) showed a significant correlation with the instrumental temperature record (Kikai-SST_{ERSST5}) (summer values: $r = -0.24$, $N_{eff} = 8.49$, n. s., 8–30 year bandpass filtered; Fig. A11a, winter values: $r = -0.23$, $N_{eff} = 11.10$, n. s., 8–30 year bandpass filtered; Fig. A11b).

Morimoto et al. (2007) documented a short-term coral Sr/Ca record from Kikai Island. Its record length (< 6 years) is insufficient to assess past interannual-to-decadal-scale variability. Although the absolute Sr/Ca values differed between our Kikai-coral Sr/Ca record and that of Morimoto et al. (2007), likely due to intercolonial differences (Corrège, 2006), the seasonal ranges of the records were largely consistent (Table A4).

3.3 Kikai-SST_{coral} (this study)

As demonstrated in Sect. 3.2.2, both the Kikai-coral Sr/Ca_{summer} and Kikai-coral Sr/Ca_{winter} time series have the potential to reconstruct long-term temperature variability around Kikai Island. Accordingly, we converted these time series into temperature values (°C, Summer Kikai-SST_{coral} and Winter Kikai-SST_{coral}; Sect. 2.5). The time series of Summer and Winter Kikai-SST_{coral} are shown in Fig. 2b and c. The spectral power analyses revealed significant peaks both with and without a 30 year high-pass filter (Fig. A12). In particular, significant spectral peaks at 16.4 and 15.2 years for Summer Kikai-SST_{coral} (at the 95 % CL, Fig. A12c) and at 18.2, 12.8, 9.3, and 8.3 years for Winter Kikai-SST_{coral} (at the 95 % CL, Fig. A12d) fell within the range of filters applied in this study (Sect. 2.6).

Significant relationships were confirmed between Summer Kikai-SST_{coral} and Kikai-SST_{ERSST5}, and between Winter Kikai-SST_{coral} and Kikai-SST_{ERSST5}, at the 95 % CL from 1950 to 2014 CE (8–30 year bandpass filtered; Fig. 3a, c, and e; Table 2a). However, for the longer period (1900–2014 CE), no significant correlations were observed (8–30 year bandpass filtered; Fig. 3a, c, and e; Table 2b). Moreover, Summer Kikai-SST_{coral} time series matched the SST time series in the CP (CP-SST_{ERSST5}). A significant negative correlation was observed between the two time series at the 99 % CL from 1950 to 2014 CE (8–30 year bandpass filtered; Fig. 3b and d; Table 2a). Even over the longer period from 1900 to 2014 CE, the significant relationship was maintained (8–30 year bandpass filtered; Fig. 3b and d; Table 2b). While the Winter Kikai-SST_{coral} time series showed no significant relationships with CP-SST_{ERSST5} from 1950 to 2014 CE (8–30 year bandpass filtered; Fig. 3b and f; Table 2a) and from 1900 to 2014 CE (8–30 year bandpass filtered; Fig. 3b and f; Table 2b).

A significant correlation was also observed with the previously published coral-based temperature record from Palmyra, located in the central tropical Pacific, dating back to 1887 CE (referred to as "Palmyra-SST_{coral}") (Nurhati et al., 2011). Summer Kikai-SST_{coral} correlated with Palmyra-SST_{coral} at the 95 % CL (8–30 year bandpass filtered; Fig. A13a and c; Table 2c), whereas no significant relationship was obtained for Winter Kikai-SST_{coral} (8–30 year bandpass filtered; Fig. A13a and e; Table 2c). In addition, no significant correlation was observed with the previously published coral $\delta^{18}O$ record from Clarion Island, located in the northeastern Pacific (NEP), dating back to 1820 CE (referred to as "Clarion-$\delta^{18}O_{coral}$") (Sanchez et al., 2016) (8–30 year bandpass filtered; Fig. A13b, d, and f; Table 2c).

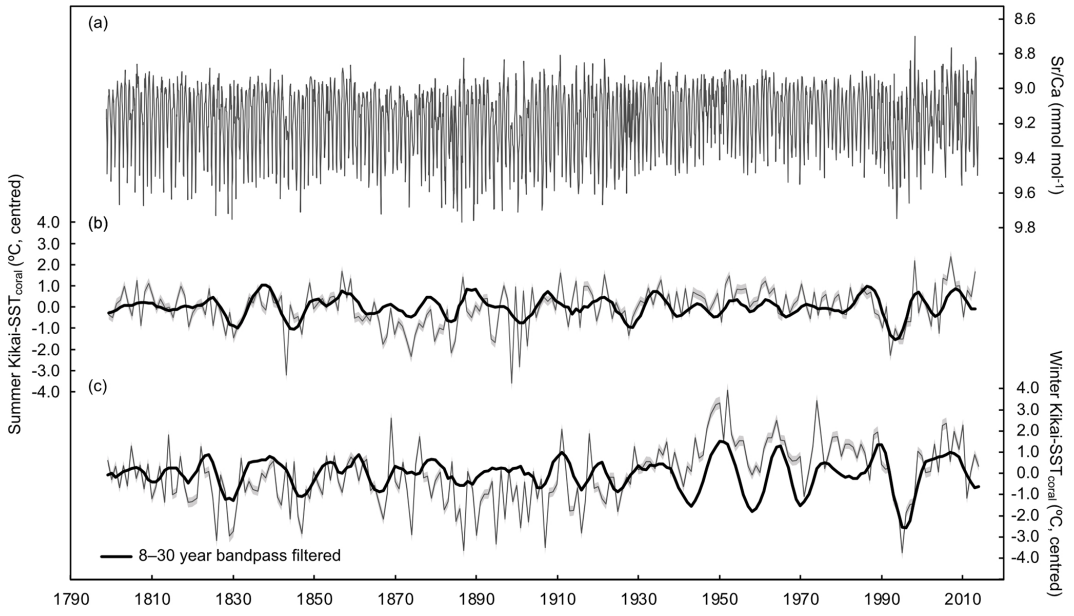


Figure 2. Kikai-coral Sr/Ca and Kikai-SST_{coral} records. The time series of **(a)** Kikai-coral Sr/Ca (mmol mol^{-1}), **(b)** Summer Kikai-SST_{coral} (°C, centred), and **(c)** Winter Kikai-SST_{coral} (°C, centred). See also Fig. A7, illustrating Kikai-coral Sr/Ca for the overlapping periods (1926–1931 CE for between Core-1 and Core-2; 1884–1886 CE for between Core-2 and Core-3). The methodology for calculating Kikai-SST_{coral} (figure panels **b** and **c**) converted from Kikai-coral Sr/Ca is described in Sect. 2.5. The uncertainty in temperature, represented by shading indicating 90 % CIs, was estimated using a Monte–Carlo approach (Watanabe and Pfeiffer, 2022).

Table 1. Summary of the Kikai-coral Sr/Ca record. Core-1 is a modern *Porites* coral core collected in June 2015 CE. Core-2 and Core-3 are sub-fossil *Porites* coral cores. U–Th dating results for the sub-fossil cores are reported in Table A2. The overlapping intervals among the three cores are shown in Fig. A7. The number of annual cycles was determined based on Sr/Ca seasonal variability, counting one year as the period from one winter peak to the subsequent winter peak.

Specimens	Mean Sr/Ca (mmol mol^{-1})	Maximum Sr/Ca (mmol mol^{-1})	Minimum Sr/Ca (mmol mol^{-1})	Number of annual cycles	Period of Sr/Ca record
Core-1	9.14	9.79	8.67	89	1926–2015 CE
Core-2	9.22	9.81	8.79	46	1884–1931 CE
Core-3	9.19	9.79	8.84	87	1798–1886 CE

3.4 Comparison among the NPGO Index, the VMDI, and Kikai-SST_{coral}

Field correlation patterns between Kikai-SST_{coral} and instrumental SST or SSHa revealed spatial structures resembling those associated with the NPGO and VM (compare Figs. 1 and 4 for the 8–30 year bandpass filtered results; see also Fig. A14 for the unfiltered results), particularly for Summer Kikai-SST_{coral}. In particular, the field correlation pattern between Summer Kikai-SST_{coral} and ERSST5 for the period 1950–2014 CE (Fig. 4a) was consistent with the documented expression of the NPGO pattern in Pacific SSTa (refer to Fig. 4b of Di Lorenzo et al., 2008) and VM-like temperature distribution in the North Pacific (refer to Fig. 1a of Wen et al., 2024). When extended back to 1900 CE (Fig. 4c), the field correlation pattern still showed an NPGO-like structure in the Pacific SSTa field. Compared to the period 1950–2014 CE (Fig. 4a), the correlation coefficients for the longer period 1900–2014 CE (Fig. 4c) were generally lower. To examine whether the weaker correspondence before 1950 CE was associated with a different dominant spatial pattern, we additionally calculated the field correlations for 1900–1949 CE. The resulting pattern did not reveal a coherent spatial structure that could be clearly attributed to an alternative dominant climate mode during this interval (Fig. A15). Possible explanations for the weaker pre-1950 correspondence, including limitations in the instrumental SST dataset, are discussed in Sect. 4.1. These spatial relationships indicate that the coral record captures NWP temperature variability associated with the NPGO, the VM, or their covariability.

Notably, Summer Kikai-SST_{coral} significantly correlated with the annual mean NPGO Index from 1950 to 2014 CE at the 99 % CL (8–30 year bandpass filtered; Fig. 5a and e; Table 3a). A significant relationship was also observed in the

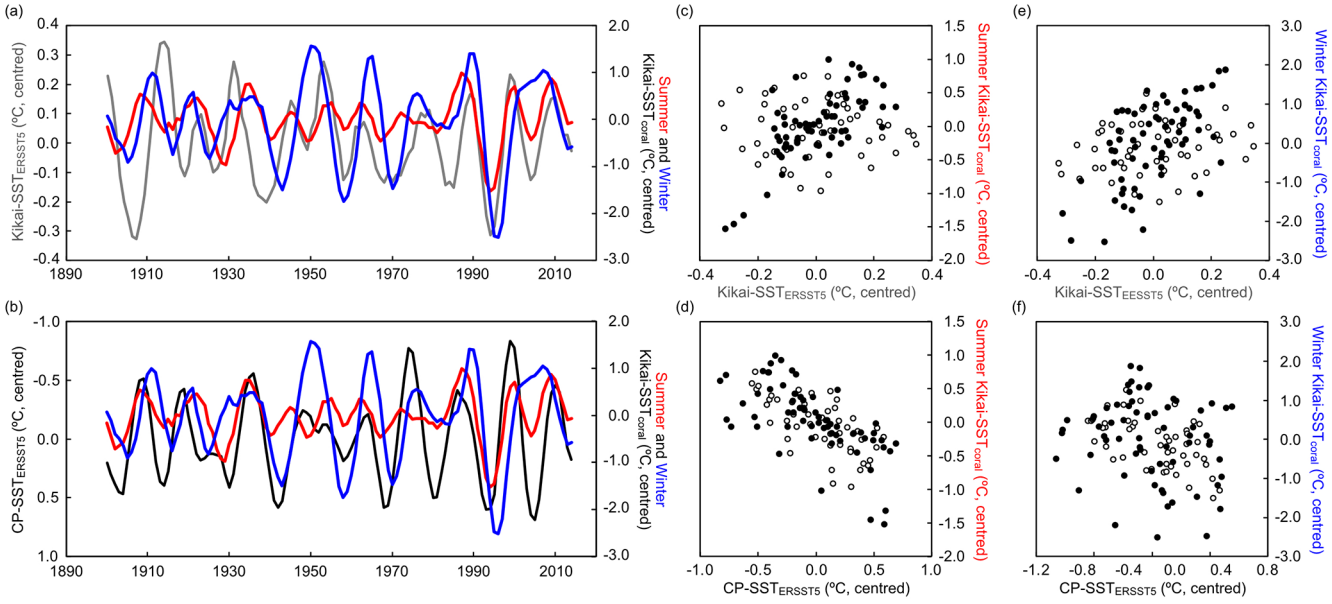


Figure 3. Time series comparisons of coral-based temperature and SST datasets from 1900 to 2014 CE. Comparison of **(a)** Summer (in red) and Winter Kikai-SST$_{coral}$ (in blue) and annual mean Kikai-SST$_{ERSST5}$ (in grey, Huang et al., 2017); **(b)** Summer (in red) and Winter Kikai-SST$_{coral}$ (in blue) and annual mean CP-SST$_{ERSST5}$ (in black). An 8–30 year bandpass filter was applied to all time series. **(c–f)** Scatter plots corresponding to **(a)** and **(b)**. Open-circle plots are data for the period 1900–1949 CE. Closed-circle plots are data for the period 1950–2014 CE.

Table 2. Correlations among Kikai-SST$_{coral}$ (this study), the instrumental SST record (ERSST5) around Kikai Island and in the CP, and previously published coral records. Correlations between Summer or Winter Kikai-SST$_{coral}$ and the instrumental SST record (ERSST5; Huang et al., 2017) for the periods **(a)** from 1950 to 2014 CE and **(b)** from 1900 to 2014 CE. **(c)** Correlation among Summer or Winter Kikai-SST$_{coral}$ and annual mean values of the previously published coral records. An 8–30 year bandpass filter was applied to all time series prior to calculating correlations.

Pair of correlation analysis	Period	r	Significance	N_{eff}
(a) Comparison of the seasonal Kikai-SST$_{coral}$ dataset and the annual mean instrumental SST records, for the period 1950–2014 CE				
Summer Kikai-SST$_{coral}$ versus Kikai-SST$_{ERSST5}$	1950–2014 CE	0.69	95 % CL	7.94
Summer Kikai-SST$_{coral}$ versus CP-SST$_{ERSST5}$	1950–2014 CE	–0.66	99 % CL	6.71
Winter Kikai-SST$_{coral}$ versus Kikai-SST$_{ERSST5}$	1950–2014 CE	0.68	95 % CL	8.94
Winter Kikai-SST$_{coral}$ versus CP-SST$_{ERSST5}$	1950–2014 CE	–0.18	n. s.	6.02
(b) Comparison of the seasonal Kikai-SST$_{coral}$ dataset and the annual mean instrumental SST records, for the period 1900–2014 CE				
Summer Kikai-SST$_{coral}$ versus Kikai-SST$_{ERSST5}$	1900–2014 CE	0.34	n. s.	15.26
Summer Kikai-SST$_{coral}$ versus CP-SST$_{ERSST5}$	1900–2014 CE	–0.65	95 % CL	9.80
Winter Kikai-SST$_{coral}$ versus Kikai-SST$_{ERSST5}$	1900–2014 CE	0.41	90 % CL	18.74
Winter Kikai-SST$_{coral}$ versus CP-SST$_{ERSST5}$	1900–2014 CE	–0.28	n. s.	10.96
(c) Comparison of the seasonal Kikai-SST$_{coral}$ dataset and the previously published coral records				
Summer Kikai-SST$_{coral}$ versus Palmyra-SST$_{coral}$	1887–1997 CE	–0.56	95 % CL	12.73
Summer Kikai-SST$_{coral}$ versus Clarion-$\delta^{18}O_{coral}$	1820–1997 CE	0.30	n. s.	21.51
Winter Kikai-SST$_{coral}$ versus Palmyra-SST$_{coral}$	1887–1997 CE	–0.16	n. s.	11.91
Winter Kikai-SST$_{coral}$ versus Clarion-$\delta^{18}O_{coral}$	1820–1997 CE	0.23	n. s.	26.39

8 year low-pass filtered data (Fig. A16a and e; Table A5a). Winter Kikai-SST_{coral} also appears to reflect NPGO variability, although the correlation between them for the same period was significant only at the 90 % CL (8–30 year bandpass filtered; Fig. 5b and f; Table 3a; see also Fig. A16b and f and Table A5a for 8 year low-pass filtered). Similarly, Summer Kikai-SST_{coral} significantly correlated with the annual mean VMDI from 1950 to 2014 CE at the 99 % CL (8–30 year bandpass filtered; Fig. 5c and g; Table 3b). A significant relationship was also observed in the 8 year low-pass filtered data (Fig. A16c and g and Table A5b). While Winter Kikai-SST_{coral} showed a significant relationship with the VMDI only at the 90 % CL (8–30 year bandpass filtered; Fig. 5d and h; Table 3b; see also Fig. A16d and h and Table A5b for 8 year low-pass filtered). For the longer period (from 1900 to 2014 CE), neither Summer Kikai-SST_{coral} nor Winter Kikai-SST_{coral} exhibited a significant relationship with the VMDI (Tables 3b and A5b).

The NPGO Index and VMDI generally covaried over their common period, although their correspondence weakened temporarily from the late 1960s through the 1970s (Fig. A2b, 8–30 year bandpass filtered). During this interval, Summer Kikai-SST_{coral} more closely tracked the annual mean VMDI (Fig. 5c) than the annual mean NPGO Index (Fig. 5a). Overall, the spatial correlation patterns and time-series comparisons showed stronger and more consistent relationships for Summer Kikai-SST_{coral} than for Winter Kikai-SST_{coral}. Based on these results, the reconstruction presented in Sect. 3.5 uses the summer coral Sr/Ca record.

4 Reconstructed NPGO–VM-related variability back to the 19th century

We reconstructed NPGO–VM-related variability from 1799 to 2014 CE using the 8 year low-pass filtered Kikai-coral Sr/Ca_{summer} record (Eq. 1; Sect. 2.7). The resulting reconstruction extends back to the early 19th century, prior to the instrumental period (Fig. 6a). Before the 1850s, the reconstruction was characterised by alternating negative and positive phases, including a relatively modest negative phase (reconstructed NPGO–VM-related variability < -1.0, corresponding to cool conditions in the NWP) from the late 1820s to the early 1830s. From the 1860s through the 1900s, a pronounced negative phase was observed. A trend change point was identified at 1873 CE (95 % CI: 1844–1877 CE; diamond symbol in Fig. 6a). Following alternating negative and positive phases during much of the 20th century, another prominent negative phase occurred in the 1990s. Since the early 2000s, the reconstruction has shifted towards a distinct positive phase (reconstructed NPGO–VM-related variability > 1.0, corresponding to warm conditions in the NWP).

The reconstructed NPGO–VM-related variability was not significantly correlated with either Palmyra-SST_{coral} ($r = -0.31$, $N_{eff} = 18.02$, n. s., from 1887 to 1997 CE; Fig. 6a and b) or Clarion-$\delta^{18}O_{coral}$ ($r = 0.22$, $N_{eff} = 26.07$, n. s., from 1820 to 1997 CE; Fig. 6a and c). Cross-wavelet coherence between the reconstruction and Palmyra-SST_{coral} was significant only within limited time-frequency regions (Fig. 6d). The reconstruction and Clarion-$\delta^{18}O_{coral}$ exhibited significant coherence at decadal to interdecadal periods during parts of their common interval (Fig. 6e).

The 30 year running correlation between the reconstructed NPGO–VM-related variability and CP-SST_{ERSST5} indicates a significant negative relationship from the early 20th century to 2014, except during the 1970s–1980s (Fig. 7a). This interval partly coincided with a period characterised by both weak correspondence between Summer Kikai-SST_{coral} and the NPGO Index (Fig. 5a) and divergence between the NPGO Index and the VMDI (Fig. A2). The negative relationship between the reconstructed NPGO–VM-related variability and CP-SST_{ERSST5} strengthened again in the 1990s and remained significant from the 2000s onwards. Significant negative correlations were also observed with Palmyra-SST_{coral} from the mid-1920s to the early 1970s and from the early 1990s to 1997, with no significant correlation between these intervals (Fig. 7b). Similarly, the correlation with Clarion-$\delta^{18}O_{coral}$ was significantly negative from the 1910s to the mid-1940s and from the late-1970s to 1997, with no significant correlation between these intervals (Fig. 7c). For all three comparisons, the magnitude of the negative running correlations during parts of the 1920s–1950s was nearly comparable to that observed during the recent significant correlation intervals (Fig. 7).

5 Discussion

5.1 Potential of Kikai coral records to reconstruct NPGO–VM-related variability

5.1.1 Ocean–atmosphere bridge over the Central and Northwest Pacific

The VM likely explains the observed linkage between the NWP/North Pacific and CP by acting as an "oceanic bridge" that connects the NPO and CP-centred ENSO phenomena (Ding et al., 2015; Qi and Mao, 2022). In addition, temperature variability in the CP serves as a driving force for large-scale atmospheric circulation in the central North Pacific (i.e., NPO), which in turn feeds back onto ocean dynamics and excites NPGO responses. This feedback connecting the NPGO and temperature variability in the CP has been referred to as an "atmospheric bridge" (Alexander et al., 2002; Di Lorenzo et al., 2010). Given these interrelationships between oceanic and atmospheric modes, the temperature variability observed in the NWP, including at our study site, is likely influenced by NPGO–VM-related temperature variability propagated from the CP via the "ocean–atmosphere bridge," particularly on decadal and longer timescales.

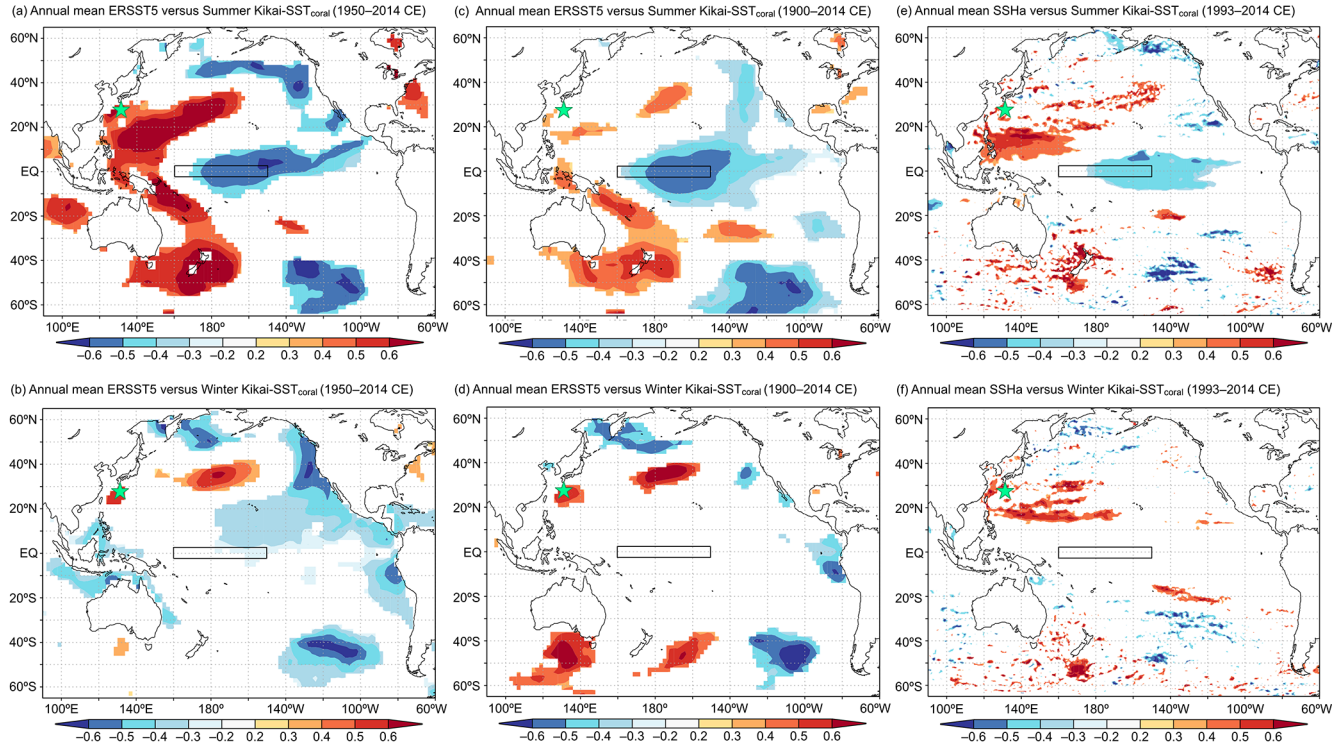


Figure 4. Field correlations between Kikai-SST$_{coral}$ record and instrumental SST and SSH records. **(a)** Field correlation map between Summer Kikai-SST$_{coral}$ (this study) and the annual mean SST time series (ERSST5; Huang et al., 2017) from 1950 to 2014 CE. **(b)** Field correlation map between Winter Kikai-SST$_{coral}$ and the annual mean SST time series (ERSST5; Huang et al., 2017) from 1950 to 2014 CE. **(c)** same as **(a)**, but covering the period from 1900 to 2014 CE. **(d)** same as **(b)**, but covering the period from 1900 to 2014 CE. **(e)** Field correlation map between Summer Kikai-SST$_{coral}$ and the annual mean SSHa time series from 1993 to 2014 CE. **(f)** Field correlation map between Winter Kikai-SST$_{coral}$ and the annual mean SSHa time series from 1993 to 2014 CE. All correlations are computed using detrended data. Only correlations with p-values < 0.1 are colour-coded. The original figures in each panel were computed using the web application KNMI Climate Explorer (https://climexp.knmi.nl/, last access: 22 October 2026) and plotted using GrADS (v2.2.1). The location of the coral sampling site (Kikai Island, Kagoshima, Japan) is marked by a star. The black box indicates the CP region (5° S–5° N, 160° E–150° W). For panels **(a)**–**(d)**, an 8–30 year bandpass filter was applied to the datasets before calculation. See also Fig. A14 for the unfiltered analyses.

Table 3. Correlations among Kikai-SST$_{coral}$ (this study), the NPGO Index, and the VMDI. Correlations between Summer or Winter Kikai-SST$_{coral}$ and **(a)** the annual mean NPGO Index (Di Lorenzo et al., 2008), **(b)** the annual mean Victoria Mode Dipole Index (VMDI; Wen et al., 2024, calculated using ERSST5). Prior to calculating correlations, an 8–30 year bandpass filter was applied to the time series. See also Table A5 for the results obtained using the 8 year low-pass filtered datasets.

(a) Comparison of the seasonal Kikai-SST$_{coral}$ dataset and the annual mean NPGO Index (8–30 year bandpass filtered)				
Pair of correlation analysis	Period	r	Significance	N_{eff}
Summer Kikai-SST$_{coral}$ versus NPGO Index	1950–2014 CE	0.67	99 % CL	7.27
Winter Kikai-SST$_{coral}$ versus NPGO Index	1950–2014 CE	0.45	90 % CL	5.80
(b) Comparison of the seasonal Kikai-SST$_{coral}$ dataset and the annual mean VMDI (8–30 year bandpass filtered)				
Summer Kikai-SST$_{coral}$ versus VMDI	1950–2014 CE	–0.82	99 % CL	7.97
Winter Kikai-SST$_{coral}$ versus VMDI	1950–2014 CE	–0.46	90 % CL	7.88
Summer Kikai-SST$_{coral}$ versus VMDI	1900–2014 CE	–0.44	n. s.	15.80
Winter Kikai-SST$_{coral}$ versus VMDI	1900–2014 CE	–0.30	n. s.	17.88

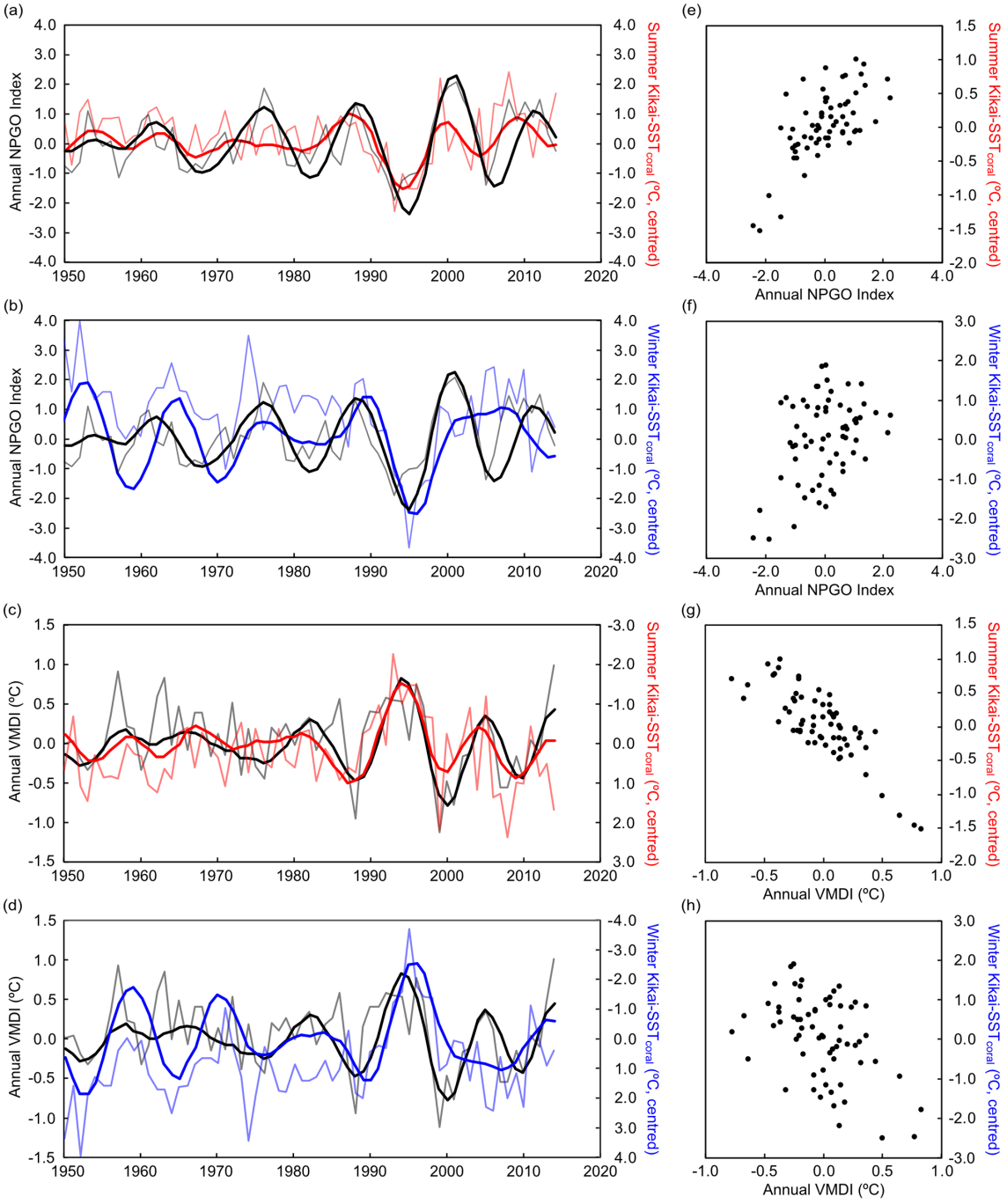


Figure 5. Comparison of the annual mean NPGO Index, annual mean VMDI, and Kikai-SST$_{coral}$ (1950–2014 CE). Time series of **(a)** the annual mean NPGO Index (thin black line, Di Lorenzo et al., 2008) and Summer Kikai-SST$_{coral}$ (thin red line); **(b)** the annual mean NPGO Index (thin black line) and Winter Kikai-SST$_{coral}$ (thin blue line); **(c)** the annual mean Victoria Mode Dipole Index (thin black line, VMDI, Wen et al., 2024, calculated using ERSST5) and Summer Kikai-SST$_{coral}$ (thin red line); **(d)** the VMDI (thin black line) and Winter Kikai-SST$_{coral}$ (thin blue line). Bold lines represent the 8–30 year bandpass filtered time series. **(e–h)** Scatter plot corresponding to **(a)**–**(d)**, for the bandpass filtered dataset. See also Fig. A16 for the 8 year low-pass filtered time series.

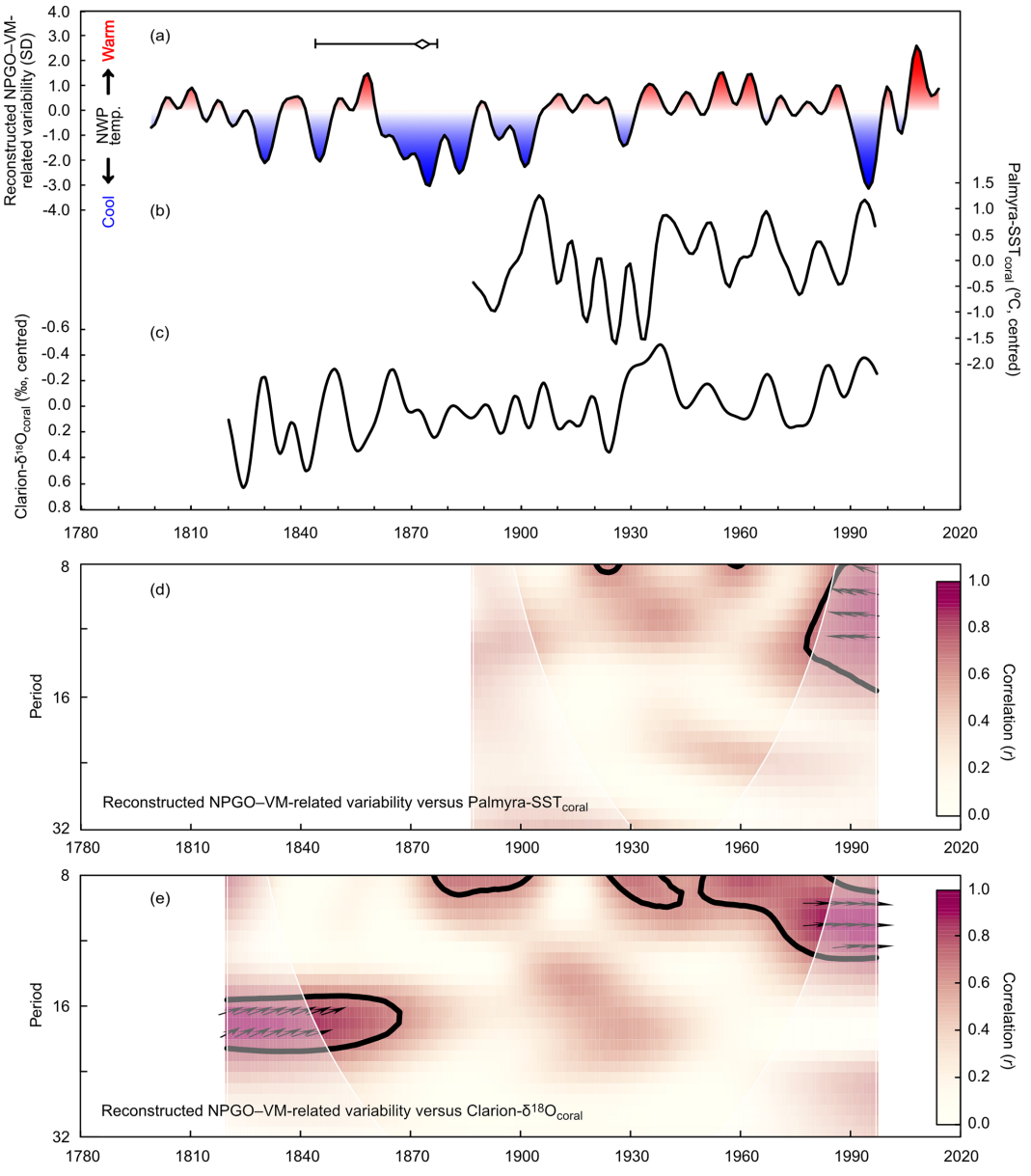


Figure 6. Reconstructed NPGO–VM-related variability extending back to 1799 CE. **(a)** Coral-based reconstruction of NPGO–VM-related variability derived from the standardised Kikai-coral Sr/Ca_{summer} record. An 8 year low-pass filter was applied to the datasets before calculation. Blue-coloured portions indicate negative phases (reconstructed NPGO–VM-related variability < 0, cool conditions in the NWP), while red-coloured portions indicate positive phases (reconstructed NPGO–VM-related variability > 0, warm conditions in the NWP). The diamond symbol denotes a detected trend change point, determined using the "SiZer" package (version 0.1-8) on R software (Chaudhuri and Marron, 1999; R Core Team, 2023; Sonderegger et al., 2009). The horizontal error bar represents the estimated uncertainty associated with the trend change point. **(b)** Palmyra-SST_{coral} dataset reported by Nurhati et al. (2011) (8 year low-pass filtered). **(c)** Clarion-$\delta^{18}O_{coral}$ dataset reported by Sanchez et al. (2016) (8 year low-pass filtered). **(d)** Cross-wavelet coherence between time series **(a, b)** from 1887 to 1997 CE. Regions of significant coherence (p-values < 0.1) are outlined by solid contours. Arrows indicate the phase relationship. The cross-wavelet coherence was computed using the "biwavelet" package (version 0.20.21) on R software (Gouhier et al., 2021; R Core Team, 2023). **(e)** same as **(d)**, but between time series **(a, c)** from 1820 to 1997 CE.

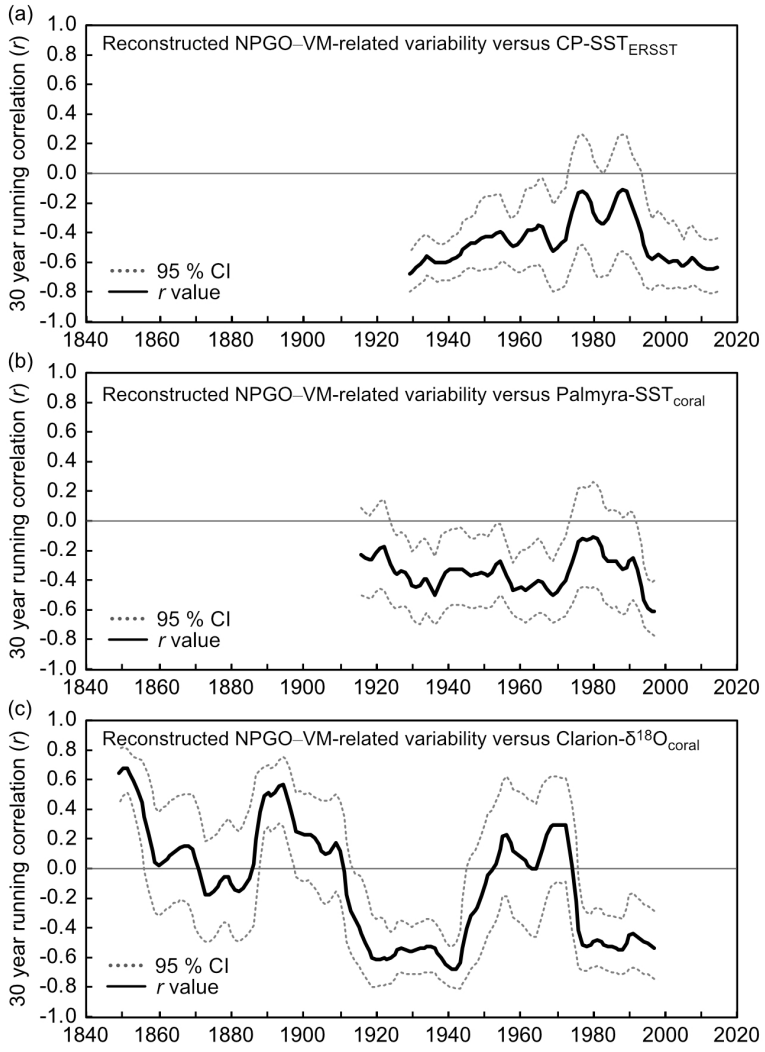


Figure 7. 30 year running correlations between the reconstructed NPGO–VM-related variability and records from the CP/NEP region. 30 year running correlation between the coral-based reconstruction of NPGO–VM-related variability and **(a)** CP-SST$_{ERSST5}$ (Huang et al., 2017), **(b)** Palmyra-SST$_{coral}$ (Nurhati et al., 2011), and **(c)** Clarion-$\delta^{18}O_{coral}$ (Sanchez et al., 2016). The solid line represents the 30 year running correlation coefficient (r), and the dashed lines indicate the 95 % confidence interval (CI). An 8 year low-pass filter was applied to all time series prior to calculating the correlation.

Indeed, the Summer Kikai-SST$_{coral}$ time series implies the effects of the "ocean–atmosphere bridge" connecting the NWP and CP. This is evidenced by its significant correlations with both CP-SST$_{ERSST5}$ (Fig. 3b and d; Table 2a and b) and Palmyra-SST$_{coral}$ (Fig. A13a and c; Table 2c). This consistency indicates a robust climatic linkage between our NWP coral-based temperature record and the temperature variability in the CP. Between 1950 and 2014 CE, CP-SST$_{ERSST5}$ significantly correlated with Kikai-SST$_{ERSST5}$ at the 95 % CL ($r = -0.43$, $N_{eff} = 6.34$, 8–30 year bandpass filtered; Fig. A17), supporting a temperature linkage between the NWP and CP regions. In contrast, no significant correlation was observed over the longer period from 1900 to 2014 CE ($r = -0.29$, $N_{eff} = 17.72$, n. s., 8–30 year bandpass filtered; Fig. A17), which is consistent with the absence of significant correlations between Summer or Winter Kikai-SST$_{coral}$ and Kikai-SST$_{ERSST5}$ over the same interval (Sect. 3.3; Fig. 3a, c, and e; Table 2b). The SST field correlation for 1900–1949 CE did not reveal a coherent spatial pattern indicative of an alternative dominant climate mode during this interval (Fig. A15). These analyses cannot determine the cause of the weaker pre-1950 correlations. However, they provide no clear evidence that a distinct coherent climate mode dominated during this period. One possible contributing factor is the reduced quality of instrumental SST datasets prior to 1950 CE (Thompson et al., 2008; Pfeiffer et al., 2017), particularly for the grid covering Kikai Island (i.e., Kikai-SST$_{ERSST5}$), which can introduce statistical biases in estimates of long-term tempera-

ture variability (Sippel et al., 2024). Such limitations complicate assessments of NPGO–VM-related temperature variability and its regional influence prior to 1950 CE. A precise, high-temporal-resolution temperature proxy record, such as a coral Sr/Ca-based temperature reconstruction, can address this limitation because it is independent of lower-quality instrumental SST records (Pfeiffer et al., 2017). In particular, coral-based temperature records derived from Kikai Island in the NWP have the capacity to reconstruct NPGO–VM-related temperature variability (Sect. 3.4). Moreover, cross-wavelet coherence analysis (Fig. A18) revealed that our coral records, especially Summer Kikai-SST_{coral}, and the NPO variability were coherent at interannual-to-decadal timescales throughout the period 1950–2014 CE. The significant spectral power near 3.6–3.7 years identified in both the NPGO and VMDI (Fig. A10), together with corresponding power in Summer Kikai-SST_{coral} (Fig. A12), suggests that part of their shared interannual variability may reflect ENSO-mediated coupling between tropical and extratropical climate variability. This shared interannual variance should therefore not be interpreted as evidence that the NPGO and VM constitute a single intrinsic climate mode. Because our reconstruction primarily focuses on NPGO–VM-related temperature variability at decadal and longer timescales, a detailed investigation of this interannual linkage is beyond the scope of this study. Taken together, the significant relationships between Kikai-SST_{coral} and CP-SST_{ERSST5} variability or NPO variability support the existence of the "ocean–atmosphere bridge," and agree with NPGO-mode-centred Pacific decadal dynamics and teleconnections, as proposed by Di Lorenzo et al. (2013) (see their Fig. 1).

5.1.2 Potential factors underlying differences in responses to the NPGO–VM-related temperature variability recorded in coral geochemical records from Kikai Island

Consistent with our results (Sect. 3.4), the previously published long-term coral Sr/Ca record from Kikai Island (Kawakubo et al., 2017) also appears to capture NPGO–VM-related temperature variability linked with the CP via the "ocean–atmosphere bridge". Our coral records showed significant correlations with both the NPGO Index and the VMDI, whereas only the summer values reported by Kawakubo et al. (2017) exhibited a significant relationship with the annual mean VMDI from 1950 to 2009 CE at the 95 % CL ($r = 0.52$, $N_{eff} = 7.60$, 8–30 year bandpass filtered); no significant relationship was identified with the NPGO Index. Thus, although the records were derived from the same region, their responses to NPGO–VM-related temperature variability differ. This difference is further supported by the relatively weak correlation between our Kikai-coral Sr/Ca record and that of Kawakubo et al. (2017) (Sect. 3.2.3). Several factors may contribute to these differences, including local environmental conditions associated with the coral core collection sites. The coral core collection sites in the previous studies by Kawakubo et al. (2017) and Morimoto et al. (2007) are located offshore of Arakizaki Point, southwest of Kikai Island (Fig. A3a). On the other hand, our coral cores were collected from Shiomichi Bay, northeast of Kikai Island (Fig. A3a). Kikai Island is a small island with a perimeter of 48.6 km; however, its coastline and surrounding coral reef environments exhibit substantial spatial heterogeneity. The area offshore of Arakizaki Point is an open ocean setting and is geomorphologically characterised by a reef slope with widely developed coral or algal cover (Fig. A3c and e), whereas Shiomichi Bay is a semi-closed bay, and is characterised by an outer-reef flat with less-developed coral or algal cover (Fig. A3b and d). Such environmental differences at coral core collection sites can influence coral geochemical signals and may explain the non-significant relationship observed in the long-term comparison analysis between our Kikai-coral Sr/Ca record and that of Kawakubo et al. (2017) (Sect. 3.2.3).

In addition to local environmental factors, differences in analytical methods and analytical precision may also affect the resulting datasets. These methodological differences are particularly significant when reconstructing paleoclimate/temperature variability, such as NPGO–VM-related temperature variability. Our coral record provides higher analytical precision compared to the previously published records. This advantage was achieved through the use of solution ICP-OES analysis (Watanabe et al., 2020). On the other hand, the previously published long-term Sr/Ca record from Kikai Island (Kawakubo et al., 2017) was obtained using laser ablation Inductively Coupled Plasma Mass Spectrometry (ICP-MS) (Kawakubo et al., 2014). The reported analytical uncertainty was 0.3 %RSD (Kawakubo et al., 2017). This uncertainty was equivalent to 0.4 °C when accounting for both the analytical uncertainty and the uncertainty of the Sr/Ca-temperature calibration slopes, as calculated following Watanabe and Pfeiffer (2022). This analytical precision (0.3 %RSD) is lower than that of our method (0.1 %RSD). Such differences in analytical precision can lead to discrepancies in the expression of coral Sr/Ca signals associated with NPGO–VM-related temperature variability across different timescales. Another coral Sr/Ca record from Kikai Island (Morimoto et al., 2007) was obtained using thermal ionisation mass spectrometry (TIMS) with the isotope dilution method (Alibert and McCulloch, 1997), which offers precision comparable to that of our analytical method. The reported analytical uncertainty was 0.1 %RSD (1σ, Morimoto et al., 2007). It was equivalent to 0.14 °C when accounting for both the analytical uncertainty and the uncertainty of the Sr/Ca-temperature calibration slopes, as calculated following Watanabe and Pfeiffer (2022). However, because the record is less than 6 years long, it is insufficient to evaluate coral Sr/Ca responses to NPGO–VM-related temperature variability or to meaningfully compare with our long-term record.

5.1.3 Growth effects on seasonal differences in the coral Sr/Ca record

Through the intercomparison analyses (Sect. 3.2, 3.3, and 3.4), we found that the winter component of the coral geochemical proxy data from Kikai Island does not accurately reflect long-term temperature variability, unlike the summer component. Seasonal variability in coral growth rates likely contributes to this discrepancy. Generally, warmer SSTs during the summer season promote faster coral growth, while cooler SSTs during the winter season lead to slower growth. Such seasonal growth-rate differences result in more data points being recorded during summer and fewer during winter (Barnes et al., 1995). This bias would be more distinct in coral geochemical proxy data from the subtropics than from the tropics due to a larger seasonal temperature amplitude. As illustrated in the histogram of Kikai-coral Sr/Ca values (Fig. A19), there were more data points in summer and mid-season, consistent with previous observations for subtropical corals (Kawakubo et al., 2014, Kikai Island) and temperate corals (Fallon et al., 1999, Shikoku region, Japan). Both our results and Kawakubo et al. (2014) suggest that biweekly-to-monthly resolved geochemical records from *Porites* corals at Kikai Island may be biased toward summer values. To better capture the winter signal in coral geochemical proxies from Kikai Island, a combined approach may be required, incorporating high-spatial-resolution techniques such as laser ablation (e.g., Kawakubo et al., 2014) alongside the high-precision analytical methods employed in this study.

Our results suggest that Summer Kikai-SST_{coral} has a strong, consistent relationship with instrumental SST datasets, the NPGO Index, and the VMDI (Sect. 3.3 and 3.4). From a theoretical perspective, because the NPGO and VM are considered to be dominant during boreal winter and spring/early summer, not only Summer Kikai-SST_{coral} but also Winter Kikai-SST_{coral} would be expected to capture signals of NPGO–VM-related temperature variability. However, Winter Kikai-SST_{coral} exhibited a weaker relationship with the VMDI than Summer Kikai-SST_{coral}. Similarly, weak or non-significant relationships were identified in comparisons with instrumental SST datasets. These discrepancies observed between the summer and winter components would be explained by a seasonal growth bias in the Kikai-coral Sr/Ca dataset. The Kikai-coral Sr/Ca_{summer} dataset is minimally affected by seasonal growth bias and more accurately reflects long-term SST variability compared to the Kikai-coral Sr/Ca_{winter} dataset. The Kikai-coral $Sr/Ca_{annual\ mean}$ dataset is also subject to bias because the annual mean incorporates both summer and winter values. Consequently, we conclude that Kikai-coral Sr/Ca_{summer} is the most appropriate dataset for reconstructing NPGO–VM-related temperature variability in this study.

5.2 Reconstructed NPGO–VM-related variability

5.2.1 Reconstructed NPGO–VM-related variability in the 19th and 20th centuries

As shown in Sect. 3.5, the coral-based reconstruction exhibited a relatively modest negative phase (reconstructed NPGO–VM-related variability < -1.0) from the late 1820s to the early 1830s, corresponding to cool conditions in the NWP (Fig. 6a). It is well-known that several major volcanic eruptions occurred between the 1800s and 1830s (the late phase of the Little Ice Age), and that these eruptions caused multi-year cooling following each event (Brönnimann et al., 2019). Both the Kikai-coral Sr/Ca record and the reconstructed NPGO–VM-related variability exhibited a cooling phase during the late 1820s to the early 1830s, coincident with this period of frequent volcanic eruptions. Although volcanic forcing cannot be entirely excluded as a contributing factor, its overall influence appears limited, given the relatively modest amplitude of the cooling signal. In contrast, the pronounced negative phase during the 1860s–1900s occurred well after the late phase of the Little Ice Age and after the period of major volcanic eruptions, suggesting that it was unlikely to have been driven primarily by volcanic forcing. Notably, this strong negative phase aligns well with previously reported low-temperature conditions recorded in coral archives from Kikai Island (Kawakubo et al., 2017) and southern Taiwan (Ramos et al., 2020). Kawakubo et al. (2017) further reported a closely concurrent reduction in atmospheric variability, inferred from the Gibraltar/Reykjavik North Atlantic Oscillation Index (Vinther et al., 2003), from 1870 to 1900 CE, which may be linked to this cool period. However, further investigations are required to elucidate the connection between reduced atmospheric variability and NPGO or VM dynamics during that time.

The pronounced negative phase (reconstructed NPGO–VM-related variability < -1.0) during the 1860s–1900s may also be related to the late onset of the warming trend in the NWP. The trend change point at 1873 CE (95 % CI: 1844–1877 CE; Fig. 6a) indicates that the onset of the warming trend in the NWP might have occurred later than previous estimates for other ocean basins and the Northern Hemisphere (estimated using "Western Pacific Ocean" archive; Abram et al., 2016). This previously used "Western Pacific Ocean" archive primarily comprises data from the southern and central western Pacific; therefore, it may be insufficient to capture temperature trends specifically in the NWP. Our Kikai-coral Sr/Ca record would complement this spatial data gap. Since a similar cool phase was also reported in other NWP coral records (Kawakubo et al., 2017; Ramos et al., 2020), the delayed onset of warming may be a regional feature specific to the NWP. However, long-term temperature reconstructions in this region remain limited, and further studies are necessary to more accurately determine the onset of warming.

Following the negative phase during the 1860s–1900s, the reconstructed NPGO–VM-related variability shows alternating negative and positive phases through the early 20th century (Fig. 6a). In the late 20th century, positive phases occurred intermittently; however, the overall amplitude of variability was relatively small (within ± 1.0 in the reconstructed NPGO–VM-related variability). This suggests a comparatively stable regime of NPGO–VM-related variability, similar to that observed prior to the 1820s. In contrast, a prominent negative phase (reconstructed NPGO–VM-related variability < -1.0, corresponding to cool conditions in the NWP) was again observed in the 1990s, with an amplitude comparable to the prolonged negative phase that occurred between the 1860s and the 1900s.

5.2.2 Reconstructed NPGO–VM-related variability in the 21st century

As described in Sect. 3.5, the coral-based reconstruction shifted towards a distinct positive phase (reconstructed NPGO–VM-related variability > 1.0, corresponding to warm conditions in the NWP) in the early 2000s (Fig. 6a). The 30 year running correlation between the reconstructed NPGO–VM-related variability and CP-SST_{ERSST5} also showed a significant relationship became significant in the 1990s and strengthened and remained significant from the 2000s onward (Fig. 7a). This shift and significant relationship are consistent with the increased occurrence of climate variability in the CP in recent decades (Yeh et al., 2011). Several previous studies have proposed that the higher frequency of climate variability in the CP due to anthropogenic warming may enhance NPGO variability and strengthen the linkage between them (e.g., Dong et al., 2022). In addition, the occurrence ratio of CP-centred ENSO compared to EP-centred ENSO (i.e., the CP / EP event ratio) has increased in response to current global warming and is projected to continue increasing under future warming scenarios (Freund et al., 2019; Shen and Yu, 2023; Yeh et al., 2009). Previous studies have also suggested that the NPO/NPGO mode has become more dominant in the North Pacific rather than the Aleutian Low/PDO mode in recent decades, reflecting the increasing prevalence of CP-centred ENSO events in the tropical Pacific (Di Lorenzo et al., 2010; Yeh et al., 2011). Furthermore, climate model projections suggest that VM variability is expected to become more pronounced in association with amplified temperature variability in the CP under an anthropogenic warming scenario with rapid greenhouse gas emissions (RCP8.5 scenario) (Ji et al., 2024). Taken together, this external evidence suggests that the positive phase of the reconstructed NPGO–VM-related variability observed in the early 21st century may be consistent with anthropogenically forced changes in Pacific climate variability. However, our coral record documents the timing and expression of this shift in the NWP but does not by itself establish its cause.

5.3 Contribution of NPGO–VM-related variability to climate variability in the North Pacific or NWP

The 30 year running correlation between CP-SST_{ERSST5} and the reconstructed NPGO–VM-related variability was significantly negative from the early 20th century to 2014, except during the 1970s–1980s (Sect. 3.5; Fig. 7a). A previous study has indicated a regime shift related to the NPGO in 1988/1989 CE (Yeh et al., 2011). However, the non-significant correlation between the reconstructed NPGO–VM-related variability and CP-SST_{ERSST5} during the 1970s–1980s cannot be explained simply by this regime shift or anomalous variation in the NPGO. The NPGO Index and the VMDI show a strong inverse relationship at decadal timescales over their common period at the 99 % CL ($r = -0.84$, $N_{eff} = 6.10$, 8–30 year bandpass filtered; Fig. A2b and e), although their correspondence weakens temporarily during the late 1960s through the 1970s. During the late 1960s through the 1970s, Summer Kikai-SST_{coral} showed closer agreement with the VMDI than with the NPGO Index (Fig. 5a), indicating that the relative expression of temperature variability associated with the NPGO and VM may vary through time. These results indicate that the relationship between the NPGO and VM is not stationary. Accordingly, the coral-based reconstruction is interpreted as representing NPGO–VM-related temperature variability, an inclusive term for temperature variability associated with the NPGO, the VM, or their covariability, rather than as a direct reconstruction of either mode or of a temporally invariant unified index.

Consistent with previous findings that the NPO/NPGO mode has became more dominant in the North Pacific in recent decades (Di Lorenzo et al., 2010; Yeh et al., 2011) and that VM variability is projected to become more pronounced under future warming (Ji et al., 2024), the strengthened and sustained negative relationship between the reconstructed NPGO–VM-related variability and CP-SST_{ERSST5} from the 2000s onwards (Fig. 7a) suggests a strong recent linkage between NPGO–VM-related variability and climate variability in the NWP and CP. This interpretation is also supported by the 30 year running correlations between coral-based NPGO–VM-related variability and other Pacific coral records that capture the NPGO-related signals (Palmyra-SST_{coral} and Clarion-$\delta^{18}O_{coral}$; Fig. 7b and c). These findings underscore the importance of the NPGO and VM in climate–ocean interactions (Ji et al., 2024) and marine ecosystem dynamics (Kilduff et al., 2015) across the North Pacific and beyond. Additionally, for all three 30 year running correlations, the magnitude of correlations during parts of the 1920s to the 1950s was comparable to that observed during the recent significant correlation intervals (Fig. 7). These relatively strong relationships during the early to mid-20th century partly coincided with a high occurrence ratio of CP-centred versus EP-centred ENSO events, as shown in instrumental records (Freund et al., 2019). As in recent decades, NPGO–VM-

related variability and climate variability in the CP were also likely dominant in the North Pacific and the tropical Pacific, respectively, during parts of the 1920s to the 1950s.

5.4 Strengths and limitations of proxy archives for reconstructing NPGO–VM-related variability

Several proxy-based NPGO reconstructions have been developed in previous studies, including tree-ring-based records (Dong et al., 2022; Sakashita et al., 2017) and coral-based records (Nurhati et al., 2011; Rafter et al., 2017; Sanchez et al., 2016). These reconstructions have provided valuable insights into past NPGO variability from different regions and through archives with different environmental sensitivities. Previous coral-based reconstructions were derived primarily from archives located in the central tropical Pacific and eastern Pacific. In contrast, our study provides the first long-term reconstruction of NPGO–VM-related variability based on a coral archive from the NWP. The following comparison evaluates the respective strengths, limitations, and complementary contributions of these proxy records to the reconstruction of Pacific climate variability.

5.4.1 Tree-ring-based reconstructions

Tree-ring-based reconstructions have the advantage of extending climate records beyond the instrumental period. Dong et al. (2022) reconstructed NPGO variability using tree-ring chronologies that extend back to 1596 CE. They identified negative-NPGO phases from the 1790s to the 1810s, which is consistent with the Dalton minimum (1790–1830 CE; Wagner and Zorita, 2005). However, the reconstructed NPGO–VM-related variability did not show a distinct, consecutive negative phase corresponding to the negative-NPGO interval reported by Dong et al. (2022) (Fig. 6a). Such differences likely reflect differences in the climatic and environmental sensitivities of the proxy archives rather than inconsistency in either reconstruction. Tree-ring chronologies integrate physiological responses of trees to multiple environmental factors, including temperature, moisture availability, and other climatic controls (Evans et al., 2006; Mann et al., 2012), which may introduce uncertainty when reconstructing past temperature variability (Björklund et al., 2023). Thus, tree-ring chronologies provide exceptionally long climate reconstructions, while complementary temperature-sensitive marine archives (e.g., corals or foraminifera) may help constrain proxy-specific uncertainties. A multi-archive approach may therefore provide a more robust reconstruction than reliance on any single proxy archive.

5.4.2 Coral δ^{18}O-based reconstructions

Sanchez et al. (2016) reported decadal NPGO variability based on coral δ^{18}O records (Clarion-$\delta^{18}O_{coral}$) derived from Clarion Island in the NEP. Comparison between Clarion-$\delta^{18}O_{coral}$ and our Kikai coral records provides an opportunity to examine how different coral geochemical proxies represent Pacific climate variability. We evaluated this relationship using the two filtering frameworks applied in this study: an 8 year low-pass filter, which retains variability at decadal and longer timescales, and an 8–30 year bandpass filter, which isolates variability within the decadal frequency band. The reconstructed NPGO–VM-related variability and Clarion-$\delta^{18}O_{coral}$ were not significantly correlated when both records were analysed using the 8 year low-pass filter (Fig. 6a and c). Similarly, Summer Kikai-SST_{coral} and Clarion-$\delta^{18}O_{coral}$ were not significantly correlated using the 8–30 year bandpass filter (Fig. A13b and d; Table 2c). Thus, the absence of significant correlations was consistent across the two filtering approaches and cannot be attributed solely to filter selection. Cross-wavelet coherence analysis nevertheless indicated that the reconstructed NPGO–VM-related variability and Clarion-$\delta^{18}O_{coral}$ were coherent at inter-decadal to decadal frequencies during limited parts of their common interval (Fig. 6e). In addition, their 30 year running correlation showed a significant relationship only during specific intervals, including the 1910s–1940s and the 1970s–1990s (Fig. 7c). These temporally intermittent relationships indicate that the records capture some common variability while also preserving different environmental information.

The differences between the records may reflect both their distinct regional climatic settings and the different environmental sensitivities of coral Sr/Ca and δ^{18}O. The SST field correlation pattern also suggests that Summer Kikai-SST_{coral} shows weaker correspondence with the Clarion Island region (18.350° N, 114.717° W) in the NEP than with parts of the CP (Fig. 4a and c). In addition, coral Sr/Ca is primarily sensitive to temperature variability (e.g., Corrège, 2006; Shen et al., 1996), whereas coral δ^{18}O is influenced by both temperature (negatively correlated, e.g., Abram et al., 2016; Watanabe et al., 2011) and δ^{18}O in seawater (positively correlated, e.g., Garas et al., 2023; Shen et al., 2005; Thompson et al., 2022). It is well established that the NPGO is also associated with changes in ocean salinity (Chhak et al., 2009; Di Lorenzo et al., 2009). Clarion Island is located at the termination of the California Current System, which is characterised by cooler (warmer) and higher (lower) salinity water during positive- (negative-) NPGO phases (Di Lorenzo et al., 2008; Sanchez et al., 2016). Although Clarion-$\delta^{18}O_{coral}$ has also been shown to capture NPGO-related variability (Sanchez et al., 2016), the combined effects of regional climatic differences and the thermal and hydrological sensitivity of Clarion-$\delta^{18}O_{coral}$ may contribute to the different long-term behaviour of the two records. This combined thermal and hydrological sensitivity does not diminish the value of the δ^{18}O archive; rather, it enables the reconstruction of coupled thermal and hydrographic variability. Because the reconstructed NPGO–VM-related variability in this study is interpreted primarily in terms of temperature variability, both

regional setting and proxy sensitivity should be considered when comparing Sr/Ca- and δ^{18}O-based reconstructions.

5.4.3 Coral Sr/Ca-based reconstructions

Coral Sr/Ca provides a temperature-sensitive archive that is well suited to reconstructing SST variability associated with ocean-circulation and temperature-anomaly modes such as the NPGO and VM. Nevertheless, Sr/Ca-based reconstructions may be affected by biological disturbances or seasonal growth biases, particularly under thermal stress, which can cause growth disturbances or anomalous seasonality (DeCarlo and Cohen, 2017; D'Olivo and McCulloch, 2017). In our study, no evidence of growth cessation or anomalous seasonality was identified (Figs. 2 and A4), suggesting that these effects were unlikely to have substantially influenced the reconstructed temperature variability. Seasonal differences in coral growth may nevertheless affect seasonal-scale analyses, as discussed in Sect. 4.1.3.

Nurhati et al. (2011) documented a coral Sr/Ca-based temperature record (Palmyra-SST_{coral}) from Palmyra Island in the CP that exhibits a strong relationship with the NPGO at the decadal timescale, reflecting dynamical linkages between temperature variability in the CP and extratropical decadal climate variability. As in the Clarion comparison (Sect. 4.4.2), we evaluated the relationship between the Kikai and Palmyra records using both the 8 year low-pass and 8–30 year bandpass filtering approaches. Summer Kikai-SST_{coral} and Palmyra-SST_{coral} were significantly correlated at decadal timescales when both were analysed using the 8–30 year bandpass filter (Fig. A13a and c; Table 2c). Although the two coral records originate from geographically distant regions, their significant relationship within the 8–30 year band indicates shared decadal-scale temperature variability between the NWP and CP. In contrast, the reconstructed NPGO–VM-related variability and Palmyra-SST_{coral} were not significantly correlated when both records were analysed using the 8 year low-pass filter (Fig. 6a and b). The contrasting results under the two filtering approaches indicate that the relationship depends on the frequency range examined. The 8–30 year bandpass-filtered analysis isolates variability within the targeted decadal band, whereas the 8 year low-pass-filtered records retain both decadal and lower-frequency variability. Thus, the common variability between the records appears stronger within the 8–30 year band than across the broader range of variability retained by the low-pass filter. The non-significant low-pass correlation therefore does not invalidate the significant decadal-scale relationship, but neither should it be attributed to a limitation of the Palmyra record alone. Consistent with this interpretation, cross-wavelet coherence was significant only during limited periods and frequency bands (Fig. 6d), and the 30 year running correlation varied through time, with significant correlations from the mid-1920s to the early 1970s and again in the 1990s (Fig. 7b). Thus, the relationship between NWP and CP temperature variability was neither uniform across frequencies nor stationary through time. Taken together, the significant decadal-scale correlation, temporally intermittent coherence, and time-varying running correlations support an NWP–CP teleconnection consistent with the "ocean–atmosphere bridge" discussed in Sect. 4.1.1 and with NPGO-centred Pacific decadal dynamics and associated ocean–atmosphere coupling (Di Lorenzo et al., 2013).

More broadly, the comparisons presented in this section demonstrate that tree-ring, coral δ^{18}O, and coral Sr/Ca archives preserve distinct but complementary aspects of past Pacific climate variability. Combining archives with different temporal coverage and environmental sensitivities may therefore provide more robust constraints on past NPGO–VM-related variability than reliance on any single proxy archive.

6 Conclusions

We presented a new long-term reconstruction of NPGO–VM-related variability based on reef-building coral skeletons collected at Kikai Island in the NWP, extending back to the 19th century. Our Summer Kikai-SST_{coral} showed significant correlations with temperature variability in the CP, the NPGO Index, and the VMDI. These findings suggest an extra-tropical linkage between NPGO–VM-related temperature variability in the NWP and temperature variability in the CP via the ocean–atmosphere bridge. Over the past two centuries, the reconstructed NPGO–VM-related variability showed substantial changes, although its relationship with temperature variability in the CP weakened during the 1970s–1980s. Furthermore, the relationship between the reconstructed NPGO–VM-related variability and temperature anomalies in the CP became significant in the 1990s and remained significant from the 2000s onward. Additionally, a pronounced negative phase (cool conditions in the NWP) was identified during the 1860s–1900s. This phase may have contributed to the delayed onset of the warming trend in the NWP.

The NPGO and VM can influence large-scale climate variability through their linkage with temperature anomalies in the CP (Di Lorenzo, 2013). Their climatic influence extends beyond temperature variability in the North Pacific and NWP, affecting hydrological conditions in regions such as East Asia (e.g., Ye et al., 2016). Given this strong linkage between the CP and NPGO–VM-related variability, as well as the projected increase in the frequency of CP-centred ENSO events, the climatic influence of the NPGO and VM in the North Pacific, NWP, and East Asia is expected to intensify under future warming scenarios. Despite the recognised importance, long-term reconstructions of NPGO–VM-related variability remain limited. Our coral record represents the first reconstruction based on a coral archive from the NWP. To improve our understanding of these ocean–atmosphere

interactions, more temperature-sensitive reconstructions are needed across broader spatiotemporal scales that can cover a wide region in the Pacific and over centennial timescales. As yet, century-long temperature records at high temporal resolution (monthly to seasonal) that complement or extend beyond the pre-instrumental period remain scarce in the NWP. As demonstrated in this study, coral skeletons provide high-resolution, temperature-sensitive archives for examining the thermal expression of the NPGO and VM. However, because the NWP lies near the northern limit of reef-building coral distribution and coral geochemical records may be affected by seasonal growth-related biases, particularly in winter, future efforts would benefit from multi-proxy approaches. Coral records combined with other high-resolution marine archives, such as bivalves (e.g., Tanabe et al., 2017), coralline algae (e.g., Hetzinger et al., 2009), and sclerosponges (e.g., Asami et al., 2021), will help overcome spatial limitations, reduce proxy-specific biases and enhance reconstruction robustness.

Appendix A

Table A1. List of abbreviations and terms used for datasets. All datasets are shown in figures and tables in the main text or Appendices.

Abbreviation term	Reference	Notes
(a) Sea surface temperature (SST) datasets		
Kikai-SST_{ERSST5}	Huang et al. (2017)	Instrumental SST record for the grid cell that includes the coral sampling site, Kikai Island (ERSST5, 27–29° N, 129–131° E). See also Sect. 2.4.
CP-SST_{ERSST5}	Huang et al. (2017)	Instrumental SST record for the CP (ERSST5, 5° S–5° N, 160° E–150° W). See also Sect. 2.4.
Summer Kikai-SST_{coral}	This study	Coral Sr/Ca-based SST record from Kikai Island (1799–2014 CE). Calculated by converting Kikai-coral Sr/Ca_{summer} into temperature. See also Sect. 2.5.
Winter Kikai-SST_{coral}	This study	Coral Sr/Ca-based SST record from Kikai Island (1799–2014 CE). Calculated by converting Kikai-coral Sr/Ca_{winter} into temperature. See also Sect. 2.5.
(b) Coral Sr/Ca datasets		
Kikai-coral Sr/Ca	This study	Coral skeletal Sr/Ca record (1798–2015 CE) from Kikai Island in the NWP.
Kikai-coral Sr/Ca_{summer}	This study	Extracted dataset of boreal summer values (3 month averaged) from Kikai-coral Sr/Ca.
Kikai-coral Sr/Ca_{winter}	This study	Extracted dataset of boreal winter values (3 month averaged) from Kikai-coral Sr/Ca.
Kikai-coral $Sr/Ca_{annual\ mean}$	This study	Annual mean dataset of Kikai-coral Sr/Ca, calculated by averaging values from one winter peak to the subsequent winter peak.
(c) Others		
Palmyra-SST_{coral}	Nurhati et al. (2011)	Coral Sr/Ca-based temperature reconstruction from Palmyra Island in the CP.
Clarion-$\delta^{18}O_{coral}$	Sanchez et al. (2016)	Coral δ^{18}O-based NPGO variability reconstruction from Clarion Island in the NEP.
Reconstructed NPGO–VM-related variability	This study	Reconstructed from the standardised Kikai-coral Sr/Ca_{summer} dataset after application of an 8 year low-pass filter (1799–2014 CE). See also Eq. (1) and Sect. 2.7 in the main text.

Table A2. Determined coral uranium and thorium isotopic compositions and ^{230}Th ages. The dating was carried out using MC-ICP-MS (Thermo Electron Neptune) installed at the High-Precision Mass Spectrometry and Environment Change Laboratory (HISPEC), National Taiwan University (see also Sect. 2.3). Over the past few decades, HISPEC has carefully addressed potential biases and uncertainties of the initial ^{230}Th, and has also resolved instrumental ghost signals (Cheng et al., 2013; Shen et al., 2002, 2008, 2012). The verification of the fidelity of dating young coral by MC-ICP-MS techniques was rigorously conducted and reported by Shen et al. (2008, 2012).

Sample ID	Weight g	^{238}U 10^{-9} g g^{-1} [a]	^{232}Th 10^{-12} g g^{-1}	δ^{234}U measured[a]	[^{230}Th / ^{238}U] activity[c]	[^{230}Th / ^{232}Th] atomic ($\times 10^{-6}$)	Age (CE) corrected[c,d]	$\delta^{234}U_{initial}$ corrected[b]
KISM-1	0.2064	3044.1 ± 4.2	273.9 ± 2.3	146.1 ± 1.6	0.001408 ± 0.000011	258.0 ± 3.0	1884.3 ± 1.5	146.2 ± 1.6
KISM-2	0.1740	2600.4 ± 2.7	397.5 ± 2.7	147.3 ± 1.6	0.001451 ± 0.000018	156.5 ± 2.2	1883.1 ± 2.5	147.3 ± 1.6
KISM-3	0.4134	2744.6 ± 2.5	320.0 ± 1.2	145.1 ± 1.5	0.002337 ± 0.000023	330.4 ± 3.5	1797.5 ± 2.6	145.2 ± 1.5

Note. Chemistry was performed in March 2016 and July 2017 (Shen et al., 2003), and instrumental analysis on MC-ICP-MS (Shen et al., 2012). Analytical errors are 2σ of the mean. [a] $[^{238}U] = [^{235}U] \times 137.77$ (± 0.11 ‰) (Hiess et al., 2012); $\delta^{234}U = ([^{234}U / {}^{238}U]_{activity} - 1) \times 1000$. [b] $\delta^{234}U_{initial}$ corrected was calculated based on ^{230}Th age (T), i.e., $\delta^{234}U_{initial} = \delta^{234}U_{measured} \times e^{\lambda 234 T}$, and T is corrected age. [c] $[^{230}Th / {}^{238}U]_{activity} = 1 - e^{-\lambda 230 T} + (\delta^{234}U_{measured}/1000)[\lambda_{230}/(\lambda_{230} - \lambda_{234})](1 - e^{-(\lambda 230 - \lambda 234)T})$, where T is the age. Decay constants are 9.1705×10^{-6} yr^{-1} for ^{230}Th, 2.8221×10^{-6} yr^{-1} for ^{234}U (Cheng et al., 2013), and 1.55125×10^{-10} yr^{-1} for ^{238}U (Jaffey et al., 1971). [d] Age corrections were calculated using an estimated atomic ^{230}Th / ^{232}Th ratio of 4 (± 2) $\times 10^{-6}$ (Shen et al., 2008).

Table A3. The differences in coral Sr/Ca for overlapping periods. Mean values of overlapped Sr/Ca record between **(a)** Core-1 and Core-2, **(b)** Core-2 and Core-3. "Summer (Winter) peaks mean" means the average value of the annual lowest (highest) Sr/Ca in the overlapped periods. "Difference" values were shown as absolute values of the differences calculated between the two cores. The asterisk (*) indicates a significant difference (p-value < 0.05, t-test). The time series is shown in Fig. A7.

	Mean (mmol mol^{-1})	Summer peaks mean (mmol mol^{-1})	Winter peaks mean (mmol mol^{-1})
(a) Overlap between Core-1 and Core-2 (1926–1931 CE)			
Core-1	9.16	8.97	9.43
Core-2	9.21	8.98	9.52
Difference	0.05	< 0.01	0.08*
(b) Overlap between Core-2 and Core-3 (1884–1886 CE)			
Core-2	9.36	9.06	9.67
Core-3	9.27	9.05	9.55
Difference	0.09	0.01	0.12

Table A4. Comparison of modern coral Sr/Ca records from Kikai Island. Both coral Sr/Ca records were from *Porites* corals. Sample collection sites are shown in Fig. A3. The coral core of this study was collected on the northeastern side (Shiomichi Bay) of Kikai Island. The coral core of Morimoto et al. (2007) was collected on the southwestern side (offshore of Arakizaki Point) of Kikai Island. The seasonal range was calculated by the difference between **(a)** and **(b)**.

	(a) Mean value of the annual lowest Sr/Ca (mmol mol^{-1})	**(b)** Mean value of the annual highest Sr/Ca (mmol mol^{-1})	**(c)** Seasonal range: **(b)**−**(a)** (mmol mol^{-1})
This study (Core-1)	8.947	9.518	0.571
Morimoto et al. (2007)	8.852	9.382	0.530

Table A5. Correlations among Kikai-SST$_{coral}$ (this study), the NPGO Index, and the VMDI (8 year low-pass filtered). Correlations between Summer or Winter Kikai-SST$_{coral}$ and **(a)** the annual mean NPGO Index (Di Lorenzo et al., 2008), **(b)** the annual mean Victoria Mode Dipole Index (VMDI; Wen et al., 2024, calculated using ERSST5). Prior to calculating correlations, an 8 year low-pass filter was applied to the time series. See also Table 3 for the results obtained using the 8–30 year bandpass filtered datasets.

Pair of correlation analysis	Period	r	Significance	N_{eff}
(a) Comparison of the seasonal Kikai-SST$_{coral}$ dataset and the annual mean NPGO Index (8 year low-pass filtered)				
Summer Kikai-SST$_{coral}$ versus NPGO Index	1950–2014 CE	0.63	95 % CL	11.99
Winter Kikai-SST$_{coral}$ versus NPGO Index	1950–2014 CE	0.41	90 % CL	10.61
(b) Comparison of the seasonal Kikai-SST$_{coral}$ dataset and the annual mean VMDI (8 year low-pass filtered)				
Summer Kikai-SST$_{coral}$ versus VMDI	1950–2014 CE	–0.57	95 % CL	10.79
Winter Kikai-SST$_{coral}$ versus VMDI	1950–2014 CE	–0.46	90 % CL	10.94
Summer Kikai-SST$_{coral}$ versus VMDI	1900–2014 CE	–0.30	n. s.	21.95
Winter Kikai-SST$_{coral}$ versus VMDI	1900–2014 CE	–0.14	n. s.	17.54

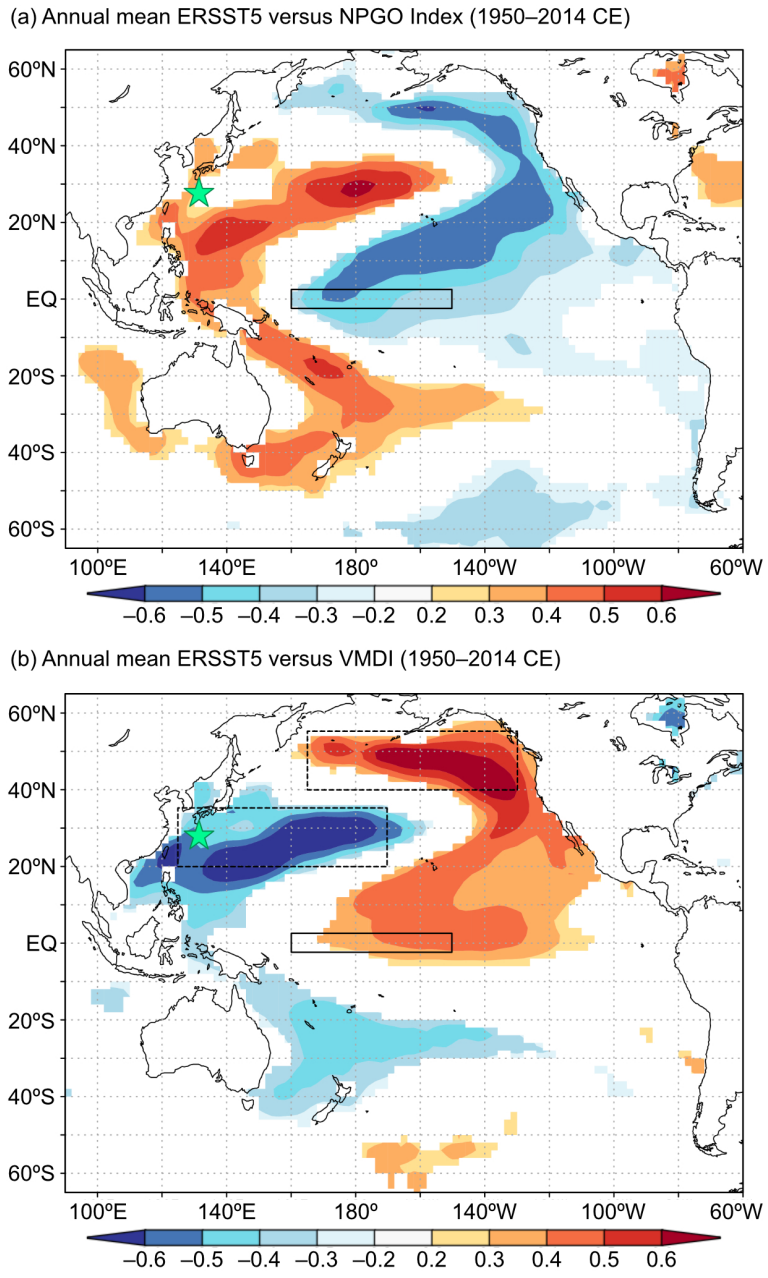


Figure A1. Spatial distribution of the NPGO and VM patterns shown in the SST field (unfiltered). **(a)** Field correlation map between the annual mean SST time series (ERSST5; Huang et al., 2017) and the NPGO Index (Di Lorenzo et al., 2008) from 1950 to 2014 CE. **(b)** Field correlation map between the annual mean SST time series (ERSST5; Huang et al., 2017) and the Victoria Mode Dipole Index (VMDI; Wen et al., 2024, calculated using ERSST5, grey boxes), from 1950 to 2014 CE. The black dashed boxes indicate the regions used to calculate the VMDI. Only correlations with p-values < 0.1 are colour-coded. The original figures in each panel were computed using the web application KNMI Climate Explorer (https://climexp.knmi.nl/, last access: 22 October 2026) and plotted using GrADS (v2.2.1). The location of the coral sampling site (Kikai Island, Kagoshima, Japan) is marked by a star. The black solid box indicates the CP region (5° S–5° N, 160° E–150° W). See also Fig. 1 for the 8–30 year bandpass filtered analyses.

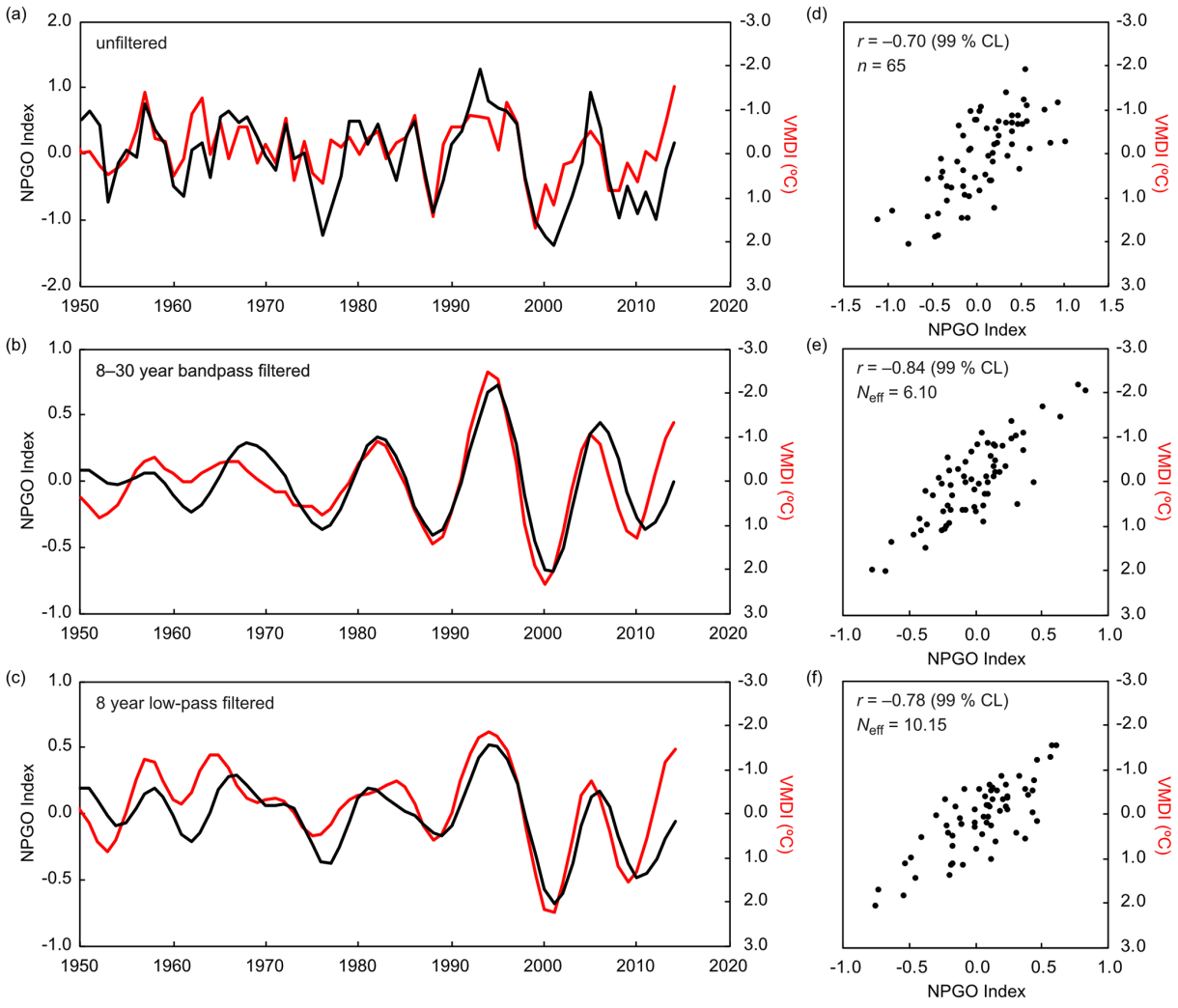


Figure A2. Comparison of the NPGO Index and the VMDI time series. **(a)** The time series of annual mean NPGO Index (Di Lorenzo et al., 2008, in black) and annual mean VMDI (Wen et al., 2024, calculated using the ERSST5 dataset, in red). **(b)** same as **(a)**, but for the 8–30 year bandpass filtered time series. **(c)** same as **(a)**, but for the 8 year lowpass filtered time series. The filtering method is described in Sect. 2.6. **(d–f)** Scatter plots corresponding to **(a)**–**(c)**. See also Sect. 2.6 for statistical analysis.

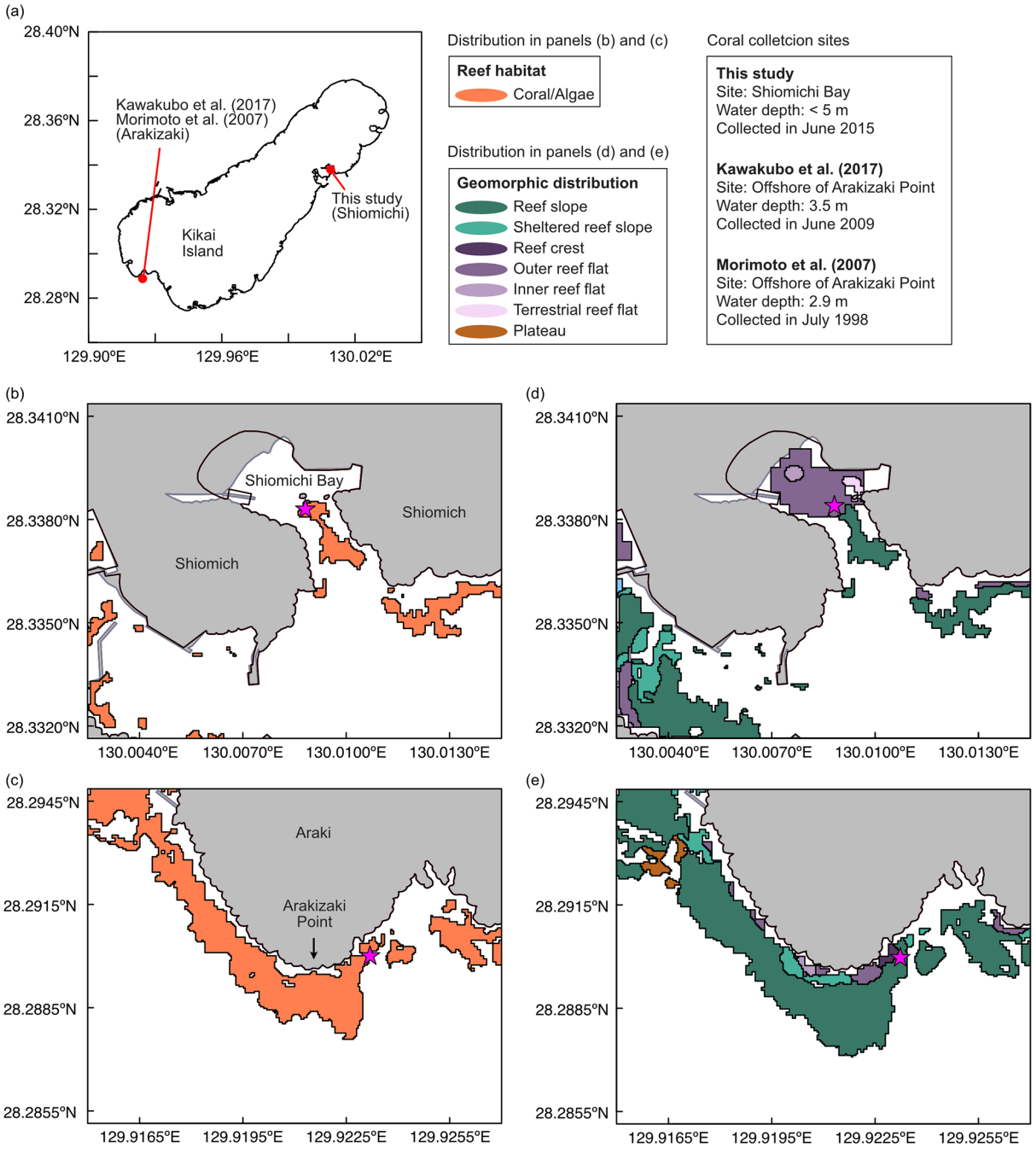


Figure A3. Maps of coral core collection sites for this study and previous studies. **(a)** Map of Kikai Island, Kagoshima, Japan. Red circles mark sites of coral core collection for this study (Shiomichi Bay) and for previous studies (Kawakubo et al., 2017; Morimoto et al., 2007; offshore of Arakizaki Point). The site for the previous studies was referred to as the location introduced in Morimoto et al. (2007) and Kubota et al. (2017). **(b)** Reef habitat distribution (coral/algae) for Shiomichi Bay. The reef habitat dataset was derived from The Allen Coral Atlas (Lyons et al., 2024). Star marks the coral core collection site. The distribution legends are shown above. **(c)** same as **(b)**, but for offshore of Arakizaki Point. **(d)** Geomorphic distribution for Shiomichi Bay. The geomorphic zonation dataset was derived from The Allen Coral Atlas (Lyons et al., 2024). **(e)** same as **(d)**, but for offshore of Arakizaki Point. For all panels, the coastline data were derived from the National Land Information Division, National Spatial Planning and Regional Policy Bureau, Ministry of Land, Infrastructure, Transport and Tourism of Japan (https://nlftp.mlit.go.jp/index.html, last access: 22 October 2026). The grey-coloured coastline and grey-shaded land are based on the latest data (2023 CE). The black line depicts the coastline prior to 2000 CE. In the Shiomichi area, land reclamation along the coast facing Shiomichi Bay was conducted in 2003 CE.

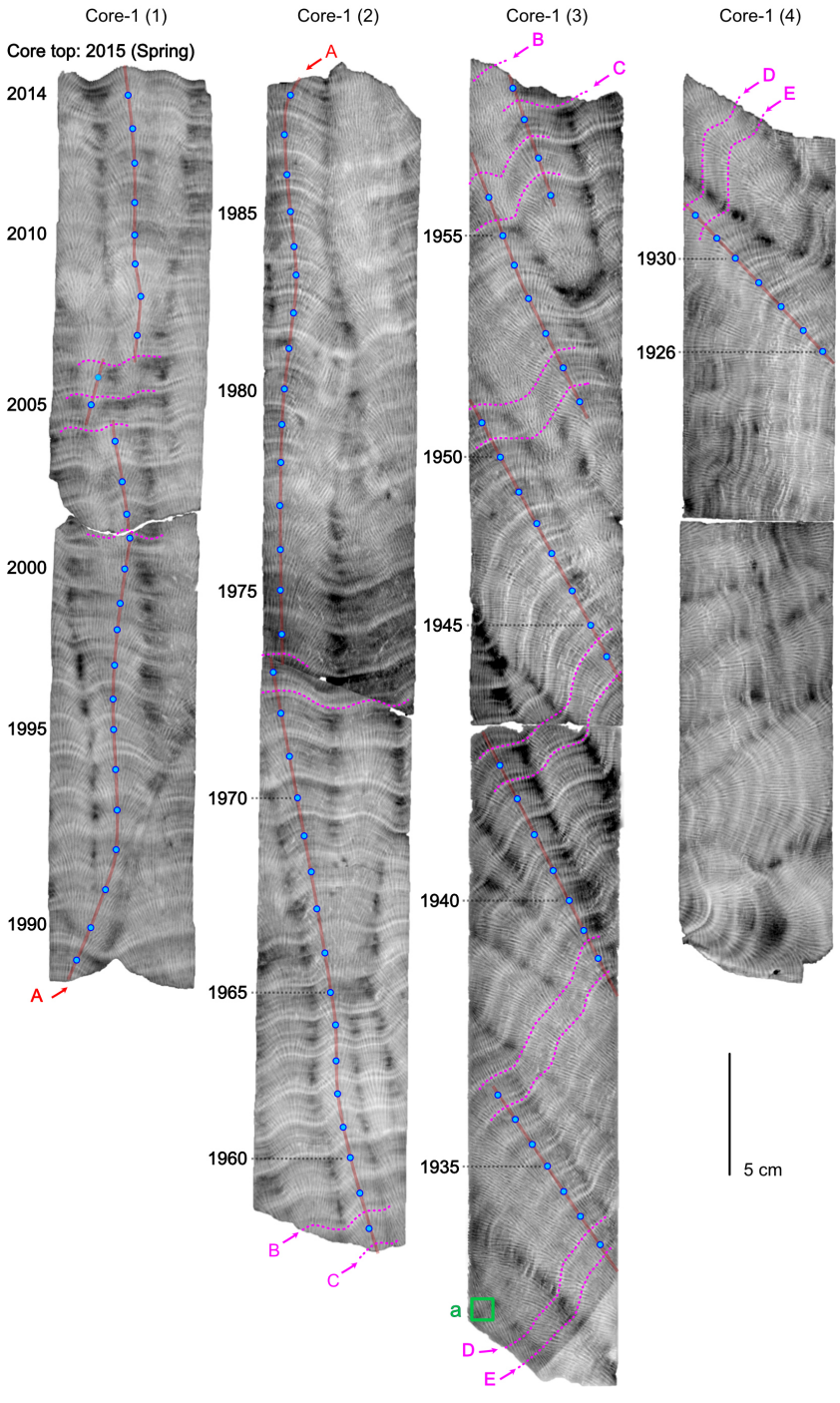

Core-1 (1)
Core-1 (2)
Core-1 (3)
Core-1 (4)
Core top: 2015 (Spring)
2014
2010
2005
2000
1995
1990
1985
1980
1975
1970
1965
1960
1955
1950
1945
1940
1935
1930
1926
A
B
C
D
E
a
5 cm

Figure A4.

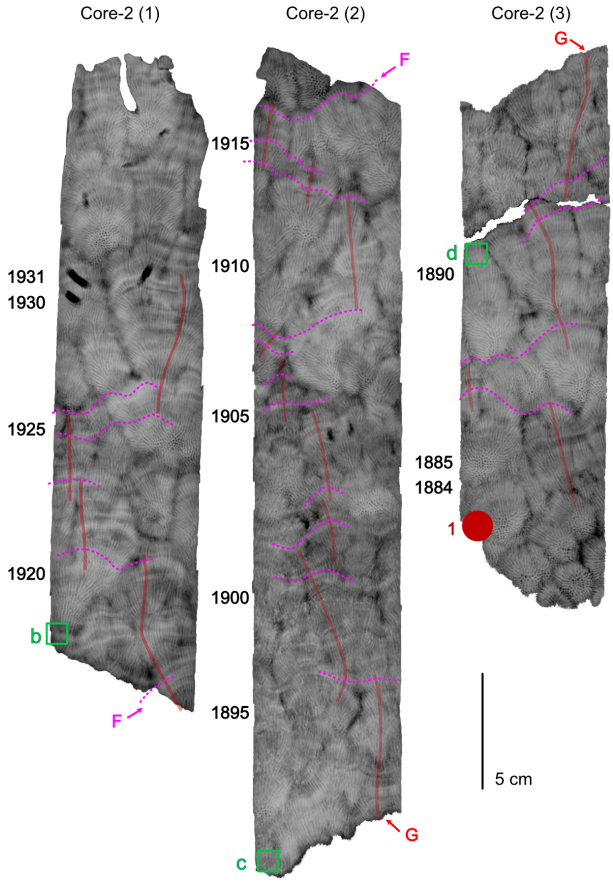

Core-2 (1)
Core-2 (2)
Core-2 (3)
1931
1930
1925
1920
1915
1910
1905
1900
1895
1890
1885
1884
F
G
b
c
d
1
5 cm

Figure A4.

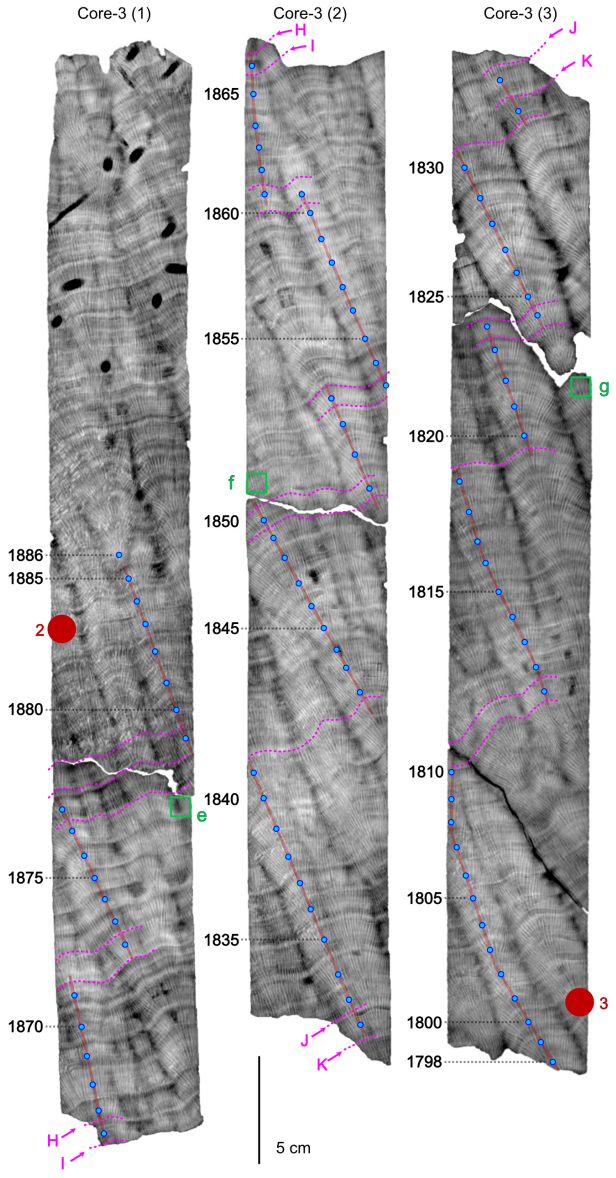


Figure A4. X-radiographs of the *Porites* coral specimens. The X-radiographs (negative) show subsampling paths indicated by red lines. The red arrows and accompanying capital letters denote the continuation of a subsampling path onto the next slab. The magenta dashed lines and accompanying capital letters mark high-density bands that help connect subsampling paths. In Core-1 and Core-3, the blue circles are marked between high-density bands, corresponding to the annual cycles identified in the skeletal Sr/Ca record. The subsampled locations for U–Th dating are marked with red circles and labelled with numbers (Sample IDs: 1 = "KISM-1", 2 = "KISM-2", and 3 = "KISM-3"); the dating results are listed in Table A2. The positions used for diagenesis screening are shown as green squares and lowercase letters. The years estimated by seasonal cycles in skeletal Sr/Ca are shown left of each slab.

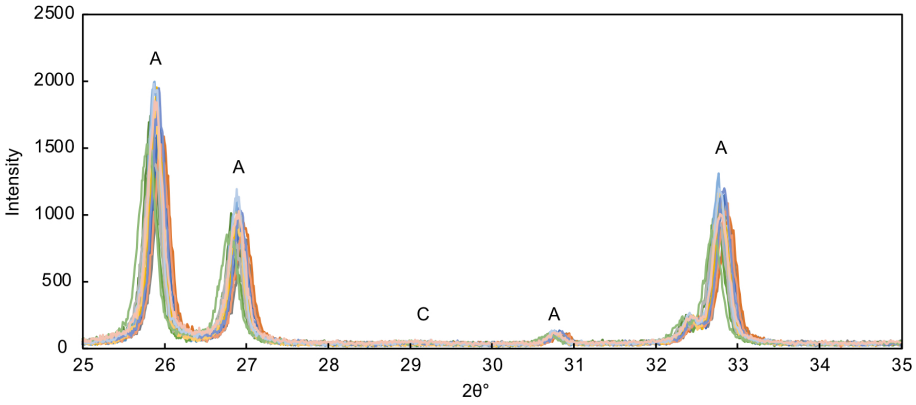


Figure A5. Diagenesis screening by X-ray diffraction analysis. Powder samples for X-ray diffraction analysis were collected along all analytical paths shown in Fig. A4. Notes "A" and "C" indicate the diffraction angles (2θ) corresponding to aragonite and calcite, respectively. The resulting peaks labelled "A" confirm that the crystalline structure of the samples is aragonite. No calcite peaks ("C") were observed in any of the samples. The calcite content for each analytical line was less than 1 %. Based on these results, we concluded that pristine aragonite is well preserved throughout all analytical paths.

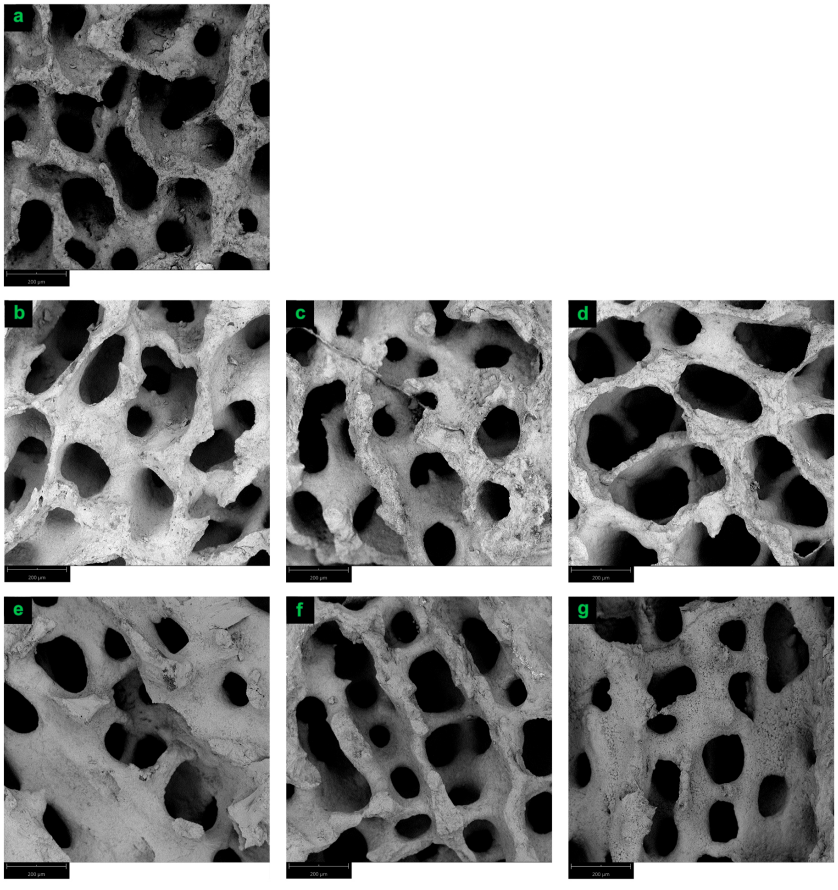


Figure A6. Diagenesis screening by scanning electron microscopy. The locations where each image was taken are shown in Fig. A4. **(a)** Core-1. **(b–d)** Core-2. **(e–g)** Core-3. These images show little to no evidence of diagenetic alteration, such as the presence of calcite, secondary aragonite, and dissolution. The results indicate that pristine aragonite is well preserved in all specimens.

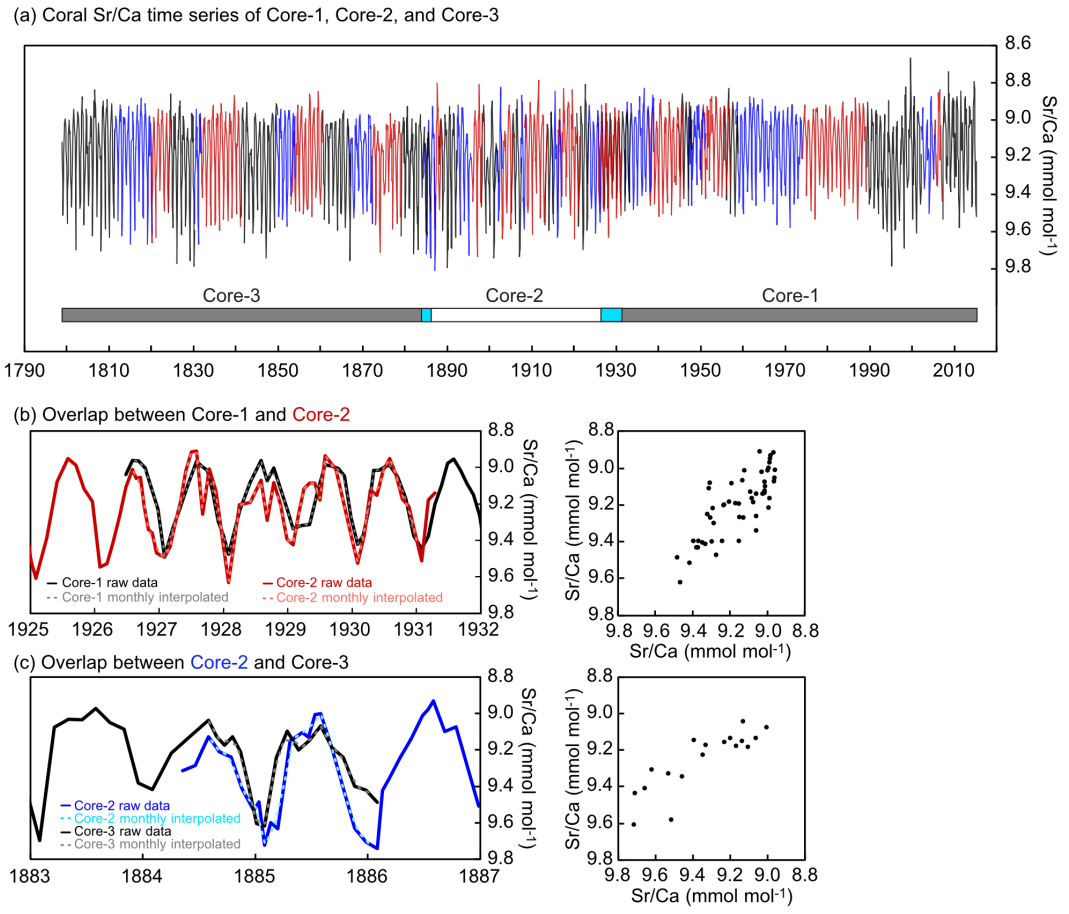


Figure A7. Individual coral Sr/Ca time series from three cores and their overlapping periods. **(a)** Coral Sr/Ca time series from Core-1, Core-2, and Core-3. Sampling transects are highlighted in different colours (in black, red, or blue). The overlapping segments of cores are shown in pale blue bars (bottom). The mean annual growth rate for each core was 11.1 ± 2.53, 14.7 ± 3.35, and 13.2 ± 1.94 mm yr^{-1} for Core-1, Core-2, and Core-3, respectively. **(b)** Left: Overlapping period between Core-1 and Core-2. Monthly interpolated coral Sr/Ca datasets of the overlapping periods are shown in grey and pale red. Right: Scatter plot of the monthly interpolated dataset. **(c)** same as **(b)**, but for the overlapping period between Core-2 and Core-3. Monthly interpolated datasets of the overlapping periods are shown in grey and pale blue. The differences in mean, summer, and winter Sr/Ca values between Core-1, Core-2, and Core-3 are reported in Table A3.

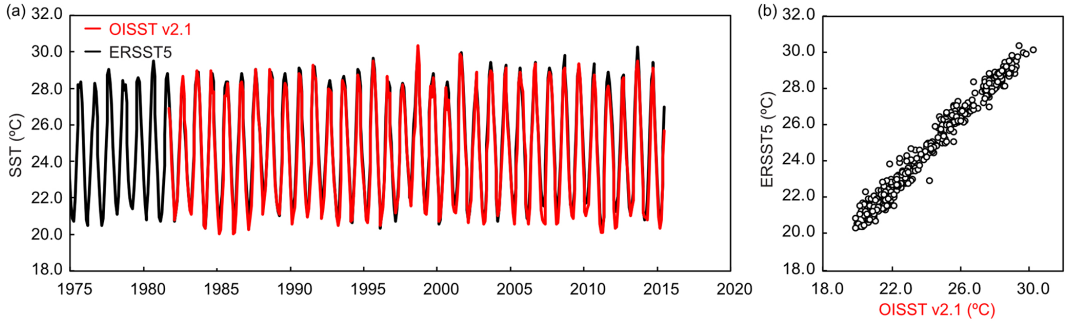


Figure A8. Comparison of instrumental temperature products (OISST v2.1 and ERSST5, covering Kikai Island). **(a)** Time series of OISST v2.1 (Huang et al., 2021, monthly resolved and converted from daily data, for the $0.25 \times 0.25°$ grid centred at 28.375° N, 130.25° E, in red) and ERSST5 (Huang et al., 2017, for the grid of 27–29° N, 129–131° E, in black). **(b)** Scatter plots for OISST v2.1 and ERSST5 for the period from September 1981 to June 2015 CE.

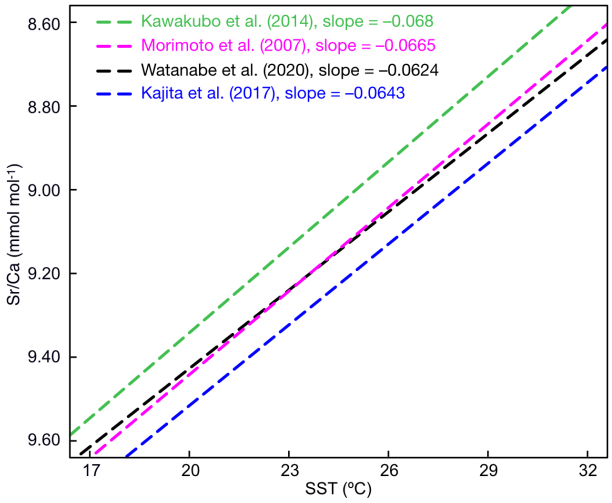


Figure A9. Previously published coral Sr/Ca-temperature slopes for Kikai Island. Slopes reported by Kawakubo et al. (2014) (by laser ablation ICP-MS analysis, in green), Morimoto et al. (2007) (by TIMS analysis with the isotope dilution method, in magenta), Watanabe et al. (2020) (by solution ICP-OES analysis, in black), and Kajita et al. (2017) (by solution ICP-OES analysis, in blue) are shown. These slopes were used to convert skeletal Sr/Ca values (mmol mol^{-1}) into temperature units (°C) in this study.

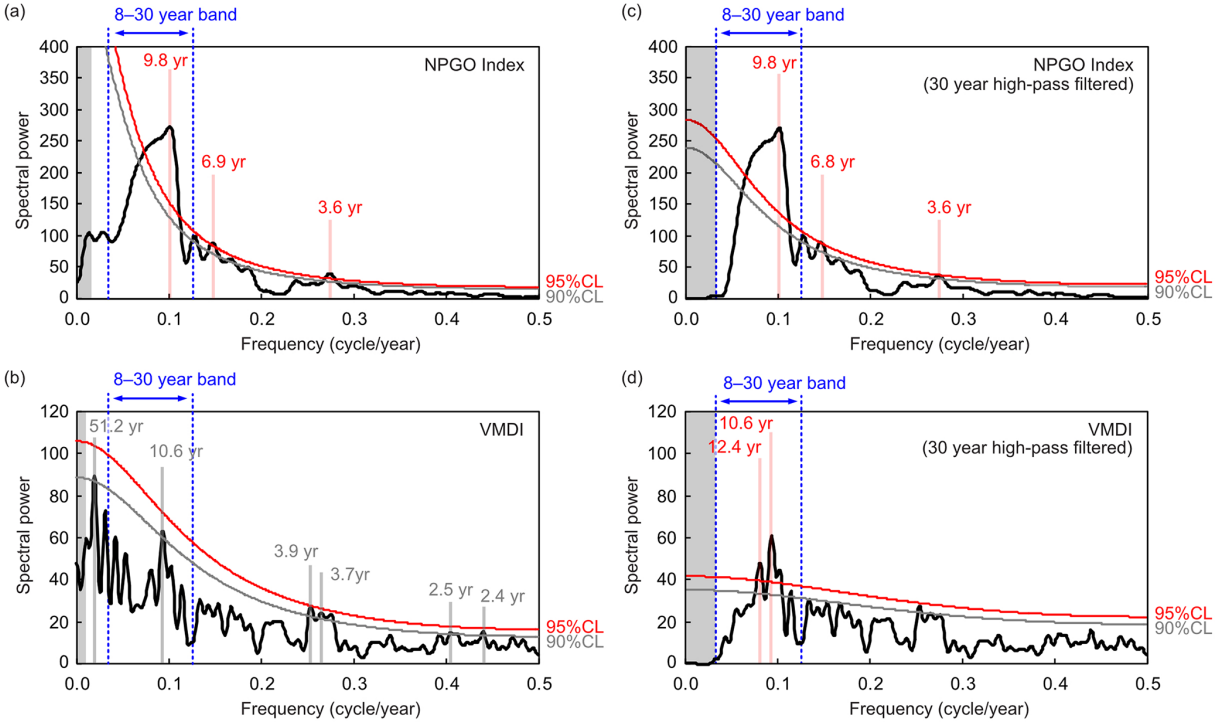


Figure A10. Spectral power analyses of the NPGO Index and the VMDI. **(a)** Annual mean time series of the NPGO Index (Di Lorenzo et al., 2008) for the period from 1950 to 2014 CE. **(b)** Annual mean time series of the Victoria Mode Dipole Index (VMDI; Wen et al., 2024, calculated using ERSST5) for the period from 1900 to 2014 CE. **(c)** and **(d)** same as **(a)** and **(b)**, but after application of a 30 year high-pass filter. Significant spectral peaks at the 95 % CL are denoted with their corresponding periods in years (yr, in red). Only in panel **(b)**, significant spectral peaks at the 90 % CL are denoted with their corresponding periods in years (yr, in grey). Periods that cannot be robustly resolved because of the limited lengths of the time series are shaded in grey. The region between the blue dashed lines labelled "8–30 year band", indicates the frequency band retained by the 8–30 year bandpass filter used in this study.

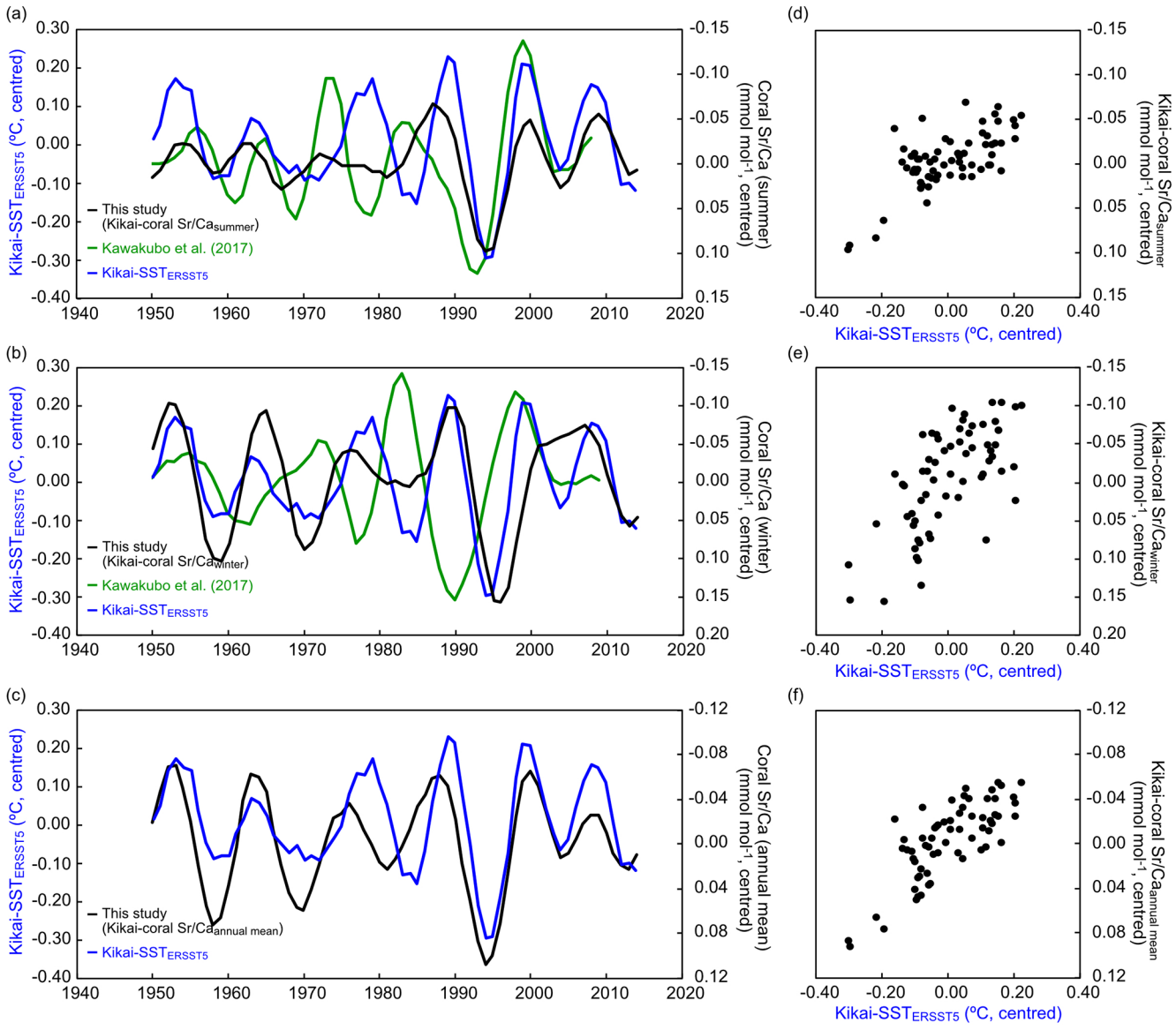


Figure A11. Comparison of coral Sr/Ca records with Kikai-SST$_{ERSST5}$. The Kikai-SST$_{ERSST5}$ time series (in blue, annual mean; Huang et al., 2017) is compared with the following coral Sr/Ca records: **(a)** Kikai-coral Sr/Ca$_{summer}$ (in black, this study) and the previously published summer data (in green, Kawakubo et al., 2017); **(b)** Kikai-coral Sr/Ca$_{winter}$ (in black, this study) and the previously published winter data (in green, Kawakubo et al., 2017); **(c)** Kikai-coral Sr/Ca$_{annual\ mean}$ (in black, this study). An 8–30 year bandpass filter was applied to all time series. **(d–f)** Scatter plots of annual mean Kikai-SST$_{ERSST5}$ and our coral records (**d**: Kikai-coral Sr/Ca$_{summer}$; **e**: Kikai-coral Sr/Ca$_{winter}$; **f**: Kikai-coral Sr/Ca$_{annual\ mean}$).

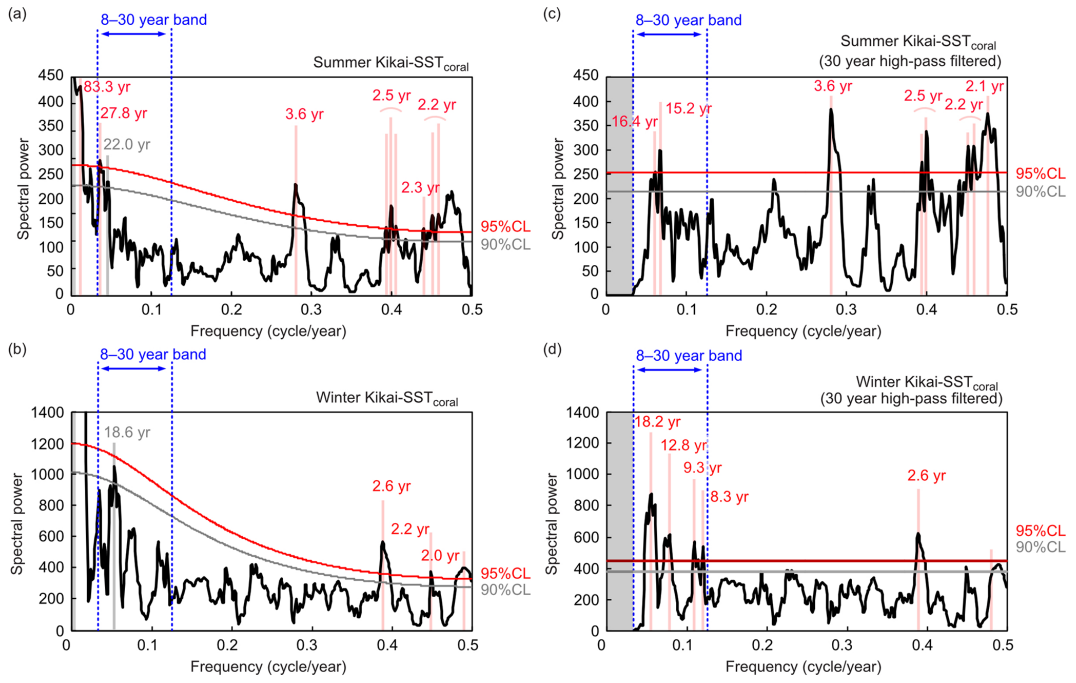


Figure A12. Spectral power analyses of Kikai-SST$_{coral}$ records. **(a)** Summer Kikai-SST$_{coral}$ and **(b)** Winter Kikai-SST$_{coral}$ datasets for the period from 1799 to 2014 CE. **(c)** and **(d)** same as **(a)** and **(b)**, but after application of a 30 year high-pass filter. Significant spectral peaks at the 95 % CL are denoted with their corresponding periods in years (yr, in red). Periods that cannot be robustly resolved because of the limited lengths of the time series are shaded in grey. The region between the blue dashed lines labelled "8–30 year band" indicates the frequency band retained by the 8–30 year bandpass filter used in this study. Focusing on the 8–30 year band, the detected significant frequencies at the 90 % CL are denoted with their corresponding periods in years (yr, in grey).

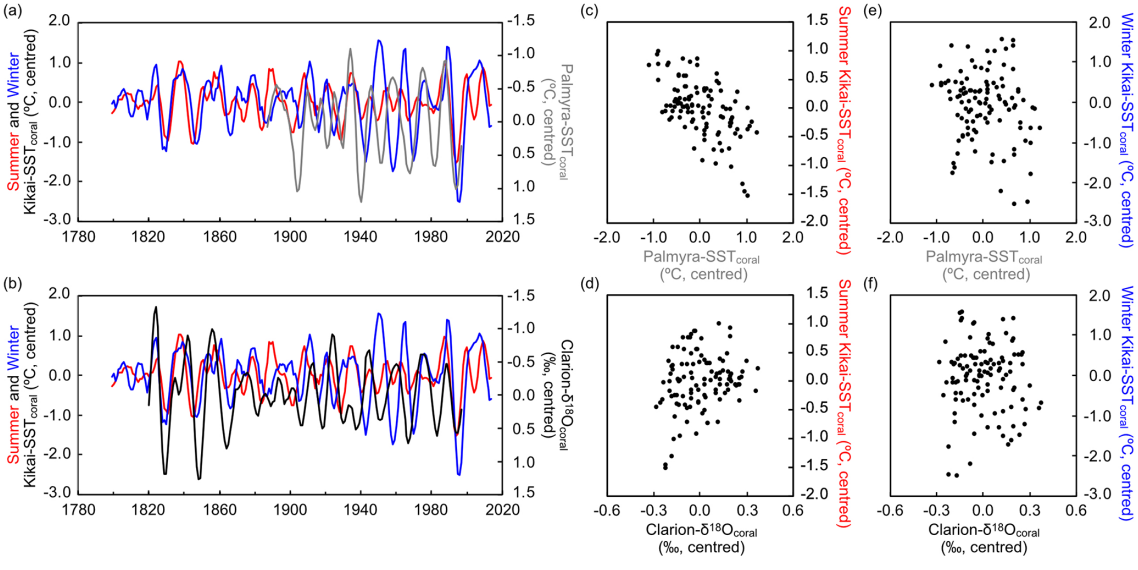


Figure A13. Comparison of the time series between our coral record from the NWP and the previously published coral record from the CP and NEP. **(a)** Time series of Summer Kikai-SST$_{coral}$ (in red, this study), Winter Kikai-SST$_{coral}$ (in blue, this study), and Palmyra-SST$_{coral}$ (in grey, annual mean values, Nurhati et al., 2011). **(b)** Time series of Summer Kikai-SST$_{coral}$ (in red, this study), Winter Kikai-SST$_{coral}$ (in blue, this study), and Clarion-$\delta^{18}O_{coral}$ (in black, annual mean values, Sanchez et al., 2016). An 8–30 year bandpass filter was applied to all time series. **(c–f)** Scatter plot corresponding to **(a)** and **(b)**.

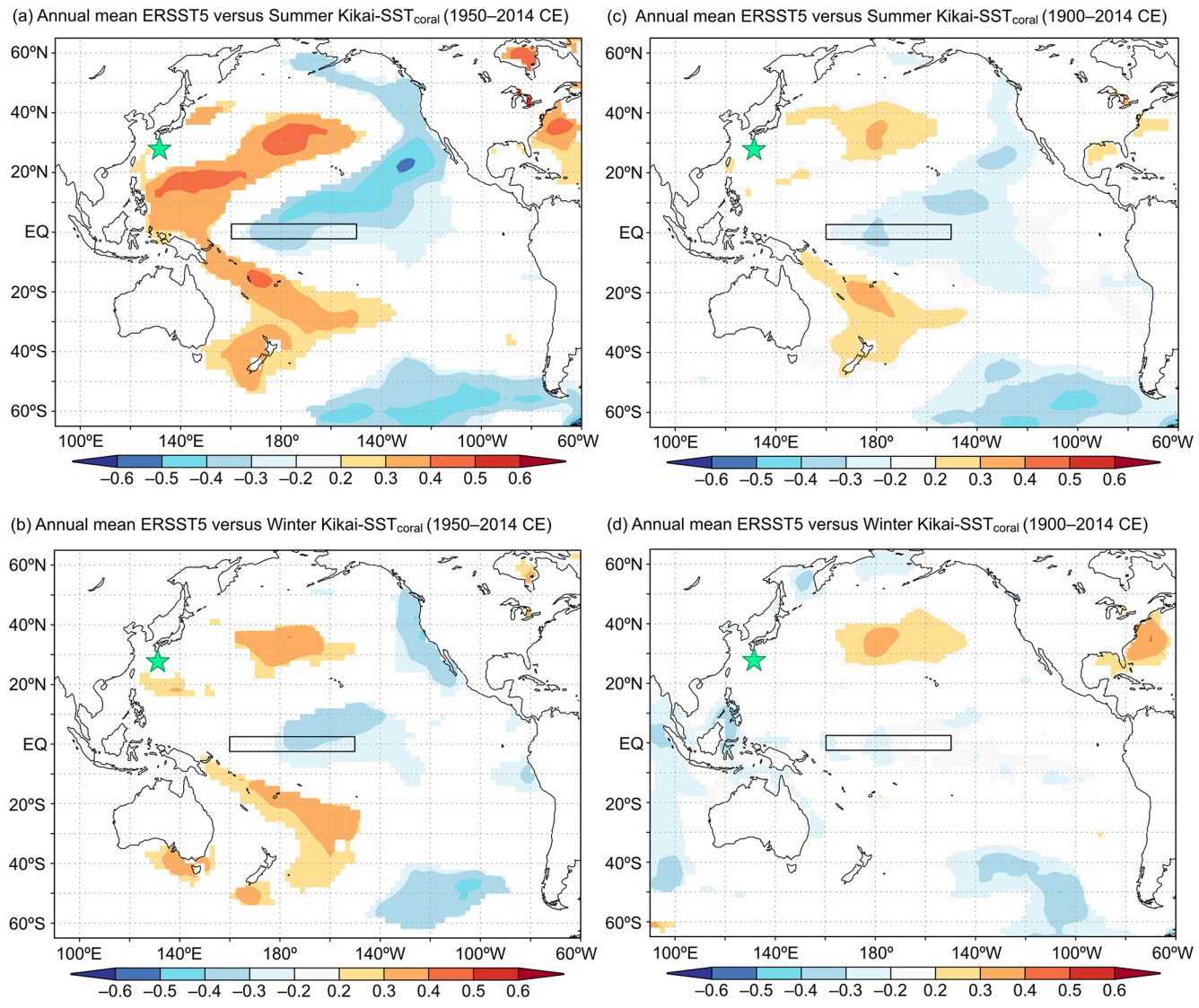


Figure A14. Field correlations between Kikai-SST$_{coral}$ and instrumental SST record (unfiltered). **(a)** Field correlation map between Summer Kikai-SST$_{coral}$ (this study) and the annual mean SST time series (ERSST5; Huang et al., 2017) from 1950 to 2014 CE. **(b)** Field correlation map between Winter Kikai-SST$_{coral}$ and the annual mean SST time series (ERSST5; Huang et al., 2017) from 1950 to 2014 CE. **(c)** same as **(a)**, but covering the period from 1900 to 2014 CE. **(d)** same as **(b)**, but covering the period from 1900 to 2014 CE. All correlations are computed using detrended data. Only correlations with p-values < 0.1 are colour-coded. The original figures in each panel were computed using the web application KNMI Climate Explorer (https://climexp.knmi.nl/, last access: 22 October 2026) and plotted using GrADS (v2.2.1). The location of the coral sampling site (Kikai Island, Kagoshima, Japan) is marked by a star. The black box indicates the CP region (5° S–5° N, 160° E–150° W). See also Fig. 4 for the 8–30 bandpass filtered analyses.

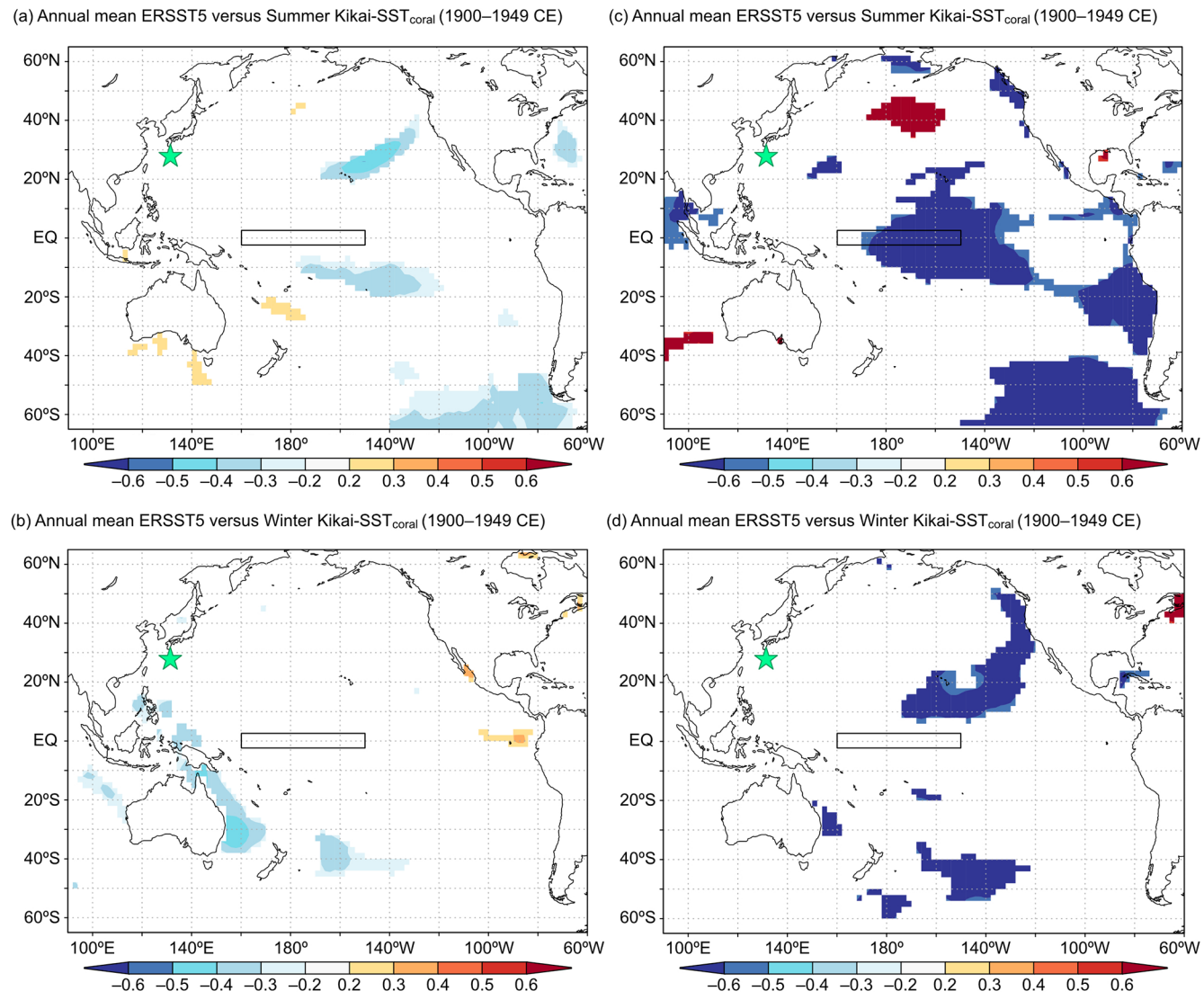


Figure A15. Field correlations between Kikai-SST$_{coral}$ and instrumental SST record (for the period 1900–1949). **(a)** Field correlation map between Summer Kikai-SST$_{coral}$ (this study) and the annual mean SST time series (ERSST5; Huang et al., 2017) from 1900 to 1949 CE. **(b)** Field correlation map between Winter Kikai-SST$_{coral}$ and the annual mean SST time series (ERSST5; Huang et al., 2017) from 1900 to 1949 CE. **(c)** same as **(a)**, but after application of an 8–30 year bandpass filter. **(d)** same as **(b)**, but after application of an 8–30 year bandpass filter. All correlations are computed using detrended data. Only correlations with p-values < 0.1 are colour-coded. The original figures in each panel were computed using the web application KNMI Climate Explorer (https://climexp.knmi.nl/, last access: 22 October 2026) and plotted using GrADS (v2.2.1). The location of the coral sampling site (Kikai Island, Kagoshima, Japan) is marked by a star. The black box indicates the CP region (5° S–5° N, 160° E–150° W).

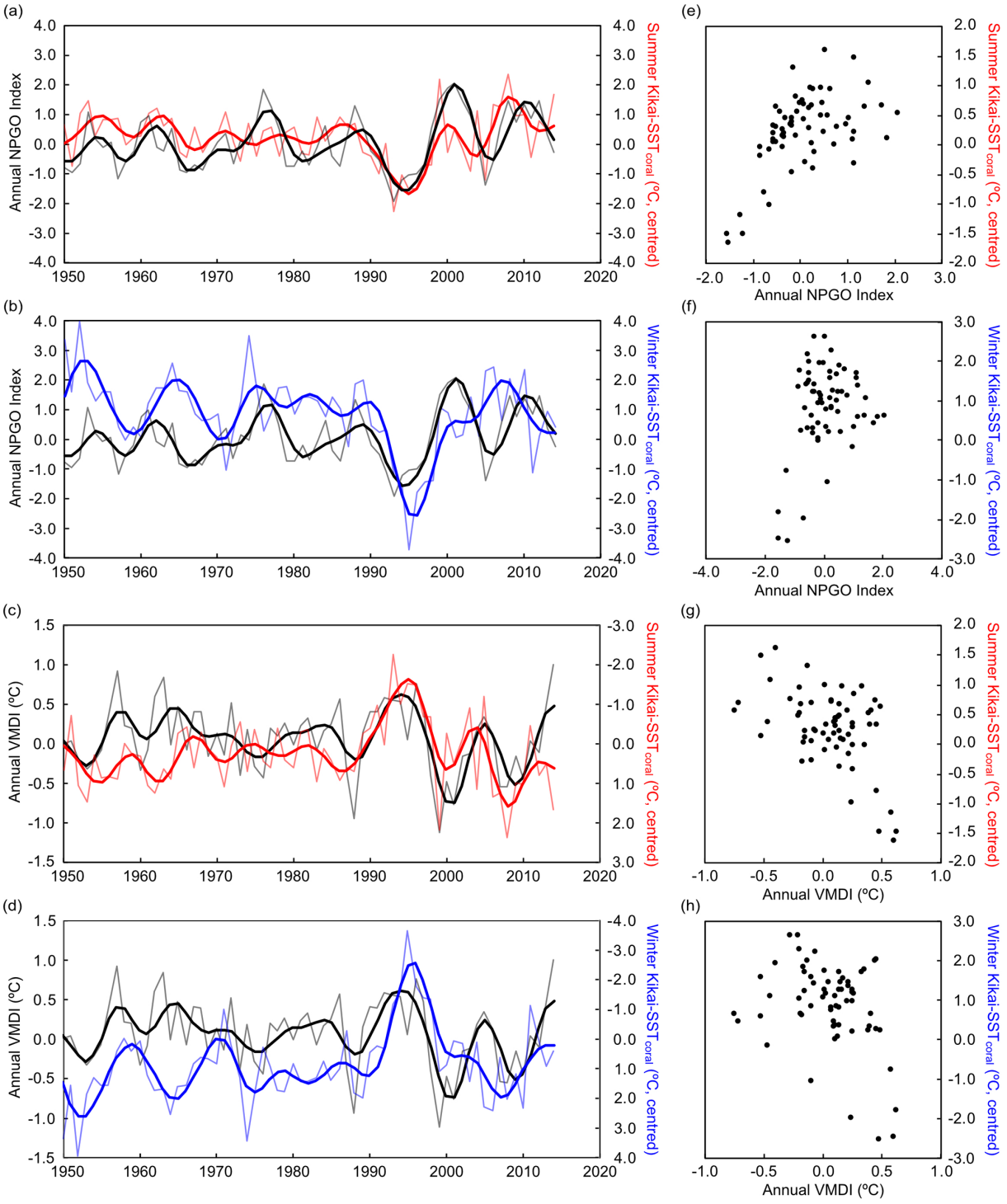


Figure A16. Comparison of the annual mean NPGO Index, annual mean VMDI, and Kikai-SST$_{coral}$ (1950–2014 CE) (8 year low-pass filtered). Time series of **(a)** the annual mean NPGO Index (thin black line, Di Lorenzo et al., 2008) and Summer Kikai-SST$_{coral}$ (thin red line); **(b)** the annual mean NPGO Index (thin black line) and Winter Kikai-SST$_{coral}$ (thin blue line); **(c)** the annual mean Victoria Mode Dipole Index (thin black line, VMDI, Wen et al., 2024, calculated using ERSST5) and Summer Kikai-SST$_{coral}$ (thin red line); **(d)** the VMDI (thin black line) and Winter Kikai-SST$_{coral}$ (thin blue line). Bold lines represent the 8 year low-pass filtered time series. **(e–h)** Scatter plot corresponding to **(a)**–**(d)**, for the low-pass filtered datasets. See also Fig. 5 for the 8–30 year bandpass filtered time series.

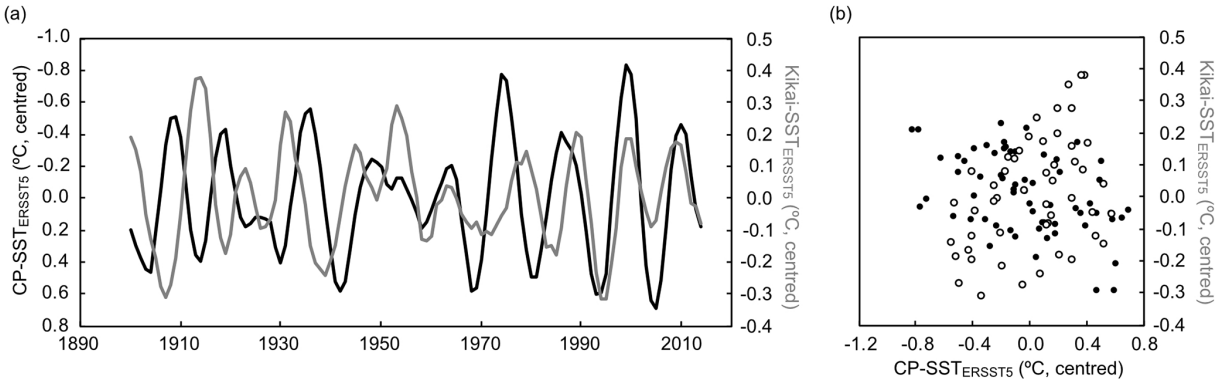


Figure A17. Comparison of time series between instrumental temperature records from the regions of the CP and Kikai Island. **(a)** Time series of CP-SST$_{ERSST5}$ (Huang et al., 2017, in black) and Kikai-SST$_{ERSST5}$ (Huang et al., 2017, in grey) for the period 1900–2014 CE. **(b)** Scatter plot corresponding to **(a)**. Open-circle plots are data for the period 1900–1949 CE. Closed-circle plots are data for the period 1950–2014 CE. An 8–30 year bandpass filter was applied to both time series.

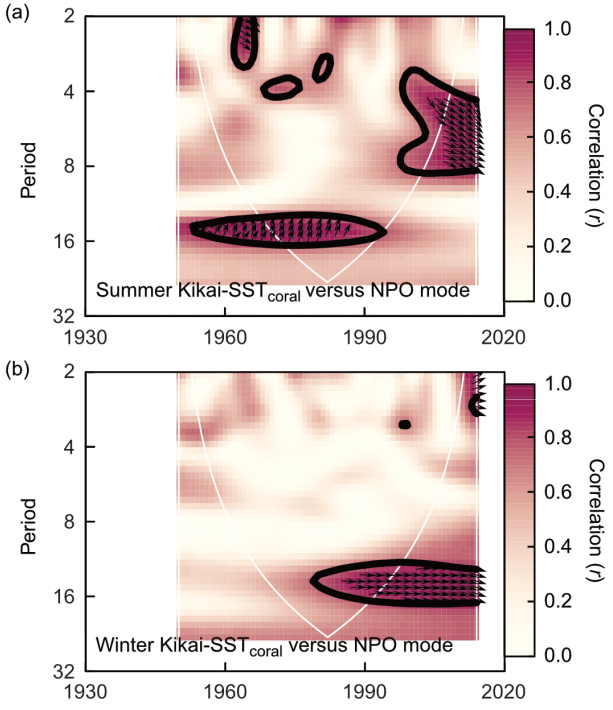


Figure A18. Cross-wavelet coherence analysis between Kikai-SST$_{coral}$ and NPO variability. **(a)** Cross-wavelet coherence between the Summer Kikai-SST$_{coral}$ time series and NPO variability (December–February) for the period 1950–2014 CE. The NPO dataset was calculated from the Hadley Centre Sea Level Pressure dataset (HadSLP2r, Allan and Ansell, 2006; 30–65° N, 160° E–140° W) using the empirical orthogonal function method of Trenberth and Hurrell (1994) at KNMI Climate Explorer. Regions of significant coherence (p-values < 0.1) are outlined by solid contours. Arrows indicate the phase relationship. **(b)** Same as **(a)**, but between Winter Kikai-SST$_{coral}$ time series and NPO variability (December–February).

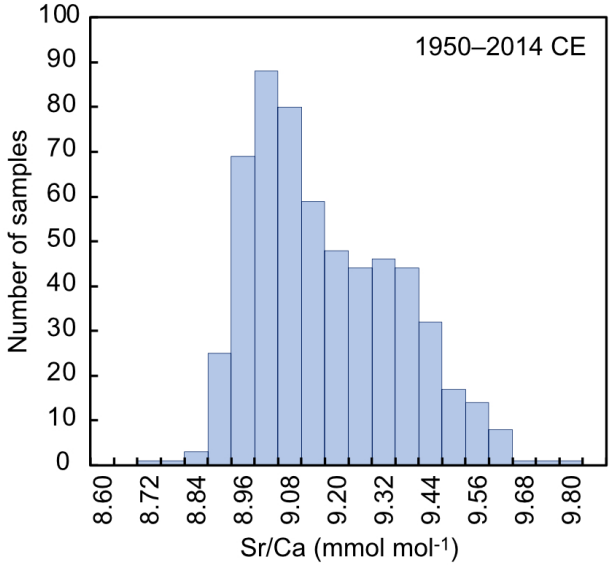


Figure A19. Histogram of the Kikai-coral Sr/Ca record from 1950 to 2014 CE. The x-axis interval is 0.06 mmol mol^{-1}, which corresponds to approximately 1 °C (Corrège, 2006). Higher (lower) Sr/Ca values indicate cooler (warmer) temperatures.

Data availability. Archiving of all data is underway, and it will be made available at the KIKAI Coral Reef Science Institute data repository (https://coralogy.kikaireefs.org/) after this manuscript is accepted.

Author contributions. S.I. conceptualised the study and designed it with T.K.W. and T.W. Coral samples were collected by S.I., A.Y., T.K., and T.W. Skeletal geochemical analysis was performed by S.I., and U–Th dating was performed by T.K.W. and C.–C.S. Diagenesis screening was conducted by S.I. (powder X-ray diffraction and scanning electron microscopy) and T.K. (scanning electron microscopy). Statistical analyses were conducted by S.I. and T.K.W. The first draft of the manuscript was written by S.I., and all authors contributed to further conceptual and content development, as well as the interpretation of the data.

Competing interests. The contact author has declared that none of the authors has any competing interests.

Disclaimer. Publisher's note: Copernicus Publications remains neutral with regard to jurisdictional claims made in the text, published maps, institutional affiliations, or any other geographical representation in this paper. The authors bear the ultimate responsibility for providing appropriate place names. Views expressed in the text are those of the authors and do not necessarily reflect the views of the publisher.

Acknowledgements. We acknowledge CREES laboratory members who assisted in collecting, cutting and microsampling coral core samples. For trace element analysis (skeletal Sr/Ca), Tung Thanh Phan, Kakeru Takeuchi, Ayuka Kuribara, Hiroto Kajita, and Yuki Kawai helped us. For X-ray diffraction analysis, Kohki Sowa established the basic method used in our analysis of coral specimens. We also thank Miriam Pfeiffer for insightful discussions regarding the temperature products and calculations for coral Sr/Ca-inferred temperature. Coral core drilling was performed with permission from Kagoshima Prefecture and Fisheries Cooperative in Kikai Town. S.I. is supported by JSPS Overseas Research Fellowships and The Deutsche Forschungsgemeinschaft (DFG, German Research Foundation, project no. 468545267 – Special Priority Programme, SPP 2299/project no. 441832482). We also appreciate two reviewers for insightful comments and discussions for publication.

Financial support. This research has been supported by the Japan Science Society (Sasakawa Scientific Research Grant (grant no. 29-702) to S.I.), the National Science and Technology Council (grant nos. 111-2116-M-002-022-MY3 and 111-2926-I-002-510-G to C.–C.S.), the Higher Education Sprout Project of the Ministry of Education, Taiwan, ROC (112L901001 to C.–C.S.) and the National Taiwan University (grant no. 112L894202 to C.–C.S.).

Review statement. This paper was edited by Julien Emile-Geay and reviewed by Sara C. Sanchez and one anonymous referee.

References

Abram, N. J., McGregor, H. V., Tierney, J. E., Evans, M. N., McKay, N. P., and Kaufman, D. S.: Early onset of industrial-era warming across the oceans and continents, Nature, 536, 411–418, https://doi.org/10.1038/nature19082, 2016.

Abram, N. J., Hargreaves, J. A., Wright, N. M., Thirumalai, K., Ummenhofer, C. C., and England, M. H.: Palaeoclimate perspectives on the Indian Ocean Dipole, Quaternary Sci. Rev., 237, 106302, https://doi.org/10.1016/j.quascirev.2020.106302, 2020.

Alexander, M. A., Bladé, I., Newman, M., Lanzante, J. R., Lau, N.-C., and Scott, J. D.: The atmospheric bridge: The influence of ENSO teleconnections on air–sea interaction over the global oceans, J. Clim., 15, 2205–2231, https://doi.org/10.1175/1520-0442(2002)015<2205:TABTIO>2.0.CO;2, 2002.

Alibert, C. and McCulloch, M. T.: Strontium / calcium ratios in modern *porites* corals From the Great Barrier Reef as a proxy for sea surface temperature: Calibration of the thermometer and monitoring of ENSO, Paleoceanography, 12, 345–363, https://doi.org/10.1029/97PA00318, 1997.

Allan, R. and Ansell, T.: A New Globally Complete Monthly Historical Gridded Mean Sea Level Pressure Dataset (HadSLP2): 1850–2004, J. Climate, 19, 5816–5842, https://doi.org/10.1175/jcli3937.1, 2006.

Asami, R., Matsumori, T., Shinjo, R., Uemura, R., Miyaoka, Y., Mizuyama, M., Ise, Y., and Sakamaki, T.: Reconstruction of ocean environment time series since the late nineteenth century using sclerosponge geochemistry in the northwestern subtropical Pacific, Prog. Earth Planet. Sci., 8, 38, https://doi.org/10.1186/s40645-021-00434-7, 2021.

Ashok, K., Behera, S. K., Rao, S. A., Weng, H., and Yamagata, T.: El Niño Modoki and its possible teleconnection, J. Geophys. Res.-Oceans, 112, C1107, https://doi.org/10.1029/2006JC003798, 2007.

Barnes, D. J., Taylor, R. B., and Lough, J. M.: On the inclusion of trace materials into massive coral skeletons. Part II: distortions in skeletal records of annual climate cycles due to growth processes, J. Exp. Mar. Biol. Ecol., 194, 251–275, https://doi.org/10.1016/0022-0981(95)00091-7, 1995.

Björklund, J., Seftigen, K., Stoffel, M., Fonti, M. V., Kottlow, S., Frank, D. C., Esper, J., Fonti, P., Goosse, H., Grudd, H., Gunnarson, B. E., Nievergelt, D., Pellizzari, E., Carrer, M., and Von Arx, G.: Fennoscandian tree-ring anatomy shows a warmer modern than medieval climate, Nature, 620, 97–103, https://doi.org/10.1038/s41586-023-06176-4, 2023.

Bond, N. A., Overland, J. E., Spillane, M., and Stabeno, P.: Recent shifts in the state of the North Pacific, Geophys. Res. Lett., 30, 2183, https://doi.org/10.1029/2003gl018597, 2003.

Brönnimann, S., Franke, J., Nussbaumer, S. U., Zumbühl, H. J., Steiner, D., Trachsel, M., Hegerl, G. C., Schurer, A., Worni, M., Malik, A., Flückiger, J., and Raible, C. C.: Last phase of the Little Ice Age forced by volcanic eruptions, Nat. Geosci., 12, 650–656, https://doi.org/10.1038/s41561-019-0402-y, 2019.

Cahyarini, S. Y., Pfeiffer, M., Timm, O., Dullo, W.-C., and Schönberg, D. G.: Reconstructing seawater δ^{18}O from paired coral δ^{18}O and Sr/Ca ratios: Methods, error analysis and problems, with examples from Tahiti (French Polynesia) and Timor (Indonesia), Geochim. Cosmochim. Acta, 72, 2841–2853, https://doi.org/10.1016/j.gca.2008.04.005, 2008.

Cahyarini, S. Y., Pfeiffer, M., Nurhati, I. S., Aldrian, E., Dullo, W.-C., and Hetzinger, S.: Twentieth century sea surface temperature and salinity variations at Timor inferred from paired coral δ^{18}O and Sr/Ca measurements, J. Geophys. Res.-Oceans, 119, 4593–4604, https://doi.org/10.1002/2013JC009594, 2014.

Cahyarini, S. Y., Pfeiffer, M., Reuning, L., Liebetrau, V., Dullo, W.-C., Takayanagi, H., Anwar, I. P., Utami, D. A., Garbe-Schönberg, D., and Hendrizan, M.: Modern and sub-fossil corals suggest reduced temperature variability in the eastern pole of the Indian Ocean Dipole during the medieval climate anomaly, Sci. Rep., 11, 14952, https://doi.org/10.1038/s41598-021-94465-1, 2021.

Charles, C. D., Hunter, D. E., and Fairbanks, R. G.: Interaction between the ENSO and the Asian monsoon in a coral record of tropical climate, Science, 277, 925–928, https://doi.org/10.1126/science.277.5328.925, 1997.

Chaudhuri, P. and Marron, J. S.: SiZer for exploration of structures in curves, J. Am. Stat. Assoc., 94, 807–823, https://doi.org/10.1080/01621459.1999.10474186, 1999.

Cheng, H., Lawrence Edwards, R., Shen, C.-C., Polyak, V. J., Asmerom, Y., Woodhead, J., Hellstrom, J., Wang, Y., Kong, X., Spötl, C., Wang, X., and Calvin Alexander, E.: Improvements in ^{230}Th dating, ^{230}Th and ^{234}U half-life values, and U–Th isotopic measurements by multi-collector inductively coupled plasma mass spectrometry, Earth Planet. Sci. Lett., 371–372, 82–91, https://doi.org/10.1016/j.epsl.2013.04.006, 2013.

Chenillat, F., Rivière, P., Capet, X., Di Lorenzo, E., and Blanke, B.: North Pacific Gyre Oscillation modulates seasonal timing and ecosystem functioning in the California Current upwelling system, Geophys. Res. Lett., 39, https://doi.org/10.1029/2011gl049966, 2012.

Chhak, K. C., Di Lorenzo, E., Schneider, N., and Cummins, P. F.: Forcing of low-frequency ocean variability in the northeast Pacific, J. Clim., 22, 1255–1276, https://doi.org/10.1175/2008JCLI2639.1, 2009.

Cobb, K. M., Charles, C. D., Cheng, H., and Edwards, R. L.: El Niño/Southern Oscillation and tropical Pacific climate during the last millennium, Nature, 424, 271–276, https://doi.org/10.1038/nature01779, 2003.

Cobb, K. M., Westphal, N., Sayani, H. R., Watson, J. T., Di Lorenzo, E., Cheng, H., Edwards, R. L., and Charles, C. D.: Highly variable El Niño–southern oscillation throughout the Holocene, Science, 339, 67–70, https://doi.org/10.1126/science.1228246, 2013.

Cole, J. E., Fairbanks, R. G., and Shen, G. T.: Recent variability in the Southern Oscillation: Isotopic results from a Tarawa Atoll coral, Science, 260, 1790–1793, https://doi.org/10.1126/science.260.5115.1790, 1993.

Corrège, T.: Sea surface temperature and salinity reconstruction from coral geochemical tracers, Palaeogeogr. Palaeocl., 232, 408–428, https://doi.org/10.1016/j.palaeo.2005.10.014, 2006.

D'Olivo, J. P. and McCulloch, M. T.: Response of coral calcification and calcifying fluid composition to thermally induced bleaching stress, Sci. Rep., 7, 2207, https://doi.org/10.1038/s41598-017-02306-x, 2017.

D'Olivo, J. P., Zinke, J., Goyal, R., England, M. H., Purich, A., Corrège, T., Zorita, E., Scholz, D., Weber, M., and Carriquiry, J. D.: Coral Sr/Ca-SST reconstruction from Fiji extending to ∼1370 CE reveals insights into the Interdecadal Pacific Oscillation, Sci. Adv., 10, https://doi.org/10.1126/sciadv.ado5107, 2024.

DeCarlo, T. M. and Cohen, A. L.: Dissepiments, density bands and signatures of thermal stress in *Porites* skeletons, Coral Reefs, 36, 749–761, https://doi.org/10.1007/s00338-017-1566-9, 2017.

DeLong, K. L., Flannery, J. A., Poore, R. Z., Quinn, T. M., Maupin, C. R., Lin, K., and Shen, C.-C.: A reconstruction of sea surface temperature variability in the southeastern Gulf of Mexico from 1734 to 2008 CE using cross-dated Sr/Ca records from the coral Siderastrea siderea, Paleoceanography, 29, 403–422, https://doi.org/10.1002/2013PA002524, 2014.

de Villiers, S., Greaves, M., and Elderfield, H.: An intensity ratio calibration method for the accurate determination of Mg/Ca and Sr/Ca of marine carbonates by ICP-AES, Geochem. Geophys. Geosyst., 3, https://doi.org/10.1029/2001GC000169, 2002.

Di Lorenzo, E., Schneider, N., Cobb, K. M., Franks, P. J. S., Chhak, K., Miller, A. J., McWilliams, J. C., Bograd, S. J., Arango, H., Curchitser, E., Powell, T. M., and Rivière, P.: North Pacific Gyre Oscillation links ocean climate and ecosystem change, Geophys. Res. Lett., 35, L08607, https://doi.org/10.1029/2007gl032838, 2008.

Di Lorenzo, E., Fiechter, J., Schneider, N., Bracco, A., Miller, A. J., Franks, P. J. S., Bograd, S. J., Moore, A. M., Thomas, A. C., Crawford, W., Peña, A., and Hermann, A. J.: Nutrient and salinity decadal variations in the central and eastern North Pacific, Geophys. Res. Lett., 36, L14601, https://doi.org/10.1029/2009gl038261, 2009.

Di Lorenzo, E., Cobb, K. M., Furtado, J. C., Schneider, N., Anderson, B. T., Bracco, A., Alexander, M. A., and Vimont, D. J.: Central Pacific El Niño and decadal climate change in the North Pacific Ocean, Nat. Geosci., 3, 762–765, https://doi.org/10.1038/ngeo984, 2010.

Di Lorenzo, E., Combes, V., Keister, J. E., Strub, P. T., Thomas, A. C., Franks, P. J. S., Ohman, M. D., Furtado, J. C., Bracco, A., Bograd, S. J., Peterson, W. T., Schwing, F. B., Chiba, S., Taguchi, B., Hormazabal, S., and Parada, C.: Synthesis of Pacific Ocean climate and ecosystem dynamics, Oceanography, 26, 68–81, https://doi.org/10.5670/oceanog.2013.76, 2013.

Ding, R., Li, J., Tseng, Y.-H., Sun, C., and Guo, Y.: The Victoria mode in the North Pacific linking extratropical sea level pressure variations to ENSO, J. Geophys. Res.-Atmos., 120, 27–45, https://doi.org/10.1002/2014jd022221, 2015.

Dong, Z., Zhou, F., Zheng, Z., and Fang, K.: Increased amplitude of the North Pacific Gyre Oscillation towards recent: Evidence from tree-ring-based reconstruction since 1596, Int. J. Climatol., 42, 6403–6412, https://doi.org/10.1002/joc.7596, 2022.

Draper, N. R. and Smith, H.: Applied regression analysis, 2nd, John Wiley & Sons, New York, ISBN 978-0-471-02995-3, 1981.

Evans, M. N., Reichert, B. K., Kaplan, A., Anchukaitis, K. J., Vaganov, E. A., Hughes, M. K., and Cane, M. A.: A forward modeling approach to paleoclimatic interpretation of tree-ring data, J. Geophys. Res. Biogeosci., 111, https://doi.org/10.1029/2006jg000166, 2006.

Fallon, S. J., McCulloch, M. T., van Woesik, R., and Sinclair, D. J.: Corals at their latitudinal limits: laser ablation trace element systematics in *Porites* from Shirigai Bay, Japan, Earth Planet. Sci. Lett., 172, 221–238, https://doi.org/10.1016/S0012-821X(99)00200-9, 1999.

Felis, T., Pätzold, J., Loya, Y., Fine, M., Nawar, A. H., and Wefer, G.: A coral oxygen isotope record from the northern Red Sea documenting NAO, ENSO, and North Pacific teleconnections on Middle East climate variability since the year 1750, Paleoceanography, 15, 679–694, https://doi.org/10.1029/1999PA000477, 2000.

Felis, T., Suzuki, A., Kuhnert, H., Rimbu, N., and Kawahata, H.: Pacific Decadal Oscillation documented in a coral record of North Pacific winter temperature since 1873, Geophys. Res. Lett., 37, L14605, https://doi.org/10.1029/2010GL043572, 2010.

Felis, T., Ionita, M., Rimbu, N., Lohmann, G., and Kölling, M.: Mild and arid climate in the eastern Sahara-Arabian Desert during the late Little Ice Age, Geophys. Res. Lett., 45, 7112–7119, https://doi.org/10.1029/2018GL078617, 2018.

Freund, M. B., Henley, B. J., Karoly, D. J., McGregor, H. V., Abram, N. J., and Dommenget, D.: Higher frequency of Central Pacific El Niño events in recent decades relative to past centuries, Nat. Geosci., 12, 450–455, https://doi.org/10.1038/s41561-019-0353-3, 2019.

Garas, K. L., Watanabe, T., and Yamazaki, A.: Hydroclimate seasonality from paired coral Sr/Ca and δ^{18}O records of Kikai Island, Southern Japan: Evidence of East Asian monsoon during mid-to late Holocene, Quaternary Sci. Rev., 301, 107926, https://doi.org/10.1016/j.quascirev.2022.107926, 2023.

Gouhier, T. C., Grinsted, A., and Simko, V.: R package biwavelet: Conduct Univariate and Bivariate Wavelet Analyses [code], https://doi.org/10.32614/CRAN.package.biwavelet, 2021.

Hammer, Ø., Harper, D. A., and Ryan, P. D.: PAST: Paleontological statistics software package for education and data analysis, Palaeontol. Electron., 4, 9, https://palaeo-electronica.org/2001_1/past/issue1_01.htm (last access: 22 October 2026), 2001.

Hendy, E. J., Gagan, M. K., Alibert, C. A., McCulloch, M. T., Lough, J. M., and Isdale, P. J.: Abrupt decrease in tropical Pacific sea surface salinity at end of Little Ice Age, Science, 295, 1511–1514, https://doi.org/10.1126/science.1067693, 2002.

Hetzinger, S., Halfar, J., Kronz, A., Steneck, R. S., Adey, W., Lebednik, P. A., and Schone, B. R.: High-resolution Mg/Ca ratios in a coralline red alga as a proxy for Bering Sea temperature variations from 1902 to 1967, PALAIOS, 24, 406–412, https://doi.org/10.2110/palo.2008.p08-116r, 2009.

Hiess, J., Condon, D. J., McLean, N., and Noble, S. R.: ^{238}U / ^{235}U systematics in terrestrial uranium-bearing minerals, Science, 335, 1610–1614, https://doi.org/10.1126/science.1215507, 2012.

Huang, B., Thorne, P. W., Banzon, V. F., Boyer, T., Chepurin, G., Lawrimore, J. H., Menne, M. J., Smith, T. M., Vose, R. S., and Zhang, H.-M.: Extended reconstructed sea surface temperature, version 5 (ERSSTv5): upgrades, validations, and intercomparisons, J. Clim., 30, 8179–8205, https://doi.org/10.1175/JCLI-D-16-0836.1, 2017.

Huang, B., Liu, C., Banzon, V., Freeman, E., Graham, G., Hankins, B., Smith, T., and Zhang, H.-M.: Improvements of the Daily Optimum Interpolation Sea Surface Temperature (DOISST) Version 2.1, J. Clim., 34, 2923–2939, https://doi.org/10.1175/jcli-d-20-0166.1, 2021.

Ito, S., Watanabe, T., Yano, M., and Watanabe, T. K.: Influence of local industrial changes on reef coral calcification, Sci. Rep., 10, 7892, https://doi.org/10.1038/s41598-020-64877-6, 2020.

Jaffey, A. H., Flynn, K. F., Glendenin, L. E., Bentley, W. C., and Essling, A. M.: Precision measurement of half-lives and specific activities of 235U and 238U, Phys. Rev. C, 4, 1889–1906, https://doi.org/10.1103/PhysRevC.4.1889, 1971.

Ji, K., Yu, J.-Y., Li, J., Hu, Z.-Z., Tseng, Y.-H., Shi, J., Zhao, Y., Sun, C., and Ding, R.: Enhanced North Pacific Victoria mode in a warming climate, npj Clim. Atmos. Sci., 7, 49, https://doi.org/10.1038/s41612-024-00599-0, 2024.

Kajita, H., Yamazaki, A., Watanabe, T., Wu, C.-C., Shen, C.-C., and Watanabe, T.: Holocene sea surface temperature variations recorded in corals from Kikai Island, Japan, Geochem. J., 51, e9–e14, https://doi.org/10.2343/geochemj.2.0482, 2017.

Kao, H.-Y. and Yu, J.-Y.: Contrasting eastern-Pacific and central-Pacific types of ENSO, J. Clim., 22, 615–632, https://doi.org/10.1175/2008jcli2309.1, 2009.

Kawakubo, Y., Yokoyama, Y., Suzuki, A., Okai, T., Alibert, C., Kinsley, L., and Eggins, S.: Precise determination of Sr/Ca by laser ablation ICP-MS compared to ICP-AES and application to multi-century temperate corals, Geochem. J., 48, 145–152, https://doi.org/10.2343/geochemj.2.0295, 2014.

Kawakubo, Y., Alibert, C., and Yokoyama, Y.: A reconstruction of subtropical western North Pacific SST variability back to 1578, based on a *Porites* Coral Sr/Ca record from the northern Ryukyus, Japan, Paleoceanography, 32, 1352–1370, https://doi.org/10.1002/2017PA003203, 2017.

Kilduff, D. P., Di Lorenzo, E., Botsford, L. W., and Teo, S. L. H.: Changing central Pacific El Niños reduce stability of North American salmon survival rates, P. Natl. Acad. Sci., 112, 10962–10966, https://doi.org/10.1073/pnas.1503190112, 2015.

Kubota, K., Yokoyama, Y., Ishikawa, T., Suzuki, A., and Ishii, M.: Rapid decline in pH of coral calcification fluid due to incorporation of anthropogenic CO_2, Sci. Rep., 7, 7694, https://doi.org/10.1038/s41598-017-07680-0, 2017.

Larkin, N. K. and Harrison, D. E.: Global seasonal temperature and precipitation anomalies during El Niño autumn and winter, Geophys. Res. Lett., 32, L16705, https://doi.org/10.1029/2005gl022860, 2005.

Lee, T. and McPhaden, M. J.: Increasing intensity of El Niño in the central-equatorial Pacific, Geophys. Res. Lett., 37, L14603, https://doi.org/10.1029/2010gl044007, 2010.

Lyons, M. B., Murray, N. J., Kennedy, E. V., Kovacs, E. M., Castro-Sanguino, C., Phinn, S. R., Acevedo, R. B., Alvarez, A. O., Say, C., and Tudman, P.: New global area estimates for coral reefs from high-resolution mapping, Cell Reports Sustainability, 1, https://doi.org/10.1016/j.crsus.2024.100015, 2024.

Mann, M. E., Fuentes, J. D., and Rutherford, S.: Underestimation of volcanic cooling in tree-ring-based reconstructions of hemispheric temperatures, Nat. Geosci., 5, 202–205, https://doi.org/10.1038/ngeo1394, 2012.

Mantua, N. J., Hare, S. R., Zhang, Y., Wallace, J. M., and Francis, R. C.: A Pacific interdecadal climate oscillation with impacts on salmon production, Bull. Am. Meteorol. Soc., 78, 1069–1079, https://doi.org/10.1175/1520-0477(1997)078<1069:apicow>2.0.co;2, 1997.

McGregor, H. V., Fischer, M. J., Gagan, M. K., Fink, D., Phipps, S. J., Wong, H., and Woodroffe, C. D.: A weak El Niño/Southern Oscillation with delayed seasonal growth around 4,300 years ago, Nat. Geosci., 6, 949–953, https://doi.org/10.1038/ngeo1936, 2013.

McPhaden, M. J., Zebiak, S. E., and Glantz, M. H.: ENSO as an integrating concept in earth science, Science, 314, 1740–1745, https://doi.org/10.1126/science.1132588, 2006.

Messié, M. and Chavez, F.: Global modes of sea surface temperature variability in relation to regional climate indices, J. Clim., 24, 4314–4331, https://doi.org/10.1175/2011JCLI3941.1, 2011.

Morimoto, M., Kayanne, H., Abe, O., and McCulloch, M. T.: Intensified mid-Holocene Asian monsoon recorded in corals from Kikai Island, subtropical northwestern Pacific, Quaternary Res., 67, 204–214, https://doi.org/10.1016/j.yqres.2006.12.005, 2007.

Nurhati, I. S., Cobb, K. M., and Di Lorenzo, E.: Decadal-scale SST and salinity variations in the central tropical Pacific: Signatures of natural and anthropogenic climate change, J. Clim., 24, 3294–3308, https://doi.org/10.1175/2011JCLI3852.1, 2011.

Okai, T., Suzuki, A., Kawahata, H., Terashima, S., and Imai, N.: Preparation of a new Geological Survey of Japan geochemical reference material: Coral JCp-1, Geostand. Geoanal. Res., 26, 95–99, https://doi.org/10.1111/j.1751-908X.2002.tb00627.x, 2002.

Pfeiffer, M., Dullo, W.-C., Zinke, J., and Garbe-Schönberg, D.: Three monthly coral Sr/Ca records from the Chagos Archipelago covering the period of 1950–1995 AD: reproducibility and implications for quantitative reconstructions of sea surface temperature variations, Int. J. Earth Sci., 98, 53–66, https://doi.org/10.1007/s00531-008-0326-z, 2009.

Pfeiffer, M., Zinke, J., Dullo, W. C., Garbe-Schönberg, D., Latif, M., and Weber, M. E.: Indian Ocean corals reveal crucial role of World War II bias for twentieth century warming estimates, Sci. Rep., 7, 14434, https://doi.org/10.1038/s41598-017-14352-6, 2017.

Philander, S. G. H.: El Niño Southern Oscillation phenomena, Nature, 302, 295–301, https://doi.org/10.1038/302295a0, 1983.

Qi, L. and Mao, X.: The North Pacific Victoria mode: More effective prediction signal for the Central Pacific El Niño than the North Pacific Oscillation, Int. J. Climatol., 42, 493–506, https://doi.org/10.1002/joc.7256, 2022.

Quinn, T. M., Crowley, T. J., Taylor, F. W., Henin, C., Joannot, P., and Join, Y.: A multicentury stable isotope record from a New Caledonia coral: Interannual and decadal sea surface temperature variability in the southwest Pacific since 1657 AD, Paleoceanography, 13, 412–426, https://doi.org/10.1029/98PA00401, 1998.

R Core Team: R: A language and environment for statistical computing, R Foundation for Statistical Computing, https://www.R-project.org/ (last access: 22 October 2026), 2023.

Rafter, P. A., Sanchez, S. C., Ferguson, J., Carriquiry, J. D., Druffel, E. R., Villaescusa, J., and Southon, J. R.: Eastern tropical North Pacific coral radiocarbon reveals North Pacific Gyre Oscillation (NPGO) variability, Quaternary Sci. Rev., 160, 108–115, https://doi.org/10.1016/j.quascirev.2017.02.002, 2017.

Ramos, R. D., Goodkin, N. F., and Fan, T. Y.: Coral records at the northern edge of the Western Pacific Warm Pool reveal multiple drivers of sea surface temperature, salinity, and rainfall variability since the end of the Little Ice Age, Paleoceanography and Paleoclimatology, 35, https://doi.org/10.1029/2019pa003826, 2020.

Rogers, J. C.: The North Pacific Oscillation, J. Climatol., 1, 39–57, https://doi.org/10.1002/joc.3370010106, 1981.

Sakashita, W., Miyahara, H., Yokoyama, Y., Aze, T., Obrochta, S. P., and Nakatsuka, T.: Relationship between the Northern Pacific Gyre Oscillation and tree-ring cellulose oxygen isotopes in northeastern Japan, Geosci. Lett., 4, 29, https://doi.org/10.1186/s40562-017-0095-2, 2017.

Sanchez, S. C., Charles, C. D., Carriquiry, J. D., and Villaescusa, J. A.: Two centuries of coherent decadal climate variability across the Pacific North American region, Geophys. Res. Lett., 43, 9208–9216, https://doi.org/10.1002/2016gl069037, 2016.

Shen, C.-C., Lee, T., Chen, C.-Y., Wang, C.-H., Dai, C.-F., and Li, L.-A.: The calibration of D[Sr/Ca] versus sea surface temperature relationship for *Porites* corals, Geochim. Cosmochim. Acta, 60, 3849–3858, https://doi.org/10.1016/0016-7037(96)00205-0, 1996.

Shen, C.-C., Lawrence Edwards, R., Cheng, H., Dorale, J. A., Thomas, R. B., Bradley Moran, S., Weinstein, S. E., and Edmonds, H. N.: Uranium and thorium isotopic and concentration measurements by magnetic sector inductively coupled plasma mass spectrometry, Chem. Geol., 185, 165–178, https://doi.org/10.1016/S0009-2541(01)00404-1, 2002.

Shen, C.-C., Cheng, H., Edwards, R. L., Moran, S. B., Edmonds, H. N., Hoff, J. A., and Thomas, R. B.: Measurement of attogram quantities of ^{231}Pa in dissolved and particulate fractions of seawater by isotope dilution thermal ionization mass spectroscopy, Anal. Chem., 75, 1075–1079, https://doi.org/10.1021/ac026247r, 2003.

Shen, C.-C., Lee, T., Liu, K.-K., Hsu, H.-H., Edwards, R. L., Wang, C.-H., Lee, M.-Y., Chen, Y.-G., Lee, H.-J., and Sun, H.-T.: An evaluation of quantitative reconstruction of past precipitation records using coral skeletal Sr/Ca and δ^{18}O data, Earth Planet. Sci. Lett., 237, 370–386, https://doi.org/10.1016/j.epsl.2005.06.042, 2005.

Shen, C.-C., Li, K.-S., Sieh, K., Natawidjaja, D., Cheng, H., Wang, X., Edwards, R. L., Lam, D. D., Hsieh, Y.-T., Fan, T.-Y., Meltzner, A. J., Taylor, F. W., Quinn, T. M., Chiang, H.-W., and Kilbourne, K. H.: Variation of initial ^{230}Th/^{232}Th and limits of high precision U–Th dating of shallow-water corals, Geochim. Cosmochim. Acta, 72, 4201–4223, https://doi.org/10.1016/j.gca.2008.06.011, 2008.

Shen, C.-C., Wu, C.-C., Cheng, H., Lawrence Edwards, R., Hsieh, Y.-T., Gallet, S., Chang, C.-C., Li, T.-Y., Lam, D. D., Kano, A., Hori, M., and Spötl, C.: High-precision and high-resolution carbonate ^{230}Th dating by MC-ICP-MS with SEM protocols, Geochim. Cosmochim. Acta, 99, 71–86, https://doi.org/10.1016/j.gca.2012.09.018, 2012.

Shen, M.-H. and Yu, J.-Y.: Changes in El Niño characteristics and air–sea feedback mechanisms under progressive global warming, Terrestrial, Atmos. Ocean. Sci., 34, 19, https://doi.org/10.1007/s44195-023-00051-5, 2023.

Sippel, S., Kent, E. C., Meinshausen, N., Chan, D., Kadow, C., Neukom, R., Fischer, E. M., Humphrey, V., Rohde, R., De Vries, I., and Knutti, R.: Early-twentieth-century cold bias in ocean surface temperature observations, Nature, 635, 618–624, https://doi.org/10.1038/s41586-024-08230-1, 2024.

Sonderegger, D. L., Wang, H., Clements, W. H., and Noon, B. R.: Using SiZer to detect thresholds in ecological data, Front. Ecol. Environ., 7, 190–195, https://doi.org/10.1890/070179, 2009.

Tanabe, K., Mimura, T., Miyaji, T., Shirai, K., Kubota, K., Murakami-Sugihara, N., and Schöne, B. R.: Interannual to decadal variability of summer sea surface temperature in the Sea of Okhotsk recorded in the shell growth history of Stimpson's hard clams (Mercenaria stimpsoni), Glob. Planet. Change, 157, 35–47, https://doi.org/10.1016/j.gloplacha.2017.08.010, 2017.

Tangri, N., Dunbar, R. B., Linsley, B. K., and Mucciarone, D. M.: ENSO's shrinking twentieth-century footprint revealed in a half-millennium coral core from the South Pacific Convergence Zone, Paleoceanography and Paleoclimatology, 33, 1136–1150, https://doi.org/10.1029/2017PA003310, 2018.

Thompson, D. M., Conroy, J. L., Konecky, B. L., Stevenson, S., Delong, K. L., McKay, N., Reed, E., Jonkers, L., and Carré, M.: Identifying Hydro-Sensitive Coral δ^{18}O Records for Improved High-Resolution Temperature and Salinity Reconstructions, Geophys. Res. Lett., 49, https://doi.org/10.1029/2021gl096153, 2022.

Thompson, D. W. J., Kennedy, J. J., Wallace, J. M., and Jones, P. D.: A large discontinuity in the mid-twentieth century in observed global-mean surface temperature, Nature, 453, 646–649, https://doi.org/10.1038/nature06982, 2008.

Trenberth, K. E. and Hurrell, J. W.: Decadal atmosphere-ocean variations in the Pacific, Clim. Dynam., 9, 303–319, https://doi.org/10.1007/bf00204745, 1994.

Vimont, D. J., Battisti, D. S., and Hirst, A. C.: Footprinting: A seasonal connection between the tropics and mid-latitudes, Geophys. Res. Lett., 28, 3923–3926, https://doi.org/10.1029/2001gl013435, 2001.

Vimont, D. J., Wallace, J. M., and Battisti, D. S.: The Seasonal Footprinting Mechanism in the Pacific: Implications for ENSO, J. Clim., 16, 2668–2675, https://doi.org/10.1175/1520-0442(2003)016<2668:tsfmit>2.0.co;2, 2003.

Vinther, B. M., Andersen, K. K., Hansen, A. W., Schmith, T., and Jones, P. D.: Improving the Gibraltar/Reykjavik NAO index, Geophys. Res. Lett., 30, 2222, https://doi.org/10.1029/2003gl018220, 2003.

Wagner, S. and Zorita, E.: The influence of volcanic, solar and CO_2 forcing on the temperatures in the Dalton Minimum (1790–1830): a model study, Climate Dynamics, 25, 205–218, https://doi.org/10.1007/s00382-005-0029-0, 2005.

Walker, G. T. and Bliss, E. W.: World weather V, Mem. R. Metrol. Soc., 4, 53–84, 1932.

Watanabe, T., Suzuki, A., Minobe, S., Kawashima, T., Kameo, K., Minoshima, K., Aguilar, Y. M., Wani, R., Kawahata, H., Sowa, K., Nagai, T., and Kase, T.: Permanent El Niño during the Pliocene warm period not supported by coral evidence, Nature, 471, 209–211, https://doi.org/10.1038/nature09777, 2011.

Watanabe, T., Kawamura, T., Yamazaki, A., Murayama, M., and Yamano, H.: A 106 year monthly coral record reveals that the East Asian summer monsoon modulates winter PDO variability, Geophys. Res. Lett., 41, 3609–3614, https://doi.org/10.1002/2014GL060037, 2014.

Watanabe, T. K., Watanabe, T., Ohmori, K., and Yamazaki, A.: Improving analytical method of Sr/Ca ratios in coral skeletons for paleo-SST reconstructions using ICP-OES, Limnol. Oceanog.-Methods, 18, 297–310, https://doi.org/10.1002/lom3.10357, 2020.

Watanabe, T. K. and Pfeiffer, M.: A simple Monte Carlo approach to estimate the uncertainties of SST and $\delta^{18}O_{sw}$ inferred from coral proxies, Geochem. Geophys. Geosyst., 23, https://doi.org/10.1029/2021gc009813, 2022.

Wen, T., Ding, R., Shi, L., and Ji, K.: A new dipole index for the North Pacific Victoria mode, Clim. Dynam., 62, 8169–8179, https://doi.org/10.1007/s00382-024-07330-y, 2024.

Xu, Y.-Y., Pearson, S., and Halimeda Kilbourne, K.: Assessing coral Sr/Ca–SST calibration techniques using the species *Diploria strigosa*, Palaeogeogr. Palaeoclimatol., 440, 353–362, https://doi.org/10.1016/j.palaeo.2015.09.016, 2015.

Ye, X., Zhang, W., and Luo, M.: The North Pacific gyre oscillation and East Asian summer precipitation, Atmos. Sci. Lett., 17, 531–537, https://doi.org/10.1002/asl.688, 2016.

Yeh, S.-W., Kug, J.-S., Dewitte, B., Kwon, M.-H., Kirtman, B. P., and Jin, F.-F.: El Niño in a changing climate, Nature, 461, 511–514, https://doi.org/10.1038/nature08316, 2009.

Yeh, S.-W., Kang, Y.-J., Noh, Y., and Miller, A. J.: The North Pacific Climate Transitions of the Winters of 1976/77 and 1988/89, J. Clim., 24, 1170–1183, https://doi.org/10.1175/2010jcli3325.1, 2011.

Yu, J.-Y. and Kim, S. T.: Relationships between Extratropical Sea Level Pressure Variations and the Central Pacific and Eastern Pacific Types of ENSO, J. Climate, 24, 708–720, https://doi.org/10.1175/2010jcli3688.1, 2011.

Zhang, S., Qu, X., and Huang, G.: Enhanced impacts of the North Pacific Victoria mode on the Indian summer monsoon onset in recent decades, Geosci. Lett., 11, 6, https://doi.org/10.1186/s40562-024-00324-y, 2024a.

Zhang, S., Hu, P., Huang, G., and Qu, X.: Observed impacts of the North Pacific Victoria Mode on Indian summer monsoon onset, Atmos. Res., 297, 107126, https://doi.org/10.1016/j.atmosres.2023.107126, 2024b.